UCONN
LIBRARY

Doctoral Dissertations

University of Connecticut Graduate School

9-29-2014

Design, Synthesis and Biological Evaluation of Small Molecule Inhibitors of the Hedgehog Signaling Pathway

Upasana Banerjee
upasana.banerjee@uconn.edu

Follow this and additional works at: https://opencommons.uconn.edu/dissertations

Design, Synthesis and Biological Evaluation of Small Molecule Inhibitors of the Hedgehog Signaling Pathway

Upasana Banerjee, PhD

University of Connecticut, 2014

The Hedgehog (Hh) signaling is an important embryonic developmental pathway normally responsible for tissue growth, differentiation and patterning. However, aberrant activity of this signaling cascade has been implicated in several types of cancer. Therefore, inhibition of the dysregulated pathway is a promising therapeutic target for treating Hh-dependent malignancies such as basal cell carcinoma (BCC) and medulloblastoma (MB). Previous studies resulted in the FDA approval of Vismodegib, a small molecule inhibitor of the Hh pathway, for the treatment of advanced BCC. Similarly, several other small molecule Hh antagonists have progressed into clinical trials. Moreover, several components within the Hh pathway have proven to be druggable in 'proof-of-concept' studies. Nonetheless, several challenges in the discovery and development process for small molecules targeting this pathway have been noted. For instance, multiple mechanisms of resistance to Hh inhibitors have been identified. This has prompted extensive search for novel inhibitors that function via mechanisms that will retain activity in the presence of pathway signaling resistant to current therapy. Consequently, a ligand based approach was undertaken to develop Hh inhibitors based on two distinct lead structures namely Vitamin D3 (VD3) and Itraconazole (ITZ). An interdisciplinary approach utilizing synthetic organic chemistry transformations and molecular biology techniques was adopted to study the Hh inhibitory effects of probing relevant biological systems with aforementioned small molecule modulators and their derivatives. Information thus obtained guided the design of improved second-generation Hh inhibitors. A structure-activity-relationship study to identify the Hh inhibitory pharmacophore of VD3 was pursued. Based on the findings, VD3 based anti-Hh

analogues with improved potency and selectivity were designed, synthesized and evaluated. Next, a synthetic methodology for preparing ITZ derivatives with stereochemically defined hydroxylated side chains was optimized. Preliminary evaluation of resultant hybrid ITZ analogues obtained via this synthetic route identified Hh inhibitors demonstrating nanomolar potencies. Taken together, the preliminary identification of several improved Hh inhibitory scaffolds through these studies will facilitate further comprehensive biological evaluation of the promising derivatives.

Design, Synthesis and Biological Evaluation of Small Molecule Inhibitors of the Hedgehog Signaling Pathway

Upasana Banerjee

B. Pharm, University of Delhi, India, 2009

A Dissertation

Submitted in Partial Fulfillment of the

Requirements for the Degree of

Doctor of Philosophy

at the

University of Connecticut

2014

Copyright by

Upasana Banerjee

2014

APPROVAL PAGE

Doctor of Philosophy Dissertation

Design, Synthesis and Biological Evaluation of Small Molecule Inhibitors of the
Hedgehog Signaling Pathway

Presented by

Upasana Banerjee, B. Pharm

Major Advisor
_____
M. Kyle Hadden, PhD

Associate Advisor
_____
Dennis L. Wright, PhD

Associate Advisor
_____
Charles Giardina, PhD

University of Connecticut
2014

DEDICATION

To my wonderful family members: *the Banerjees, the Chakrabortys and the Talapatras*

ACKNOWLEDGEMENTS

During the five years of my graduate career, I have had the privilege of working with truly inspiring mentors and extremely supportive peers and co-workers. Needless to say, this has contributed greatly towards shaping my doctoral dissertation projects and towards the successful completion of these goals. First, I would like to express sincere gratitude to my major advisor, Dr. M. Kyle Hadden, for providing me with valuable guidance, strong motivation and unwavering support. I am extremely thankful to him for encouraging me to be an independent thinker and giving me the opportunity to work on multiple exciting projects. Next, I am grateful for the support I have received from the members of the Hadden Lab. Teamwork is essential for the success of interdisciplinary drug discovery endeavors, I have been fortunate to work with the best and the brightest team players. Dr. Manuka Ghosh helped me learn the basics of practical synthetic chemistry while Vibhavari Sail trained me on various molecular biology techniques. Dr. Albert M. Deberardinis has been a great teacher, loyal friend and awesome labmate over the last few years. Long discussions about science and life with him and the newer members of the team i.e. Jen Pace and Chad Mashchinot have unfailingly provided clarity during the darkest of times. I gratefully acknowledge the time all of them have spent in guiding and assisting me. Also, past and present undergraduate members including Audrey, Steve, Dan DeCarlo, Michelle, Dan Madden, Dan Raccucia, Evrett, Kelly, thank you for your friendship and support.

I am indebted to my thesis committee members Dr. Dennis L. Wright and Dr. Charles Giardina for their constructive comments and discussions over the course of the years. With their sound advice I have been able to direct my efforts meaningfully and troubleshoot problems. I am grateful to our collaborator, Dr. Ervin Epstein, for

generously providing us with the ASZ cell line which enabled further biological evaluation of the newly synthesized molecules.

I would like to express my deepest gratitude to all my teachers who have taught me over the last several years, especially, Dr. D. K. Majumdar, my undergraduate advisor, for sharing his great depth of knowledge in the field of Pharmaceutical Science. I greatly appreciate the efforts of Dr. Zhaoming Xiong, my internship advisor at Boehringer Ingelheim, for training me in the field of Medicinal Chemistry in an industrial setting.

I would like to thank UConn's Nuclear Magnetic Resonance facility (Dr. Morton, Dr. Pacheco, Dr. Gorbatyuk) and Mass Spectrometry facility (Dr. You-Jun) for their hard work in efficiently maintaining these core facilities for the convenience of researchers. Day to day functioning in the department would not have been possible without the efforts of Pharmaceutical Sciences staff members. Special thanks to Ms. Lebel, Mr. Armati, Mr. Shea and Ms. Kathy Koji for facilitating critical administrative tasks necessary for uninterrupted research.

I am extremely thankful to my friends Suravi, Pankaj, Dhruv, and Megha for always being by side and celebrating life with me. Finally, I owe every bit of my success to my family. Ma, Baba, Puche, Pinu, Dida and Dadu have been my greatest supporters throughout. Thank you for always believing in me. Thanks to my loving husband, Siddharth, who has stood by me like a rock and to my extended family especially Ma, Baba, Bubu di, Manas da and sweet little Neil for everything. I fall short of words in thanking my family enough for their unconditional love and support.

TABLE OF CONTENTS

LIST OF FIGURES

x

Chapter IV

Chapter V

LIST OF SCHEMES

LIST OF TABLES

CHAPTER I: Recent Advances in the Design of Hedgehog Pathway Inhibitors for the Treatment of Malignancies

1. Introduction

The Hedgehog (Hh) signaling pathway is a developmental pathway that plays an essential role in tissue growth and differentiation during embryogenesis. The Hh pathway has been implicated in the proper patterning of a variety of human tissues, including, bone and cartilage, hair follicles, heart and lung muscle, and the central and peripheral nervous system [1]. Hh signaling is significantly less active in adult tissues, where its primary role appears to be the maintenance of stem cell populations in skin and the central nervous system. Aberrant regulation of pathway signaling causes constitutive activation, resulting in uncontrolled cellular proliferation and tumor growth; most notably in basal cell carcinoma (BCC) and medulloblastoma (MB).

Hh signaling is primarily controlled by two membrane-bound receptors: Patched (Ptch), a 12 transmembrane domain (TM) cell surface receptor; Smoothened (Smo), a 7 TM G-protein coupled receptor (GPCR)-like receptor; and the glioma-associated oncogene (Gli) family of zinc-finger transcription factors, which act in a concerted fashion to regulate pathway activity (Figure 1). In the absence of an Hh ligand [Sonic Hh (Shh), Indian Hh (IHh), and Desert Hh (DHh)], Ptch represses the activity of Smo through a complicated mechanism that is not completely understood. In this state, Gli and Suppressor of Fused (Sufu) form a heteroprotein complex in the cytosol. Sufu serves as a negative regulator of Gli by promoting phosphorylation of the Gli proteins, ultimately leading to their ubiquitin/proteasome-mediated proteolysis and the generation of N-terminal truncated forms (Gli^R) that serve as transcriptional repressors of Hh target genes. On binding of an Hh ligand, Ptch is internalized and its inhibition of Smo is alleviated. Smo is phosphorylated at its intracellular C-terminus and translocates to the cell surface membrane of non-motile cilia. The activation and translocation of Smo disrupts the Sufu-Gli complex, leading to the production of intact, active forms of Gli

2

(Gli^A). Gli^A acts a transcriptional activator in the nucleus to stimulate production of the ubiquitous Hh target genes *Gli1*, *Ptch1*, and *HHIP* (Hh interacting protein). Within the context of Hh signaling, Gli^A primarily consists of Gli2 and/or Gli3, while Gli1 is the predominant Hh-responsive activator that mediates the downstream effects of pathway activation.
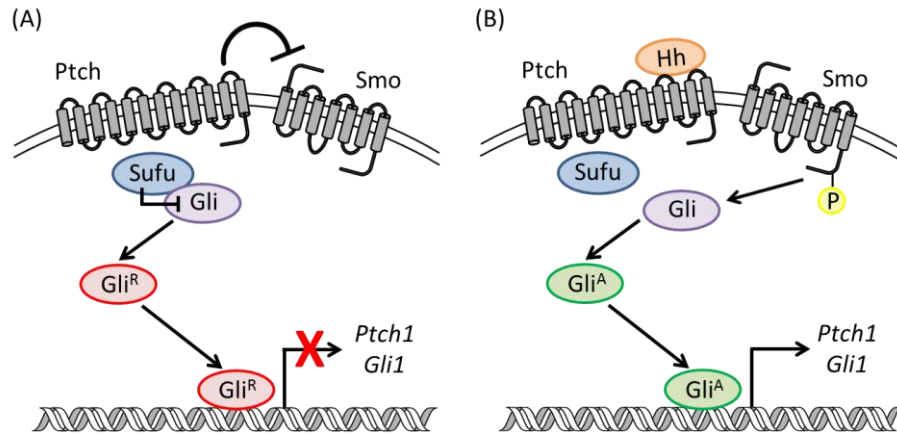
Figure 1. General scheme for the Hh signaling cascade.[2] Gli: Glioma-associated oncogene; Hh: Hedgehog; Ptch: Patched; Smo: Smoothened; Sufu: Suppressor of Fused.

2. Hh Signaling Pathway and Cancer

2.1 Cellular Mechanisms of Dysregulation

Aberrant regulation of pathway signaling results in its constitutive activation, which can ultimately drive uncontrolled cellular proliferation and tumor growth. While multiple mechanisms through which dysregulated or hyperactive Hh signaling contributes to tumor formation, growth, and metastasis have been identified, the best characterized are Hh ligand independent. These forms of Hh-dependent cancer are characterized by mutations in key pathway signal transducers, i.e. Ptch and Smo. Basal cell carcinoma (BCC) is the most common human cancer, accounting for ~80% of nonmelanoma skin cancers and affecting approximately 10 million people worldwide on an annual basis [3, 4]. Genetic analyses have demonstrated that a majority of sporadic BCCs exhibit detectable genetic mutations in *Ptch1* (~75%), *Smo* (10%), or *Sufu* (~5%)

3

[5, 6]. Mutations in *Ptch* and *Sufu* have also been implicated as primary factors contributing to the development of Hh-dependent medulloblastomas (MB) and rhabdomyosarcomas (RMS) [7-10]. Studies have also identified several ligand-dependent mechanisms that contribute to constitutive pathway activation. These include autocrine, paracrine, and reverse-paracrine signaling modalities and have been implicated in a variety of human cancers, including pancreatic adenocarcinoma [11-13], gastrointestinal [14], prostate [15-17], breast [18, 19], colon [12, 20-22], and hematologic cancers [23, 24]. It is important to note that while these ligand-dependent mechanisms may contribute to tumor growth in these tissues; it is unclear whether cancers that exhibit these forms of aberrant signaling can be defined as Hh-dependent. More detailed descriptions of the ways in which Hh signaling contributes to human cancer and cancer stem cell populations can be found in several recently published review articles [25-30].

2.2 Resistance to Smo Antagonists

To date, several Hh pathway inhibitors that target Smo have progressed from preclinical development and into clinical trials; however, the development of resistance to these compounds has become a major hurdle for their continued development [25]. The most advanced of these compounds, the small molecule GDC-0449 (Vismodegib/Erivedge™), was approved by the FDA for the treatment of metastatic BCC; however, the trials against MB were less successful [31]. Although treatment of an MB patient with GDC-0449 also demonstrated initial positive results, relapse occurred when a point mutation in Smo (D473H), the molecular target of GDC-0449, rendered the patient insensitive to further GDC-0449 treatment (Figure 2A) [32-34]. The preclinical evaluation of NVP-LDE225, a small molecule pathway inhibitor under development by Novartis, in murine models of Hh-dependent MB demonstrated tumor regrowth following initial regression, indicating the development of resistance for this compound as well [35].

4

In these studies, treatment with NVP-LDE225 resulted in chromosomal amplification of Gli2 and downstream re-activation of Hh signaling, as well as additional point mutations in Smo [35]. In addition to the development of resistance in MB, a recent study reported that 21% of patients receiving continuous GDC-0449 treatment for BCC developed regrowth of at least one BCC [36]. While the molecular mechanisms that govern this secondary acquired resistance have not been described, the results suggest that resistance to Smo antagonists in BCC patients will also be an issue moving forward.
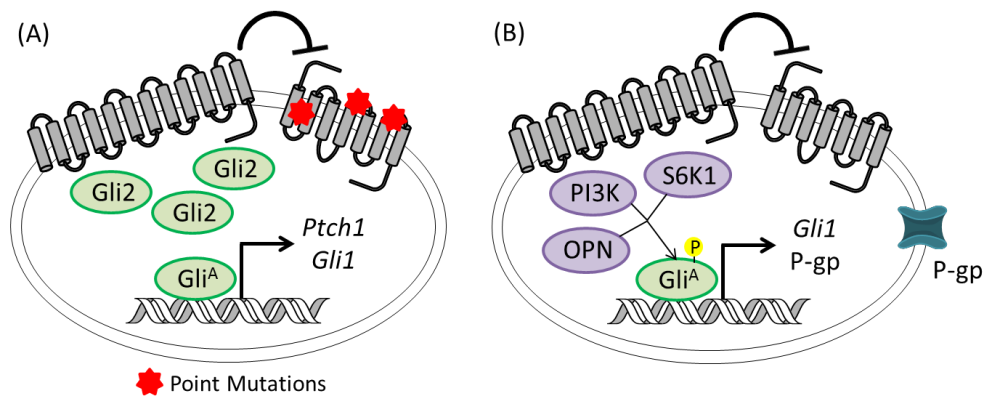
Figure 2. Cellular mechanisms of resistance to Hh pathway inhibitors. Gli: Glioma; P-gp: P-glycoprotein; PI3K: Phosphoinositide 3-kinase; Ptch: Patched; S6K1: S6 kinase 1.

Additional mechanisms of tumor resistance independent of canonical Hh signaling have also been reported for Smo antagonists (Figure 2B). Treatment with IPI-926 (Saridegib), a semi-synthetic derivative of a natural product Hh pathway inhibitor cyclopamine (Cyc), resulted in decreased tumor size and prolonged survival in mouse models of MB; however, resistance to this compound also developed [37]. In contrast to both GDC-0449 and NVP-LDE225, the resistance for IPI-926 was unrelated to either Gli amplification or Smo mutations [37]. Follow-up studies with IPI-926 linked resistance to induction of P-glycoprotein (P-gp) in the tumor cells, suggesting that its decreased activity was a result of active efflux from the tumor. MB tumors resistant to NVP-LDE225 demonstrated upregulation of components in the phosphoinositide 3-kinase (PI3K)

pathway [35]. PI3K signaling was previously shown to enhance Gli-dependent transcription when SHh is present at low levels, suggesting PI3K signaling may partially compensate for inhibition of Hh signaling by Smo antagonists to promote tumor resistance [38]. In esophageal adenocarcinoma (EAC), the mTOR pathway component S6 kinase 1 (S6K1) phosphorylates Gli1, resulting in its Smo-independent dissociation from Sufu and activation of Hh signaling [39]. Although this mechanism has not been explored in other Hh-dependent cancers, it provides evidence of another mechanism that is capable of promoting resistance to Hh pathway inhibitors that function at or prior to the level of Smo. The inflammatory cytokine osteopontin (OPN) has also been shown to activate Gli-mediated transcription through a non-classical mechanism by modulation of Akt/GSK3β signaling [40]. OPN inactivates GSK3β, which ultimately results in Sufu/Gli dissociation and accumulation of Gli[A] within the nucleus. Interestingly, OPN also up-regulated P-gp through a Gli-dependent process, suggesting that it may mediate resistance to Smo antagonists through multiple distinct mechanisms.

3. Small Molecule Smo Antagonists

3.1 Current Status of Important Smo Antagonists

The first-in-class Hh pathway inhibitor, GDC-0449 (**2**, Figure 3), was a product of collaborative research by scientists at Curis and Genentech [41]. A series of iterative medicinal chemistry studies optimized the initial lead compound (**1**, Figure 3) for potency, pharmacokinetic (PK) and physicochemical properties to provide GDC-0449 as a potent inhibitor of Hh signaling (IC_{50} values = 3 - 22 nM). Currently, it is approved for the treatment of advanced/metastatic BCC unmanageable by surgery or radiation therapy [42]. As noted above, these initial successes of GDC-0449 have been countered by the emergence of resistant forms of Smo that result in its complete loss of efficacy [32]. Even with the ongoing resistance issues, there is still continued interest in GDC-0449 for

several indications as evidenced by currently active clinical trials in which it is being studied as both monotherapy or in combination to evaluate its safety and efficacy. Moreover, several trials are underway to assess drug interactions and determine appropriate drug regimens. Researchers at Genentech seeking to identify structurally-related compounds that could inhibit Smo D473H and E518K screened a panel of 53 compounds exhibiting high potency against wild type Smo for their activity against the mutant receptors [33]. Among these, compound **3** (Figure 3) was selected for further evaluation due to its robust activity against both wild-type and Smo D473H (IC_{50} values = 300 nM and 700 nM, respectively) and its enhanced half-life (22 hrs). Compound **3** reduced tumor volume in subcutaneous allografts of the murine Hh-dependent MB tumor line SG274 following oral administration (100 mg/kg, once daily [q.d.] dosing); however, neither additional studies nor clinical trials for this compound have been reported [33].

The second small-molecule inhibitor of Hh signaling that has demonstrated promising clinical efficacy is NVP-LDE225 (Sonidegib, Erismodegib), a *meta*-bisphenyl carboxamide compound developed by Novartis (**5**, Figure 3) [43]. NVP-LDE225 was recently advanced to Phase III studies for advanced BCC and a phase III study for relapsed MB is being initiated to study the comparative safety and efficacy of NVP-LDE225 and Temozolomide (TMZ). Additionally, volunteers are currently being recruited to evaluate efficacy against new indications such as resectable pancreatic cancer, relapsed acute leukemia, myelofibrosis and Ptch- and Smo-mutant-activated solid and hematological tumors. Although clinical resistance has not been reported for NVP-LDE225, the development of multiple forms of resistance to the compound in mouse models of MB remains a critical concern for this scaffold.

7
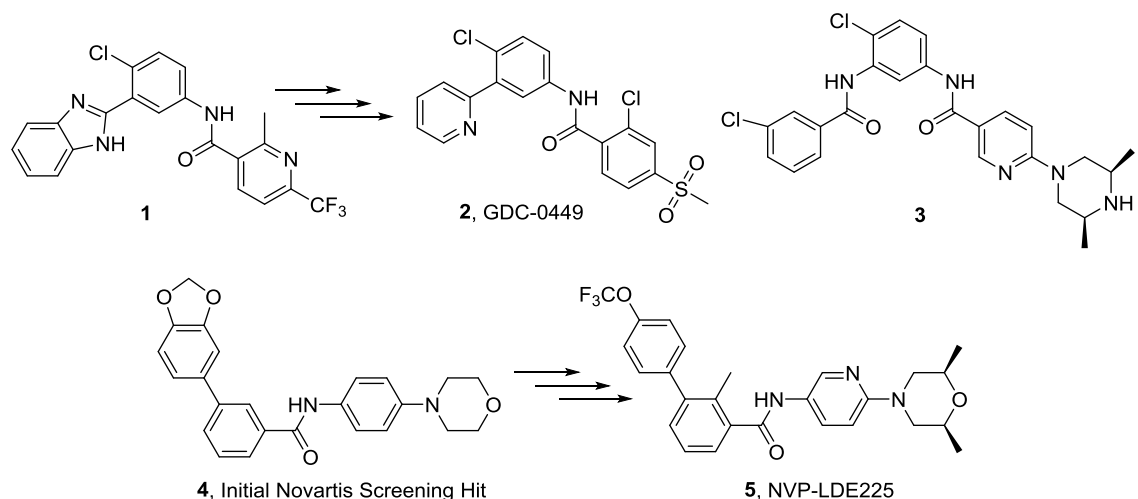
Figure 3. General structural optimization of GDC-0449 and NVP-LDE225.

Cyclopamine (**6**, Figure 4), an alkaloid natural product derived from corn lilies, was the first known small-molecule Hh inhibitor. Extensive research using this prototype Hh/Smo inhibitor not only led to crucial revelations about multiple binding sites, mechanisms of SMO activation and post binding cellular events [44-46], but also pushed forward the search for related small-molecule inhibitors for dysregulated Hh pathway signaling [44-48]. Due to poor physicochemical properties and moderate activity, Cyc was unsuitable as a clinical candidate [49]; however, second and third generation Cyc analogues developed by Infinity Pharmaceuticals improved on the core scaffold and ultimately resulted in IPI-926 (**7,** Figure 4), a clinical candidate that demonstrated improved potency and drug-like properties [37, 50]. When tested in mouse MB allograft models, IPI-926 demonstrated complete regression upon multi-day oral administration and abrogated tumor recurrence during a 21-day post treatment period. Despite the initial promise, IPI-926 failed to deliver satisfactory results in Phase II clinical trials for pancreatic cancer, inoperable chondrosarcoma and myelofibrosis [51]. It is important to note that, to date, IPI-926 has not been evaluated in forms of human cancer generally considered to be Hh-dependent. Although the initial success of IPI-926 suggests the

potential clinical efficacy of this class of pathway inhibitor, further development of this scaffold has been nominal.
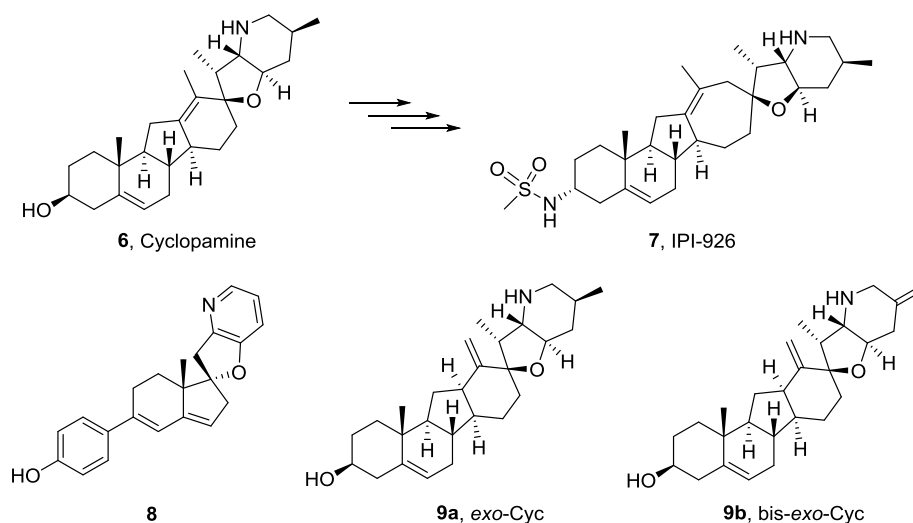
Figure 4. Structures of Cyc and its key analogues.

Researchers at the University of Pennsylvania described medicinal chemistry efforts to identify the Hh inhibitory pharmacophore of Cyc and ultimately developed a simplified analogue (**8**, Figure 4) inspired by the Cyc structure [52]. Key modifications included replacement of the C-nor-D-homo steroidal structure with an androstane ring system, the piperidine ring with a pyridine moiety and homoallyl alcohol by a phenol. Analogue **8** and its precursor molecules showed comparable inhibition of Hh signaling in reporter gene luciferase assays (IC_{50} values not reported). Further, analogue **8** was equipotent to Cyc in a cell viability assay in MB and three times more potent than Cyc in a granule neuron precursors proliferation assay [52]. More recently, the preparation and *in vitro* evaluation of a series of Cyc analogues incorporating an exocyclic olefin (**9a & 9b**, Figure 4) were reported by researchers at the University of Leipzig [53, 54]. Both analogues were significantly more active at inhibiting pathway signaling in Shh-Light II cells, an Hh-dependent clonal mouse fibroblast cell line incorporating a stably transfected Gli-dependent luciferase reporter (10- to 25-fold) with the most potent analogue

demonstrating an IC_{50} against Hh signaling of 0.2 μM [54]. Interestingly, removal or truncation of the piperidine ring abolished the anti-Hh activity of the *exo*-Cyc analogues, suggesting this functionality is essential for the Hh inhibitory activity of the Cyc scaffold [54]. A comprehensive description of other Cyc analogues can be found in a previously reported review [55].

3.2 Additional Smo Antagonists

3.2.1 Other Key Smo Antagonists in Clinical Trials

The results of a medicinal chemistry program at Pfizer designed to improve the metabolic profile and enhance the solubility of a class of benzimidazole inhibitors of Hh signaling culminated in PF-04449913 (**10**, Figure 5) a potent, urea-based inhibitor of Hh activity (IC_{50} = 5 nM) [56]. PF-04449913 demonstrated improved PK parameters, including a predicted half-life of 30 h and an oral bioavailability of 55% in humans [56]. Although detailed descriptions of the *in vivo* activity of this compound have not been disclosed, it has been advanced into multiple Phase I and II clinical trials for the treatment of acute myeloid leukemia and high-risk myelodysplastic syndrome either alone or in combination with other agents. Its efficacy in preventing or decreasing disease relapse in acute leukemia patients who have undergone donor stem cell transplant is also a current topic of investigation. Researchers at Pfizer have also reported on the preclinical development of another potent small-molecule Smo antagonist, PF-5274857 (**11**, Figure 5) [56]. PF-5274857 specifically binds to Smo, presumably in the GDC-0449/Cyc binding region, with high affinity (K_i = 4.6 nM). PF-5274857 demonstrated potent pathway inhibition *in vitro* and in an *in vivo* model of Hh-dependent MB with IC_{50} values of 2.7 and 8.9 nM, respectively [57]. *In vivo* inhibition of Hh signaling following oral administration (30 and 100 mg/kg) correlated well with increased survival and significant concentrations of intact PF-

5274857 was measured in the cerebrospinal fluid, indicating pharmacologically effective doses achieved blood-brain barrier penetration [57].

Researchers at Novartis have recently detailed lead optimization studies on their initial substituted phthalazine series that ultimately led to the identification of 1-piperazino-4-benzylpyridazine NVP-LEQ506 (**12**, Figure 5) as a potent pathway inhibitor currently in clinical development [58, 59]. NVP-LEQ506 demonstrates potent inhibition of pathway signaling *in vitro* against both wild-type and D473H Smo (IC_{50} values ~1 and 96 nM, respectively). Competitive displacement assays demonstrated that NVP-LEQ506 bound with high affinity to human Smo (IC_{50} = 2 nM) and *in vitro* PK assays showed its enhanced solubility and minimal hERG binding. Preclinical PK studies across multiple species demonstrated that NVP-LEQ506 possesses good bioavailability, low clearance, and the ability to cross the blood-brain barrier [59]. Finally, NVP-LEQ506 reduced Gli mRNA expression and promoted tumor regression in a murine allograft of Hh-dependent MB following oral dosing (10 – 40 mg/kg, q.d. dosing).

10, PF-04449913   **11**, PF-5274857   **12**, NVP-LEQ506

13, TAK-441   **14**, LY2940680   **15**, XL-139/BMS-833293
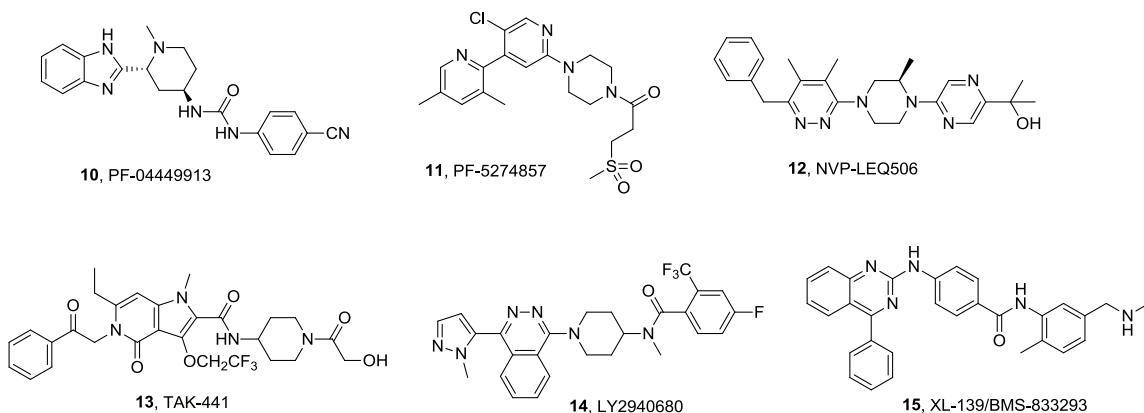
Figure 5. Additional Smo antagonists under clinical development.

TAK-441 (**13**, Figure 5) was developed by researchers at Takeda Pharmaceuticals by optimizing a novel pyrroloquinoline-one hit compound generated in an high-throughput screening (HTS) effort [60-63]. During lead optimization, the core N-

methylpyrrolopyridine scaffold was utilized to achieve optimal PK properties [61]. TAK-441 is a potent inhibitor of Hh signaling *in vitro* (IC_{50} = 4.6 nM) that completely abrogated tumor growth in an Hh-dependent model of MB following oral administration (25 mg/kg, twice daily [b.i.d.] for 14 days) [61]. Interestingly, even though TAK-441 shares the GDC-0449/Cyc binding site on Smo, it bound wild-type Smo and Smo D473H with comparable affinity (K_d values = 1.3nM and 7.8nM respectively) and maintained potent inhibition of pathway signaling *in vitro* in the presence of Smo D473H (IC_{50} = 79 nM) [62]. In a separate study, promising preclinical data was reported in delaying progression of castration-resistant prostate cancer *in vivo* (10 mg/kg or 25 mg/kg q.d. dosing for 7 days) [64]. Athough TAK-441 had advanced into clinical trial, following its initial Phase I Trial, Takeda Pharmaceuticals discontinued its development, citing research and development priorities in other areas [63].

LY2940680 (**14**, Figure 5), a phthalazine-based small molecule Smo antagonist under development at Eli Lilly was reported as a potent inhibitor of Hh signaling (IC_{50} = 2.4 nM) as determined in a MB cell line (Daoy) [65]. It was also reported to retain functional activity against the resistant D473H Smo mutant; however, specific data has not been reported in the literature. LY2940680 has also demonstrated efficacy in a mouse model of Hh-dependent MB following oral administration and is currently in several Phase I & II clinical trials for the treatment of a variety of human cancers [66].

Exelixis collaborated with Bristol-Myers Squibb to develop XL-139/BMS-833923 (**15**, Figure 5) another clinical candidate for Hh inhibition in Phase II trials. It was reported to inhibit the expression of Hh signaling markers such as Gli1 and Ptch1 in cell lines expressing either wild type or active mutant forms of Smo (IC_{50} value = 6-35 nM) [67]. Competitive binding inhibition of BODIPY-Cyc to Smo by XL-139/BMS-833923 with an IC_{50} of 21 nM was demonstrated by a fluorescence-activated cell sorting-based binding

12

assay. Additionally, it was shown to inhibit *in vitro* growth of multiple myeloma clones and colonogenic growth of several tumor cell lines obtained from hematological cancer patients [67].

3.2.2. Smo Antagonists in Preclinical Development

Researchers at Merck have disclosed the preclinical development of multiple small-molecule scaffolds as Hh pathway inhibitors [68-71]. The discovery and development of MK-5710 traces its origin to a structure-activity relationship (SAR) study of potent bicyclic hydantoin Smo antagonists. Overall, optimization of this scaffold afforded homochiral unsubstituted bicyclic tetrahydroimidazo[1,5-a]pyrazine-1,3(2H,5H)-diones as Hh pathway inhibitors. The most potent of these, MK-5710 (**16**, Figure 6) inhibited pathway signaling with an IC_{50} of 17 nM and displaced BODIPY-Cyc from Smo with high affinity (IC_{50} = 13 nM). The *in vivo* preclinical assessment of MK-5710 revealed favorable PK properties (oral bioavailability and low clearance) and potent Hh inhibitory activity (40-160 mg/kg, b.i.d.) against a murine allograft model of Hh-dependent MB [69]. In addition to MK-5710, a collaborative screening and lead optimization effort identified a class of piperazinyl ureas as potent inhibitors of Hh signaling [70]. The most active analogues in this series (**17-18**, Figure 6) inhibited pathway signaling with IC_{50} values of 5 nM and displaced BODIPY-Cyc from Smo (IC_{50} values = 3 and 13 nM, respectively). Further development of this scaffold to improve both potency and PK properties focused on iterative modifications to the "left-side" biaryl moiety, the central piperazine, or the "right-side" cyclohexyl ring [71]. The culmination of these modifications resulted in compound **19** (Figure 6), which inhibits Hh signaling with an IC_{50} of 4 nM and binds with high affinity to Smo (IC_{50} for BODIPY-Cyc displacement = 5 nM); however, further *in vitro* and *in vivo* characterization of these compounds have not been reported.

13

A collaborative effort from researchers of Novartis, Scripps Institute and Harvard University to screen 50K commercially available small molecules for their ability to inhibit Hh-Ag 1.5-induced luciferase expression in a stable TM3-Gli-Luc cell line identified ALLO-1 (**20**) and ALLO-2 (**21**) as potent inhibitors of Hh signaling (Figure 6) [72]. Both compounds exhibited submicromolar potency in a wide-range of *in vitro* Hh inhibition assays conducted in the TM3-Gli-Luc cells. As an example, IC_{50} values for ALLO-1 and ALLO-2 against Hh signaling induced by overexpression of wild-type Smo were 410 and 41 nM, respectively. In addition, only a modest two-fold reduction in activity against the mouse homologue of Smo D473H (D477G) overexpressed in TM3-Gli-Luc was seen for ALLO-1 (IC_{50} = 1 μM) and ALLO-2 (IC_{50} = 83 nM) compared to the 175-fold loss in potency demonstrated for KAAD-Cyc analogue [72]. Anti-proliferation assays in murine *Ptch1$^{+/-}$p53$^{-/-}$* MB cells overexpressing wild-type Smo or Smo D477G demonstrated GI_{50} values comparable to the IC_{50} values obtained in the Hh-dependent TM3 cell line. Mechanism of action studies suggested that these analogues occupy binding sites on Smo distinct from that of either the well-characterized Smo agonist SAG or Cyc. Finally, it is noteworthy that ALLO-2 is structurally similar to kinase inhibitors but didn't demonstrate significant inhibition of a 99-kinases panel even when tested at high concentrations (5 μM) [72].

Researchers at Oslo University identified MS-0022 (**22**, Figure 6) as an Hh pathway inhibitor via a screen of 12K compounds for their ability to prevent Hh-dependent differentiation of C3H10T1/2 cells [73]. MS-0022 demonstrated an IC_{50} of 100 nM against pathway signaling and modest anti-proliferative effects across several cancer cell lines including pancreatic adenocarcinoma, prostate carcinoma and melanoma. A decrease in tumor volume of 38% was reported following intraperitoneal (i.p.) administration of MS-0022 in a xenograft model of pancreatic adenocarcinoma (50

14

mg/kg, q.i.d.). Studies detailing the mechanism of action for this molecule suggested a dual Smo inhibition (IC_{50} = 259 nM for competitive displacement of BODIPY-Cyc) accompanied by micromolar activity against downstream components of the Hh signaling cascade. Further experiments are warranted to clarify the specific molecular effects of this compound [73].

Screening of the Novartis chemical compound collection resulted in the identification of LAB687 (**23a**, Figure 6) as a micromolar inhibitor of Hh signaling (IC_{50} 1.2 μM). Interestingly, this molecule had been originally synthesized as a nanomolar inhibitor (IC_{50} 0.9 nM) of microsomal triglyceride transfer protein (MTP). As SAR studies were carried out to prepare selective Hh antagonist based on this scaffold, two derivatives exhibiting nanomolar Hh inhibition and minimal MTP activity measured were generated. In a Gli-luciferase reporter gene assay in TM3 cells, IC_{50} values for LAB687 derivative 1 and LAB687 derivative 2 (**23b** and **23c**, Figure 6) were calculated to be 8 nM and 17nM respectively [74]. It is noteworthy that this class of ortho-bisphenyl carboxamide is closely related to clinical candidate NVP-LDE225 that represents the meta-bisphenyl carboxamide family of analogues.

uHTS screening of Wuxi's screening collection utilizing Shh-Light II cells amounted to the identification and development of 4-[3-(quinolin-2-yl)-1,2,4-oxadiazol-5-yl]piperazinyl urea class of analogues. Optimization of this class was performed through SAR study leading to improved derivatives Wuxi 91 and Wuxi 94 (**24a** and **24b**, Figure 6). Both analogues demonstrated IC_{50} values of 5 nM in Gli-dependent reporter gene assay conducted in Shh-Light II cells. Smo binding IC_{50} values for these derivatives when measured in presence of 2% FBS were determined to be 3 nM and 13 nM for Wuxi 91 and Wuxi 94 respectively. However, based on PK assessment of the potent

15

derivatives, Wuxi 94 was shown to possess better intrinsic clearance rate in rats and dogs [70].
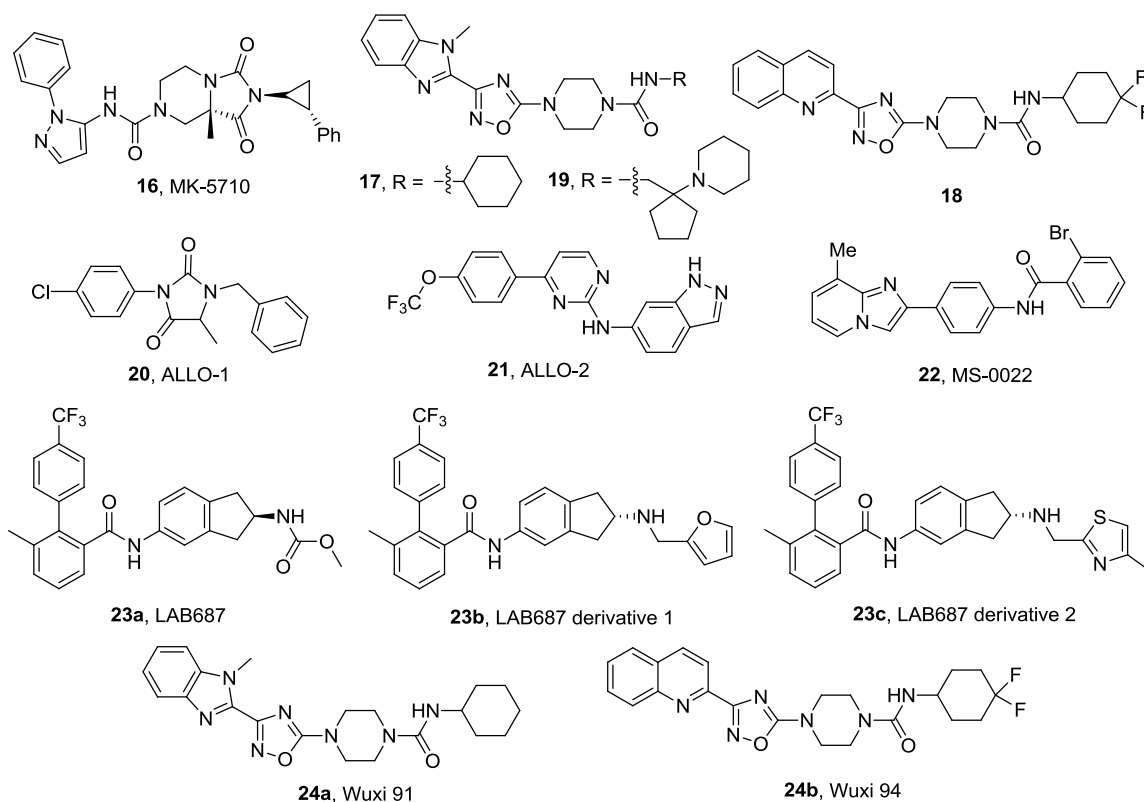
Figure 6. Structures of synthetic Smo antagonists in preclinical development.

A high content screen of FDA approved drugs, clinical candidates, and small molecules with known biological activity was conducted by researchers at Harvard University to identify compounds that inhibited Smo accumulation in the primary cilia [75]. This screen identified two small molecules, DY131 (**25**, Figure 7) and SMANT (**26**, Figure 7), as modest inhibitors of pathway signaling (IC_{50} values = 0.8 – 2 and 1.1 – 3 µM, respectively). DY131 was originally prepared as an Estrogen Related Receptor agonist, but within the context of Hh inhibition it was shown to function via direct binding to Smo at the GDC-0449/Cyc binding site (as measured by displacement of BODIPY-Cyc). In addition, inhibition of Hh signaling by DY131 was significantly reduced in the presence of a ligand-independent, oncogenic mutant of Smo (SmoM2). By contrast,

SMANT functionally inhibited Hh signaling induced by both wild-type Smo and SmoM2 at comparable concentrations and did not compete for Smo binding with Cyc, suggesting a novel mechanism of action for this scaffold [75].
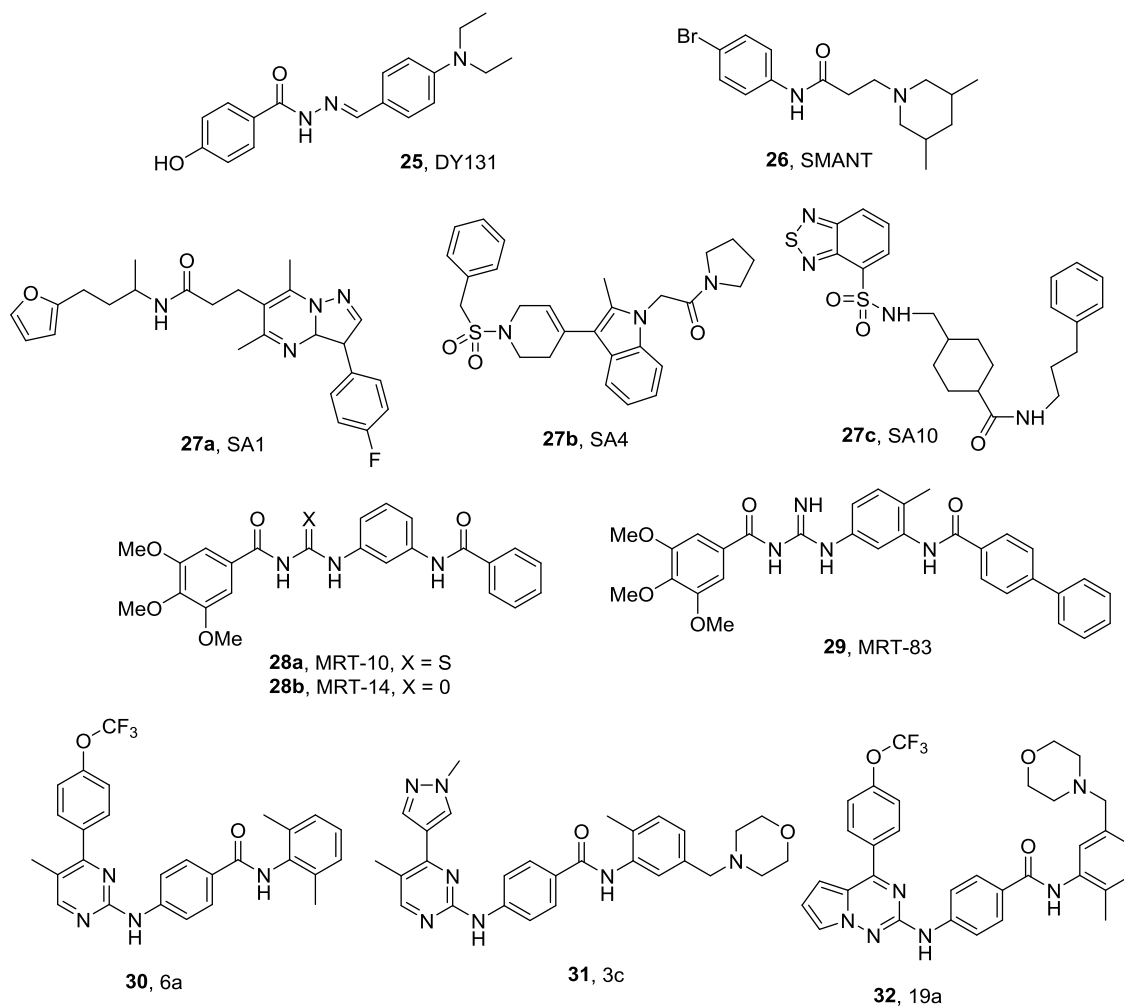
Figure 7. Structures of synthetic Smo antagonists in preclinical development.

A similar high-content screen designed by scientists at the University of California at San Francisco to select small molecules that inhibit Smo translocation to the cilia and/or ciliogenesis identified ten compounds including SA1 and SA4 (**27a** and **27b** respectively, Figure 7) as modest inhibitors of Hh signaling (IC_{50} value range 0.92 – 19 μM) that function via inhibition of Smo localization in the cilia [76]. All ten compounds reduced Gli1 mRNA expression in *Ptch*1[-/-] mouse embryonic fibroblasts (MEFs) and

BCC cells, but only compounds SA1-9 displaced BODIPY-Cyc from Smo, demonstrating that they function via direct binding to Smo. Nonetheless, although SA10 (**27c**, Figure 7) did not displace BODIPY-Cyc, it was inactive in $Sufu^{-/-}$ cells, indicating that it also functions at the level of Smo, albeit through an undefined mechanism. In addition, SA1-10 (25 µM) inhibited Hh signaling in the presence of the oncogenic SmoM2 construct. Finally, this screen also identified two other small molecules that inhibited ciliogenesis; however, neither of these compounds inhibited Hh signaling in cell culture [76].

Based on the knowledge that many of the Smo antagonists share structural features and bind in the same location on the receptor, a small molecule Smo antagonist pharmacophore was generated and used by a group at the Centre National de la Recherche Scientifique as the basis for a virtual screening effort to identify novel inhibitory scaffolds [77, 78]. Based on the screening results, the acylthiourea MRT-10 (**28a**, Figure 7) and its corresponding acylurea MRT-14 (**28b**, Figure 7) were synthesized and validated as Hh pathway inhibitors (IC_{50} values = 0.64 and 0.16 µM, respectively) [77]. In addition, both MRT-10 (IC_{50} = 0.5 µM) and MRT-14 (IC_{50} = 0.12 µM) displaced BODIPY-Cyc from Smo at concentrations that correlated well with their Hh inhibitory activity. Additional medicinal chemisty studies on this scaffold resulted in the identification of MRT-83 (**29**, Figure 7), which demonstrated an enhanced ability to inhibit Hh signaling (IC_{50} = 15 nM), prevent proliferation of cerebellar granule cell precursors (IC_{50} = 6 nM), and displace BODIPY-Cyc from Smo (IC_{50} = 5 nM) [78].

A fragment-based design approach was applied towards the discovery and development of novel *N*-(2-pyrimidinylamino) benzamide derivatives as potent inhibitors of Hh signaling by researchers at Jiangsu Pharmaceutical [79, 80]. Combining key structural features of Smo antagonists such as ALLO-2 and NVP-LDE225, lead compound 6a (**30**, Figure 7) was designed and synthesized [79]. Interestingly, this compound exhibited

18

greater potency (IC_{50} = 1.3 nM) as compared to NVP-LDE225 (IC_{50} 5.5 nM) and GDC-0449 (IC_{50} 7.2 nM) in Hh-dependent cells. Extensive SAR studies guided modifications to the terminal aromatic rings ultimately resulted analogue 3c (**31**, Figure 7), which demonstrated comparable potency (IC_{50} 1.3 nM) and improved permeability (AlogP 3.6) [80]. Continuing the search for improved leads based on this scaffold, an additional series of analogues incorporating a pyrrolotriazine isostere in lieu of the pyrimidine was prepared and evaluated. Many of the derivatives from this class demonstrated potent Hh inhibition (IC_{50} range 0.62 – 12.3 nM); most notably, compound 19a (**32**, Figure 7) not only exhibited potent anti-Hh activity (IC_{50} = 0.83 nM), but also superior *in vivo* plasma exposure and an increased half-life [81]. To date, additional *in vitro* assays or *in vivo* studies to assess Hh inhibitory efficacy and tumor regression have not been reported for these compounds.

Several sterol based Smo antagonists have also been recently identified by several different academic research groups [82-84]. The azasterol 22-NHC (**33**, Figure 8) inhibits Hh signaling with an IC_{50} of 3 μM and does not affect the interaction between Smo and other known Smo inhibitors acting on the TM region of Smo [82]. The synthetic glucocorticoids Budesonide (**34a**) and Ciclesonide (**34b**) were identified as pathway inhibitors through their ability to inhibit Smo ciliary accumulation (Figure 8) [83]. In a panel of *in vitro* assays, Budesonide demonstrated modest and comparable inhibition of pathway signaling against both wild-type and D473H Smo (IC_{50} values ~50 μM). The sterol-based Smo antagonists, 20(*R*)-yne (**35**) and 20-keto-yne (**36**), were identified as modest Hh pathway inhibitors with IC_{50} values of approximately 5 – 10 μM (Figure 8) [84]. In addition, both **35** and **36** inhibited Smo D477G-mediated pathway inhibition at levels comparable to their inhibition of wild-type Smo (~75% inhibition of signaling at 25 μM). Follow-up studies for these sterols have demonstrated that, in contrast to the Smo

antagonists described above, each of these function through direct binding to a newly identified binding site on the extracellular cysteine rich domain of Smo (CRD, described in more detail in Section 3.3 below).
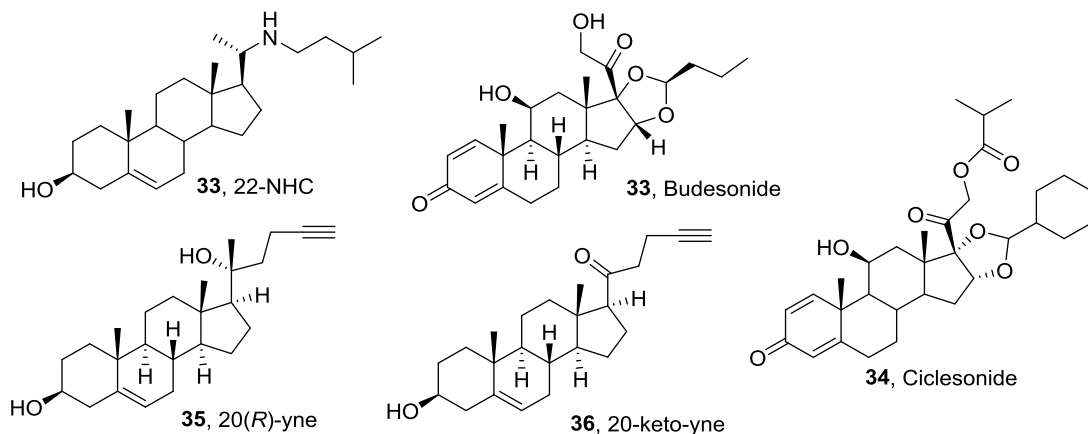
Figure 8. Sterol related Smo antagonists.

3.3 Identification and Mapping of Smo Binding Sites

Numerous groups have actively sought to probe several distinct small molecule binding sites on Smo in order to: (i) facilitate the rational design of future Smo antagonists; and (ii) better understand to what extent endogenous small molecules regulate pathway signaling via direct binding to Smo [82-88]. More detailed information on Smo binding sites could potentially mitigate the problem of drug resistance and permit combination therapy or allosteric modulation for improved potency. The first attempts to identify a small molecule binding region on Smo utilized photoaffinity labeling studies with an azide-I^{125} labeled Cyc analogue and deletion mutants of Smo to localize the Cyc binding pocket to the heptahelical bundle of Smo [46]. Since that time, a similar BODIPY-labeled Cyc analogue has been routinely utilized to demonstrate that multiple small molecule Smo antagonists and agonists bind in the same region as Cyc. Further information on the GDC-0449/Smo binding site came with the identification that the Smo D473H mutant resulted in the loss of both affinity and efficacy. Further evidence to

corroborate this binding site was achieved by mapping the location of D473 to the C-terminal end of transmembrane loop 6 on a rhodopsin-based molecular model of Smo [34]. Indeed, the Asp residue was found to occupy an extracellular site facing the central binding cavity of Smo. Interestingly, this position is a highly conserved region among Smo orthologs and Wnt signaling proteins that belong to the Frizzled family [87].

Table 1. Key Hh pathway inhibitors that function through direct inhibition of Smo.

Compound	IC_{50} wild-type Smo[a]	IC_{50} D473H/D477G[a]	Development Status	Reference
GDC-0449	3-22 nM	Loss of activity	Clinically Approved	41
IPI-926	7 nM	244 nM	Clinical (Phase II)	37, 50
NVP-LDE225	2.5 nM	Loss of activity	Clinical (Phase III)	43, 89
PF-04449913	5 nM	ND	Clinical (Phase II)	56
NVP-LEQ506	1 nM	96 nM	Clinical(Phase I)	59
TAK-0441	4.6 nM	79 nM	Clinical (discontinued)	61, 62
LY2940680	2.4 nM	Active[b]	Clinical (Phase II)	66
XL-139/BMS	21 nM	ND	Clinical (Phase II)	67
PF-5274857	2.7 nM	ND	Preclinical	57
MK-5710	17 nM	ND	Preclinical	69
19	5 nM	ND	Preclinical	71
ALLO-1	410 nM	1 μM	Preclinical	72
ALLO-2	41 nM	83 nM	Preclinical	72
MS-0022	100 nM	ND	Preclinical	73
LAB 687	1.2 μM	ND	Preclinical	74
23b	8 nM	ND	Preclinical	74
23c	17 nM	ND	Preclinical	74
Wuxi 91	5 nM	ND	Preclinical	70
Wuxi 94	5 nM	ND	Preclinical	70
DY 131	0.8-2 μM	ND	Preclinical	75
SMANT	1.1 – 3 μM	ND	Preclinical	75
MRT-83	15nM	ND	Preclinical	78
32	0.83 nM	ND	Preclinical	81
33	3 μM	ND	Preclinical	82
Budesonide	50 μM	50 μM	Preclinical	83
35	5-10 μM	~30 μM	Preclinical	84
36	5-10 μM	~30 μM	Preclinical	84

[a] Values assessed using different assay methods described in text
[b] Specific IC_{50} values were not provided
ND=not determined/ reported

More detailed structural information about the small-molecule binding site(s) on the 7TM domain region of Smo has come from two recently published co-crystal

21

structures describing this region in complex with either LY2940680 [87] or Cyc [88]. A lipidic mesophase method was utilized to solve a co-crystal structure of an engineered human Smo receptor in complex with LY2940680 to 2.5 Å (Protein Data Bank ID 4JKV) [87]. The overall structure of Smo is characterized by an elaborate arrangement of long extracellular loops that are stabilized by four disulfide bonds and within this context, the binding pocket of LY2940680 is at the extracellular end of the 7TM helical structure and is linked to the extracellular environment by a small opening characterized by the extracellular domain and extracellular loops 2 and 3. Two water molecules form a structured hydrogen-bonding network between R400, H470, D473, E518, and N521 that help define the binding pocket; however, they do not make direct interactions with LY2940680. Key hydrogen-bonding interactions occur between the guanidinium of R400 and the phthalazine nitrogens and between the carboxamide of N219 and the carbonyl oxygen. Direct contact between LY2940680 and D473 is minimal (4.04 – 4.31 Å between the aspartic acid carboxylate and the Smo antagonist) and these limited interactions help to explain how the compound retains potent activity in the presence of Smo D473H (Figure 9). More recently, a lipidic cubic phase method was utilized to solve the co-crystal structure of Cyc in complex with the same engineered human Smo receptor (3.2-4.0 Å) [88]. The Cyc binding region was localized to the same vicinity as LY2940680; however, the low resolution of the complex prevented the definitive identification of the Cyc orientation within the binding pocket. The authors provide evidence that the pyridine ring is positioned towards the solvent exposed extracellular space of the binding region, but further refinement is necessary to conclusively identify the binding site and key molecular interactions between Cyc and Smo.

In addition to small molecule binding sites within the 7TM domain of Smo, several independent research groups have explored the ability of Hh pathway

22

modulators to exert their activity through direct binding interactions with the extracellular cysteine rich domain (SmoCRD) [82-86]. These studies have all focused on exploring the role of the SmoCRD in binding Hh agonists and antagonists with a sterol or sterol-like scaffold. Initial assays utilizing Smo deletion and/or ligand affinity protocols demonstrated that the Hh agonist properties of oxysterols (OHCs) are mediated through direct binding to the SmoCRD and that small molecules that bind in this location can be agonists or antagonists, depending on structure [82-85]. In addition, these experiments provided strong evidence that the OHC binding site is localized to "site 1" of the CRD, a hydrophobic pocket formed by side chain α-helices that is analogous to the lipid-binding grove previously identified in the Frizzled CRD. Two recent reports have provided additional detailed structural insights into this small molecule binding site via the crystal structure of the zebrafish SmoCRD (zSmoCRD, 2.3 Å resolution) [84] and the NMR solution structure of the *Drosophila* SmoCRD (dSmoCRD) [86]. Molecular docking studies between zSmoCRD and 20(*S*)-OHC, a well-characterized pathway agonist, suggested the tetracyclic core of the OHC scaffold lies in the base of the lipid-binding groove at site 1 lined by W87 and L90. This docking model predicts that the 3β-hydroxy of 20(*S*)-OHC orients towards helix 1 residues L90 and N92, while the 20(*S*)-hydroxy and side chain are in close proximity to residues P142 and F144 [84]. Mutagenesis studies on residues within the predicted binding site supported the structure-based model of the OHC binding pocket; however, specific molecular interactions between the OHC scaffold and these residues have not been detailed [84]. The solution structure of Budesonide in complex with dSmoCRD further supports the site 1 lipid-binding groove as the key binding pocket for sterol-based pathway modulators of Hh signaling within the CRD [86]. Chemical shift perturbations identified potential binding interactions between budesonide and R161, W109, G111, and L112, all of which reside within site 1 and were previously identified as key for 20(*S*)-OHC binding.

23
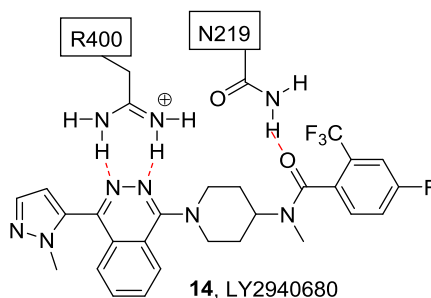
Figure 9. Key binding site interactions between Smo and LY2940680.

4. Small Molecule Non-Smo Antagonists

4.1 Compounds Acting Upstream of Smo

Maturation of a fully active Hh ligand results from a series of post-translational modifications of the secreted protein, including the covalent attachment of a palmitoyl moiety at the N-terminus [90]. For this modification, hedgehog acyltransferase (Hhat) catalyzes the attachment of a palmitoyl group to the N-terminal cysteine of SHh through an amide bond. A high-throughput screen (~64K compounds) was conducted to identify small molecules that inhibit Hhat-mediated SHh palmitoylation [91]. Secondary analysis of the hit compounds to identify potent inhibitors with promising drug-like properties identified four structurally-related thiophene piperidines with IC_{50} values ranging between 0.2-5μM. One compound RU-SKI 43 (**37**, Figure 10) with an IC_{50} of 0.85 μM was chosen for further evaluation as a Hhat inhibitor. It was a noncompetitive inhibitor ($K_i = 6.9$ μM) with respect to [I^{125}] iodo-palmitoyl CoA and an uncompetitive inhibitor with respect to SHh; moreover, inhibition by RU-SKI 43 was selective to Hhat and not a broad activity against other fatty acyltransferases. Finally, several cellular assays demonstrated that the Hh inhibitory activity of RU-SKI 43 is mediated at the level of SHh [91].

Several macrolactones that inhibit Hh signaling through direct binding to SHh were identified in a microarray-based screen (10K compounds) by researchers at the Broad Institute [92]. Optimization of the lead scaffold led to robotnikinin (**38**, Figure 10),

24

which bound to SHhN (an active N-terminal fragment of SHh) with a K_d value of 3.1 μM as determined via surface plasmon resonance. Binding to Hh ligand is thought to induce conformational changes in the protein preventing its interaction with Ptch and repressing SHh-mediated Gli overexpression. When tested in a Gli-luciferase reporter gene assay in Hh-dependent cells, it inhibited Hh signaling with an IC_{50} of 4 μM [92]. Further SAR studies on the macrolactone scaffold produced a series of analogues including BRD6851 (**39**, Figure 10), as an Hh inhibitor with improved activity (IC_{50} = 0.4 μM) [93]. Interestingly, cellular studies into the mechanism of BRD6851 suggested it functions at the level of Smo; however, these studies were indirect and displacement of a known small molecule Smo antagonist by BRD6851 has not been demonstrated. To date, *in vivo* data in Hh-dependent models of cancer have not been reported.

37, RU-SKI 43   **38**, Robotnikinin   **39**, BRD 6851

40, GK 03795   **41**, BAS 13382537   **42**, BAS 06350510
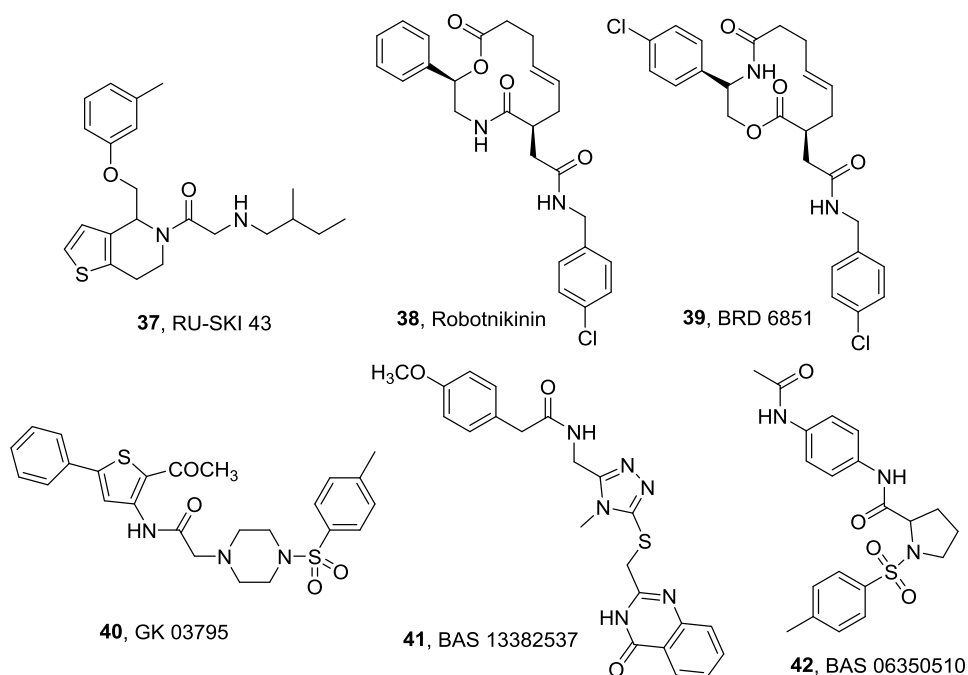
Figure 10. Structures of inhibitors upstream of Smo.

Computational approaches to design small molecules that perturb SHh/Ptch binding interactions have been undertaken at Gyeongsang National University in Korea [94, 95]. First, robotnikin and related analogues were used to develop a 3D-pharmacophore

25

model that was used in a virtual screening of >100K to identify structurally-related small molecules as possible Hh pathway inhibitors [94]. This screen and follow-up modeling studies suggested that GK 03795 (**40**, Figure 10) should bind SHh in the same location as robotnikin. A second virtual screen of >200K utilizing a computational model of key SHh/Ptch binding interactions was performed to identify small molecules that disrupt this specific interaction. Additional docking and computational analysis of two hit compounds, BAS 13382637 (**41**) and BAS 06350510 (**42**), suggest their potential to bind SHh with high affinity (Figure 10) [95]. To date, experimental verification of these simulation results in *in vitro* or *in vivo* assays has not been reported.

4.2 Compounds Acting Downstream of Smo

Two small molecules, GANT-58 & GANT-61 (**43** & **44,** Figure 11), were identified as inhibitors of Gli-mediated transcription through a screen in HEK293 cells overexpressing Gli1 by researchers at the Karolinska Institutet [96]. Both compounds inhibited Hh signaling and Gli expression with an IC_{50} value of approximately 5μM [96]. Their ability to maintain potent Hh antagonism in Sufu$^{-/-}$ cells verified that these agents act downstream of Smo. Interestingly, GANT-61 was shown to disrupt Gli1 DNA binding in live cells. Selectivity for Hh-mediated Gli expression was corroborated using a microarray analysis in which neither analogue was active against several unrelated signaling pathways. In addition, both compounds prevented the formation of dominant-active Smo transfected NIH3T3 colonies in soft agar. Finally, tumor growth regression and significant decrease in Ptch mRNA level were observed upon treating a mouse xenograft model of human prostate cancer with GANT-61 (s.c., 2.5 mg/kg, once daily dosing for 18 days) [96].

Studies demonstrating interactions between Gli proteins and the transcriptional coactivator TBP-associated factor 9 (TAF9) prompted the design of a small molecule,

26

FN1-8 (**45**, Figure 11), which prevents Gli/TAF9 interactions and down-regulates Gli expression [97]. The structure of this compound developed by researchers at the University of California at San Francisco was derived as a mimic of the common α-helical 'FXXϕϕ' motif contained in many Gli proteins. FN1-8 (15 µM) prevented TAF9 from binding both Gli1 and Gli2 *in vitro* and led to significant reductions in Gli transcriptional activity [97]. FN1-8 (7.5 or 15 µM) prevented proliferation of non-small cell lung cancer cells (NSCLC) that over-express either Gli1 or Gli2 and its anti-proliferative effect correlated well with down-regulation of endogenous Ptch and Gli1 mRNA. Finally, FN1-8 down-regulated Ptch and Gli1 mRNA and reduced tumor volume in NSCLC xenografts (50 mg/kg, sc) [97]. Subsequent modifications to FN1-8 carried out at St. Jude Children's Research Hospital afforded a modest inhibitor of Gli1 transcription factors known as NMDA298-1 (**46**, Figure 11). Extensive SAR for the scaffold demonstrated that the tyramine amide region of this chiral molecule is essential for its biological activity. NMDA298-1 activity was selective for Gli1 compared to Gli2 in Hh-dependent cell culture (IC_{50} values = 6.9 and ~23.9 µM, respectively). Additional viability studies in cancer cells (breast, MB, prostate cancer, Burkitt's lymphoma, hepatocarcinoma, glioma) versus healthy cells (human skin fibroblasts) established that NMDA298-1 selectively targets tumor cells [98].

Historically, arsenicals have been known for their toxicological effects during embryogenesis; however, arsenic trioxide (ATO) has had pharmacological use in the clinic as a curative agent for acute promyelocytic leukemia [99]. Based on these seeming contradictions, the role of several arsenicals in inhibiting Hh signaling was evaluated by researchers at the Stanford University School of Medicine. Three arsenicals (sodium arsenite, ATO, phenylarsine oxide) and the most active, ATO, inhibited pathway activity in an Hh-dependent cell model with an IC_{50} value of 0.7 µM [100]. In murine allografts of

Hh-dependent MB, ATO inhibited tumor growth in a dose-dependent fashion following IP administration (2.5 – 10 mg/kg). In addition, ATO inhibited Smo D477G-mediated Hh signaling at a level comparable to that for wild-type Smo (IC_{50} = ~0.8 μM). ATO as a monotherapy and in combination with other Hh pathway inhibitors has demonstrated potent anti-Hh and anti-tumor effects in a variety of *in vivo* models of Hh dependent cancer [100-102]. Most notably, ATO increased survival in an orthotopic model of MB driven by Smo D477G (IP administration, 7.5 mg/kg, OD) [101]. Mechanistic studies on the target of ATO within the Hh pathway have demonstrated that it directly binds to Gli1, reducing its transcriptional activity and decreasing expression of Gli target genes [100, 102].
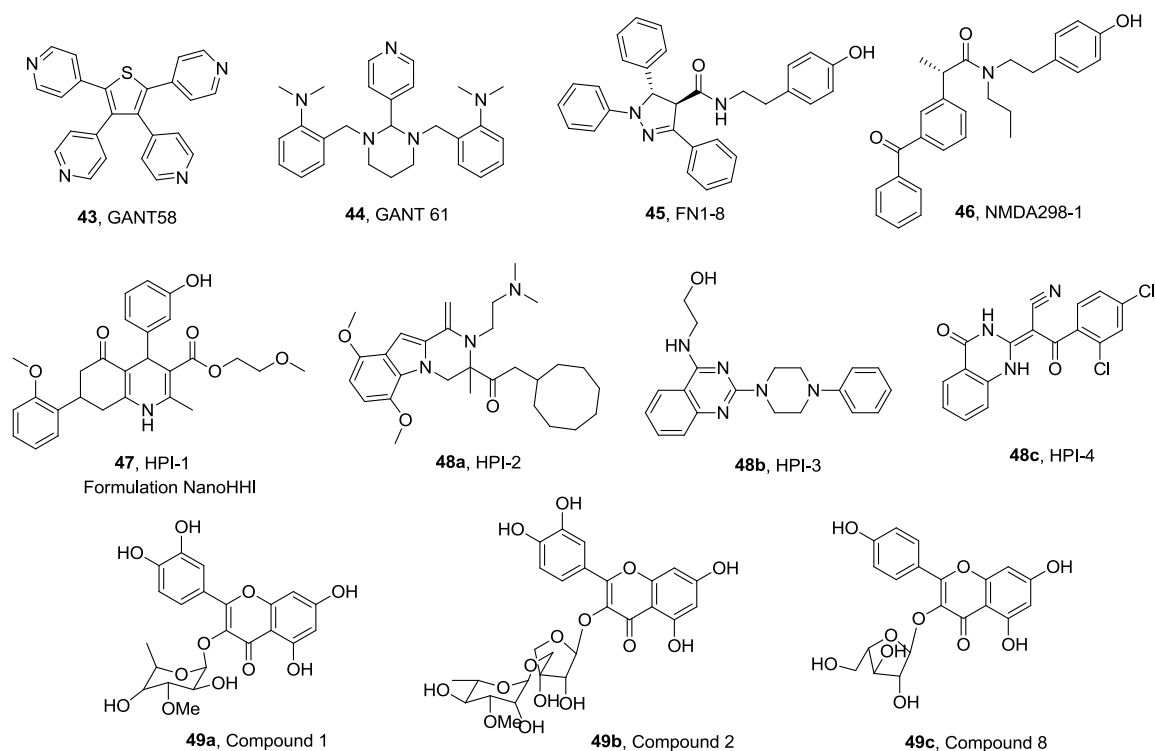
Figure 11. Synthetic Hh pathway inhibitors that target downstream of Smo.

The pathway inhibitors HPI-1 through HPI-4 (**47**, **48a-c**, Figure 11) were identified at the Stanford University through a screen of >100K compounds specifically for their ability to interfere with Hh signaling downstream of Smo [103]. Each of these

compounds demonstrated modest inhibition of Hh signaling with an IC_{50} value range of 1.5 - 7 µM. In addition, these compounds demonstrated selectivity for Hh signaling over Wnt, PKA and PI3K/MAPK signaling. Interestingly, while each HPI was able to inhibit pathway activity in the presence of the SmoM2 mutant, only HPI-1 and HPI-4 prevented SmoM2-dependent proliferation of cerebellar granule neuron precursors. The HPIs are structurally dissimilar and antagonize the hyperactive signal transduction through varied subcellular mechanisms even though they all target components downstream of Smo. The central theme underlying their inhibitory activity is disturbing the processing, trafficking and stability of Gli transcription factors [103]. In order to enhance the solubility and bioavailability profile of HPI-1, researchers at the Johns Hopkins University formulated it as a polymeric nanoparticle with poly(lactic-co-glycolic acid) conjugated to polyethylene glycol (PLGA-PEG) to provide NanoHHI [104]. In contrast to HPI-1, NanoHHI formed a uniform suspension in aqueous media, was orally bioavailable, and crossed the blood-brain barrier [104]. NanoHHI reduced tumor volume in orthotopic models of MB driven by either wild-type Smo or Smo D477G (IP administration, 30 mg/kg, b.i.d) [104]. In addition, NanoHHI inhibited *in vitro* proliferation and *in vivo* tumor growth and metastasis of hepatocellular carcinoma [105].

Naturally occurring flavonoid glycosides from *Excoecaria agallocha* leaves inhibit the Hh signal transduction by abrogating Gli1 translocation to the nucleus. Researchers at Chiba University reported that compounds 1, 2 and 8 (**49a-c**, Figure 11) antagonize Gli mediated transcriptional activity with IC_{50} values of 0.5, 19.1 and 2.0 µM respectively. In addition, these compounds exhibit selective cytotoxicity against human pancreatic cancer cells (PANC1) and human prostate cancer cells (DU145) at low micromolar concentrations. Further investigation revealed that compound 1 inhibited the expression of Hh proteins (Ptch and BCL-2) and blocked nuclear translocation of Gli1 in PANC1

cells in a dose dependent fashion. Further, experiments with siRNA mediated knockdown of Smo confirmed that Gli1 inhibition is brought about independently of Smo interference [106].

4.3 Compounds With Unknown/Undisclosed Target or Indirect Mechanism

Several members of the vitamin D class of secosteroids have also been identified as modulators of Hh pathway signaling. Vitamin D3 or VD3 (**50**, Figure 12), a metabolic precursor to the hormonally active form of vitamin D known as calcitriol, was first identified as a pathway inhibitor in studies conducted to identify physiological small molecules that control Ptch-mediated inhibition of Smo [107]. VD3 inhibition of Hh signaling *in vitro* is modest, with IC_{50} values reported between 1 and 20 µM [107-111]. VD3 has demonstrated the ability to significantly reduce *in vitro* proliferation of Hh-dependent BCC cell lines and reduce *in vivo* Gli expression in mouse models of BCC [110]. Interestingly, while VD3 inhibited the growth of pancreatic cancer cells, it failed to have an anti-tumor effect in a comparable xenograft model of pancreatic adenocarcinoma [109]. Initial studies into the mechanism of action for VD3-mediated Hh inhibition suggested that this activity was at the level of Smo; however, it has also been shown that VD3 can activate canonical vitamin D receptor (VDR) signaling in these same model systems [108-110]. Calcitriol (**51**, Figure 12), generally acknowledged as the physiologically active form of vitamin D, has also demonstrated the ability to inhibit Hh signaling *in vitro* and *in vivo* in Hh-dependent models of BCC and RMS. Similar to VD3, calcitriol appears to inhibit Hh signaling at the level of Smo, while also activating the canonical VDR pathway in these models. Taken together with the additional recent data suggesting complicated crosstalk between Hh and VDR signaling (reviewed in a previous publication [112]), further explorations into the biological activities of these secosteroids is warranted to more clearly define the mechanisms that govern their pathway modulation.

30

A medicinal chemistry approach undertaken at the University of Connecticut to design analogues of VD3 that selectively target Hh signaling demonstrated that the 'northern' region of VD3, also known as Grundmann's alcohol (**52**, Figure 12), retains ~90% of the Hh inhibitory activity of the parent scaffold (IC_{50} values = 3.1 and 4.1 µM, respectively) [111, 113]. A subsequent series of VD3 analogues designed to incorporate an aromatic A-ring isostere that maintains the approximate steric and hydrophobic features of the natural aliphatic A-ring into the secosteroid scaffold identified compound **53** (Figure 12) as a selective Hh inhibitor with improved potency (IC_{50} = 0.74 µM) [113, 114].

50, VD$_3$; $R_1 = R_2 = H$
51, Calcitriol; $R_1 = R_2 = OH$

52, Grundmann's alcohol

53

54, Desmethylveramiline

55, Itraconazole

56, R = H; BRD50837
57, R = Cl; BRD9526
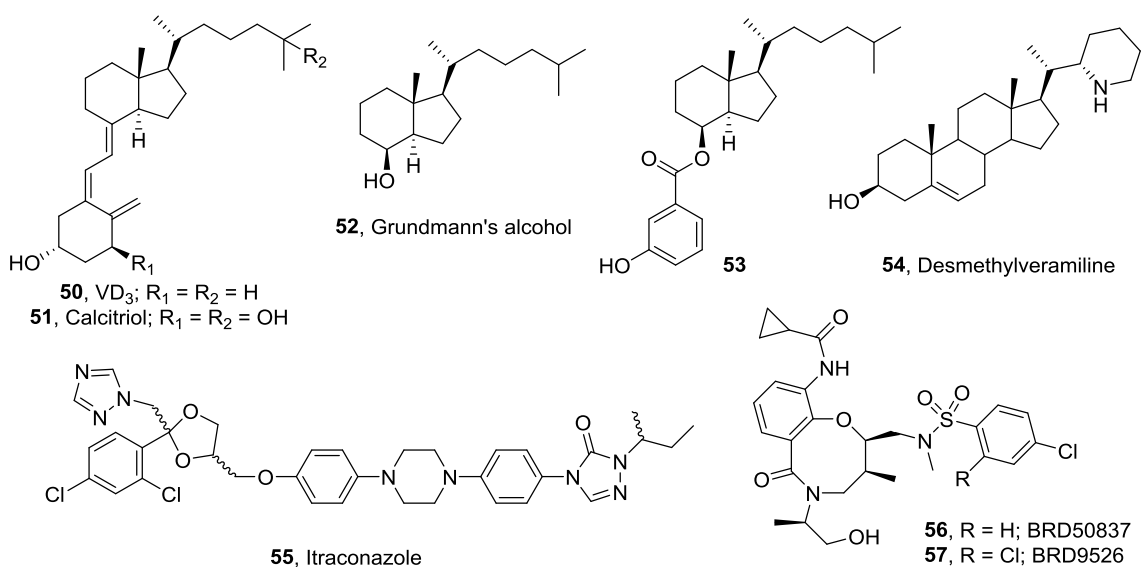
Figure 12. Compounds with indirect/unknown/undisclosed mechanism(s).

Desmethylveramiline (**54**, Figure 12), a semi-synthetic compound, belongs to the steroidal family of Hh inhibitors and shares structural features with Cyc. A seven step derivatization of teratogenic alkaloid veramiline was reported by researchers at University of Strasbourg. Using relatively straightforward synthetic manipulation of commercially available starting material, Fernholtz acid, preparation of this analogue was accomplished with the intention to mimic the complex spatial structure of Cyc [115]. At 10 µM, it inhibited ShhN-induced luciferase activity in Shh-Light II cells and SAG-induced

differentiation of C3H10T1/2 cells by 87 ± 1% and 85 ± 4% respectively. However, the specific molecular target of this micromolar inhibitor remains undetermined to date.

A screen of FDA approved drugs identified the clinically efficacious antimycotic drug itraconazole (ITZ, **55**, Figure 12) as a potent pathway inhibitor *in vitro* (IC_{50} values = 270 – 690 nM, depending on cellular context) [116]. ITZ also inhibits pathway signaling mediated by Smo D477G at a level comparable to its inhibition of wild-type Smo (IC_{50} ~500 nM) [101]. Treatment with ITZ significantly decreased tumor volume and increased survival in Smo D477G MB allografts. In addition, oral administration of ITZ (75 mg/kg, b.i.d) significantly increased survival in an orthotopic model of MB expressing SmoD477G, highlighting the ability of ITZ to be centrally active against intracranial tumors. Similar activities for ITZ in Hh-dependent BCCs have also been described [101, 116]. Studies have demonstrated that the Hh inhibitory activity of ITZ is unrelated to inhibition of 14-α-lanosterol demethylase, the physiological target responsible for its anti-fungal properties. Further investigations have suggested that it inhibits at the level of Smo; however, direct binding interactions or displacement of a known Smo antagonist have not been identified. The results of a Phase II trial into the anti-BCC effects of oral ITZ demonstrated positive results and the authors note further clinical trials are in the planning process [117]. It should be noted that ITZ was also recently identified as an inhibitor of angiogenesis, suggesting its potential application as an anti-cancer therapeutic via multiple distinct mechanisms of action [118, 119]. A single publication detailing Hh inhibitory activity for ITZ analogues with modified alkyl side chains has been reported [120]. These studies demonstrated while small aliphatic groups were well-tolerated, bulky functional groups in this region completely abolished inhibitory activity.

A recent screen of approximately 20K small molecules followed by SAR studies on the hit scaffold conducted at the Broad Institute of MIT and Harvard University

32

identified a series of small molecules that incorporate a central eight-membered heterocycle as inhibitors of pathway signaling [121]. The most potent compounds that also demonstrated promising drug-like solubility, BRD50837 and BRD9526 (**56** and **57**, Figure 12), were chosen for additional studies to probe the mechanism of action of this scaffold (IC_{50} values = 90 and 60 nm, respectively). Neither compound displaced BODIPY-Cyc from Smo, suggesting they did not bind in the known Smo binding pocket. Interestingly, while neither compound inhibited pathway signaling in Ptch$^{-/-}$ cells, they retained partial activity in SuFu-/- cells, a seemingly contradictory result [121]. It is clear that further studies are warranted to understand the cellular mechanisms that govern the Hh inhibitory activity of this scaffold.

Researchers at Novartis recently combined a high-throughput screening effort with additional *in vitro* assays to identify novel small molecule modulators of Hh signaling [122]. Their overall goal was to identify 'non-Smo' inhibitors that could then be utilized as chemical probes to identify new drug targets within the pathway. The ultimate result of these studies was the identification of the cyclohexyl-methyl aminopyrimidine (CMAP) scaffold represented by **58**, **59**, and **60** (Figure 13) as inhibitors of Gli-mediated transcription that function via agonism of the orphan GPCR GPR39. These three compounds potently inhibited Hh signaling (as measured by down-regulation of a Gli luciferase reporter) with low nanomolar potency (IC_{50} values = 4 -10 nM) [122]. Follow-up studies with these compounds demonstrated that GPR39 was required for their anti-Hh activity and it was hypothesized that activation of GPR39 stimulates multiple signaling pathways to activate MAPK, which directly inhibits the transcriptional activity of Gli proteins [122].

Researchers at Chiba University reported three naturally occurring molecules namely colubrinic acid, betulinic acid and alphitolic acid (**61**, **62** and **63**, Figure 13) found

in pentacyclic triterpenoids of *Zizyphus cambodiana* to exhibit Hh inhibitory activity [123]. These compounds inhibit Gli1 expression with micromolar IC_{50} values (38-42 µM) and also exert cytotoxic effects on pancreatic and prostate cancer cells. On the contrary, they are relatively non-lethal towards non-cancerous cells such as MEFs. Interestingly, inhibition of Hh signaling by betulinic acid in rhabdomyosarcoma cells is accompanied by induction of apoptosis [123, 124]. This pharmacological effect could be due to its role in activation of the Mitogen Activated Protein Kinase (MAPK) pathway as established earlier in human melanoma cells [125]. Nonetheless, antagonism of Hh signaling was confirmed by documenting reduction of Hh target genes such as Gli1, Gli2, Ptch1 and IGF2 in a rhabdomyosarcoma cell line with otherwise increased Hh pathway activity.

Structurally distinct compounds GW3965 and TO-901317 (**64** and **65**, Figure 13) are liver X receptor (LXR) agonists that indirectly antagonize the Hh signaling [126]. Researchers at University of California Los Angeles recorded a dose-dependent and time-dependent inhibition of Hh responsive genes (Ptch1, Gli1) following treatment in MEF M210B4 cell line. Using qRT-PCR, greater than 50% inhibition of Ptch1 and Gli1 expression was observed upon treatment with 2 µM TO-901317. Further, gene silencing experiments confirmed that abolition of LXR activity significantly affected the resultant Hh modulation. In addition to the *in vitro* activity, reduction of Hh responsive genes by TO-901317 was observed in *ex vivo* as well as *in vivo* mouse organ cultures. It is hypothesized that the pharmacological activity of cholesterol depletion due to LXR activation potentially perturbs the post-translational modification of Hh proteins and thereby leads to Hh pathway inhibition by TO-901317.

Another interesting small molecule, norcantharidin (**66**, Figure 13), was developed by researchers in Taiwan as a synthetic derivative of naturally occurring molecule, cantharidin. Previously, this compound was known to inhibit drug effux pump

34

protein, P-gp, making it useful against multidrug resistance [127]. More recently, it was reported to cause reversal of multidrug resistance in human breast cancer cells accompanied by downregulation of Shh protein and perturbation of Gli1 nuclear translocation at 10 μM concentration [128]. In accordance with its effect on P-gp, concomitant treatment of norcantharidin with Doxorubicine (DOX) also improved intracellular accumulation of the latter in MCF7 cells resistant to DOX from 30% to 80%. Other noteworthy pharmacological effects of norcantharidin include inhibition of tumor angiogenesis by blockade of VEGFR2/MEK/ERK signaling pathways [129].

58, R_1 = NH(CH$_2$)$_2$OMe; R_2 = 4-F
59, R_1 = NHMe; R_2 = 3-CN
60, R_1 = NH(CH$_2$)$_5$NHAc; R_2 = 3-CN

61, Colubrinic Acid

62, Betulinic Acid

63, Alphitolic Acid

64, GW-3965

65, TO-901317

66, Norcantharidin

67, JK-184
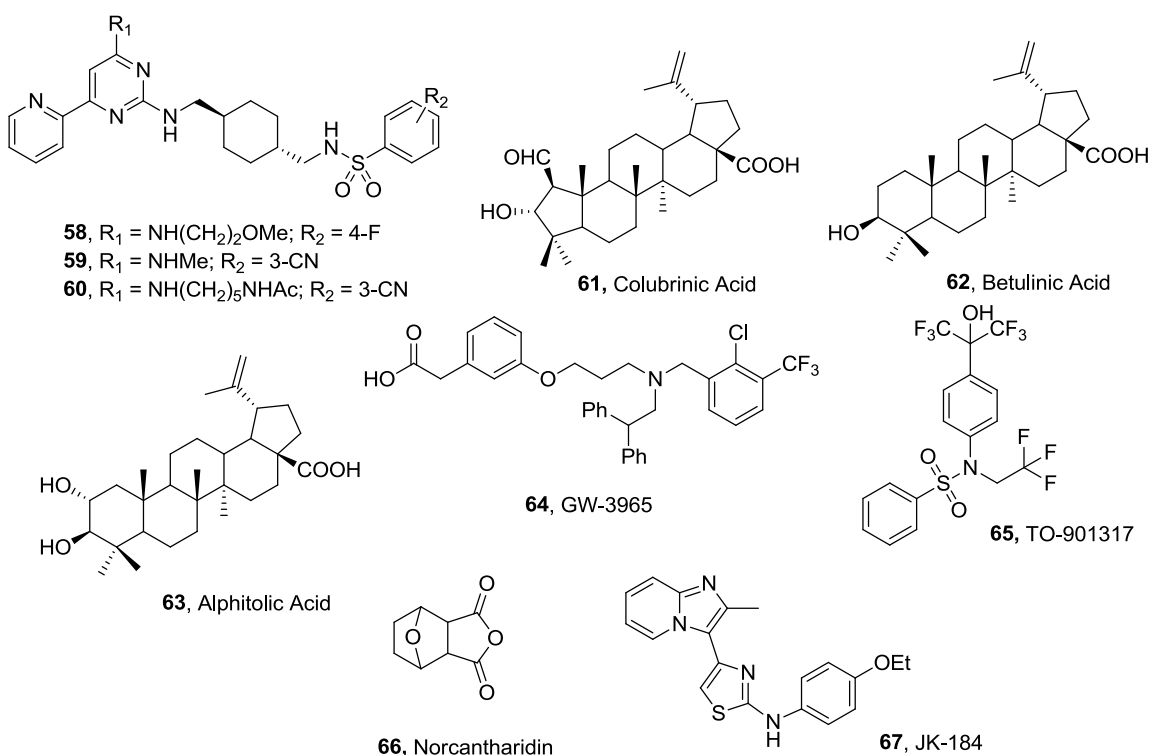
Figure 13. Compounds with indirect/unknown/undisclosed mechanism(s).

A class of compounds with 2, 4 substituted thiazole was identified in a screen of 20,000 heterocycles by researchers at The Scripps Research Institute. Within this class, JK-184 (**67**, Figure 13) proved to be nanomolar inhibitor of Gli1 (IC$_{50}$ 30 nM) as determined in a Gli dependent luciferase assay. A SAR analysis of this core led to optimization of the parent scaffold and guided the discovery of other improved

antagonists that have been patented. JK-184 exerts potent antiproliferative effects in a panel of cell lines (IC_{50} values between 3 nM and 21 nM). Preliminary, mechanistic characterization suggested that it antagonizes Hh signaling at the level of Gli. Additionally, Hh downregulatory effect of this compound is mediated indirectly by inhibition of class IV alcohol dehydrogenase 7 [Adh 7] (Kd = 348 nM) [130]. Further probing revealed other biological effects mediated by this compound such as microtubule destabilization to serve as alternate mechanism of action explaining the nanomolar anti-proliferation potency [131].

Table 2. Key 'non-Smo' Hh pathway inhibitors.

Cmpd	IC_{50} wild-type Smo[a]	IC_{50} D473H/D477G[a]	Development Status	Reference
Robotnikinin	4 µM	ND	Preclinical	92
BRD 6851	0.4 µM	ND	Preclinical	93
RU-SKI 43	0.85 µM	ND	Preclinical	91
GANT-61	5 µM	ND	Preclinical	96
NMDA298-1	6.9 µM	ND	Preclinical	98
ATO	0.7 µM	~0.8 µM	Preclinical	100, 101
HPI-1	1.5 µM	ND	Preclinical	103
NanoHHI	active[b]	Active[b]	Preclinical	104
49a-c	0.5, 19.1, 2 µM		Preclinical	106
VD3	1-20 µM	ND	Preclinical	107-110
53	0.74 µM	ND	Preclinical	113
Calcitriol	0.1 µM	ND	Preclinical	108
ITZ	0.27-0.69 µM	0.5 µM	Phase II	101,116, 117
58	4 nM	ND	Preclinical	122
61-63	38-42 µM	NND	Preclinical	123
BRD50837	90 nM	ND	Preclinical	121
BRD9526	60 nM	ND	Preclinical	121
JK 184	30 nM	ND	Preclinical	130

[a] Values assessed using different assay methods described in text
[b] Specific IC_{50} values were not provided

5. Biologics as Hh Pathway Inhibitors

In addition to the small molecule Hh pathway inhibitors described above, several protein-based Hh pathway inhibitors have been described. The best characterized of these is 5E1, which was initially generated by scientists at Genentech through mouse

36

hybridoma technology utilizing the N-terminus of rat SHh as the antigen [132]. 5E1 inhibits pathway signaling by preventing Hh ligands from interacting with Ptch through direct binding interactions with the pseudo active site groove of the Hh ligand [133]. 5E1 binds with high affinity to human SHh and IHh (K_D value ranges = 0.13 – 0.31 and 0.16 – 0.29 nM, respectively) [133, 134]. 5E1 also binds to DHh, although at a reduced affinity (K_D = 1.7 nM) [133]. The reduced affinity for DHh is likely due to the increased bulk associated with Asn179 compared to Ala179 found in the binding epitope of SHh [133]. 5E1 is a potent inhibitor of Hh signaling in multiple Hh-dependent fibroblast cell lines (IC_{50} values = 0.33 – 12.5 nM) [133, 134]. 5E1 has also demonstrated the ability to inhibit pathway signaling and decrease tumor volume in colorectal xenografts [12], orthotopic and xenograft models of pancreatic cancer [135, 136], and medulloblastoma [137], but it has not advanced beyond these preclinical studies.

A more recent report by researchers at AstraZeneca detailed the development of a series of human monoclonal antibodies against SHh as potent pathway inhibitors [134, 138]. Xeno-Mouse mice were immunized against human SHh using both recombinant human SHh and KLH-conjugated SHh. Two of the antibodies generated through this process, 3H8 and 6D7, were extensively characterized for their SHh-binding and *in vitro* anti-Hh and anti-cancer activity. Interestingly, while both antibodies bound with high affinity to human SHh (K_d values = 36 and 5 pM, respectively) only 6D7 bound IHh (K_d = 34 pM) and neither bound DHh [134]. Both antibodies inhibited pathway signaling in Hh-dependent cell culture (C3H10T1/2) in the low nanomolar range (IC_{50} values = 3.4 nM and 5.3 nM, respectively) [138]. Due to its broader substrate specificity, 6D7 was renamed MEDI-5304 and further evaluated for its *in vivo* anti-cancer effects in a compliant model (HT-29 human cancer cells and MEFs) of colorectal cancer that mimics paracrine Hh signaling [134]. MEDI-5304 decreased Hh signaling and tumor volume in this model in a

37

dose-dependent fashion (0.1-10 mg/kg); however, the overall reduction in Hh pathway target gene expression and tumor growth was modest (~30-50% reduction) [134, 138]. In addition, preliminary toxicology studies in rats and cynomolgus monkeys did not identify adverse effects up to 75 mg/kg.

6. Conclusion & future directions

Hh signaling pathway inhibitors are being developed in both academia and industry as potential anti-cancer chemotherapeutics. Thus far, pathway inhibitors have demonstrated clinical efficacy against cancers in which a specific pathway mutation is responsible for tumor formation. However, broader applications against other forms of cancer are yet to be fully explored. The initial development of Hh pathway inhibitors focused mainly on small molecules antagonists of Smo. In fact, the only pathway inhibitor approved by the FDA, Vismodegib, also acts by targeting Smo. Unfortunately, multiple mechanisms of resistance to Smo inhibitors have been reported in the recent years. Therefore, there is an urgent need to identify and develop novel inhibitors of pathway signaling that retain activity against resistant forms of Hh driven tumors. Guided by the current progress towards better understanding of structural and functional requirements of active molecules, researchers may adopt different strategies to address this issue. For instance, several research groups are working to develop pathway inhibitors that function downstream of Smo and retain activity against drug resistant Smo mutations. Further, the latest characterization of multiple small molecule binding sites on Smo can be exploited in the structure-based design of improved Smo antagonists. Nonetheless, to present date, advancement of such newer inhibitors beyond preclinical and early clinical trials has been nominal. Therefore, there is an immense need for continued research in this area.

The following chapters describe the progress towards the identification of novel small molecule inhibitors of the Hh signaling pathway using a chemical biology-dependent drug discovery strategy. Since crystal structures of drug binding receptors involved in Hh signaling were unavailable prior to 2013, adopting a structure-based drug discovery strategy was not feasible when these projects were first started. Alternately, a ligand based drug discovery approach was taken to develop Hh inhibitors based on two distinct lead structures namely VD3 and ITZ.

Based on preliminary findings, it was hypothesized that metabolic conversion of VD3 to its physiologically active form, calcitriol, can occur in cell culture leading to robust activation of VDR signaling. Over activation of VDR signaling results in hypercalcemia, hence such off-target effects preclude the clinical use of VD3 as an inhibitor of Hh pathway. Therefore, the goals of this project were to pursue a SAR study to identify the Hh inhibitory pharmacophore of VD3 and use this knowledge to improve potency and selectivity of VD3 based anti-Hh analogues.

Next, based on a comparative analysis of Hh inhibition mediated by ITZ and other marketed azole antifungal drugs that share common structural features interesting trends were discovered. This study indicated that integrating structural features of Posaconazole (PSZ) with ITZ could potentially lead to superior second generation analogues. Thus, the aim for this project was to synthesize and evaluate ITZ derivatives with stereochemically defined hydroxylated side chains as mimics of the PSZ side arm.

CHAPTER II: Design, Synthesis and Evaluation of Vitamin D3 A-Ring Analogues as Hedgehog Pathway Inhibitors

1. Introduction
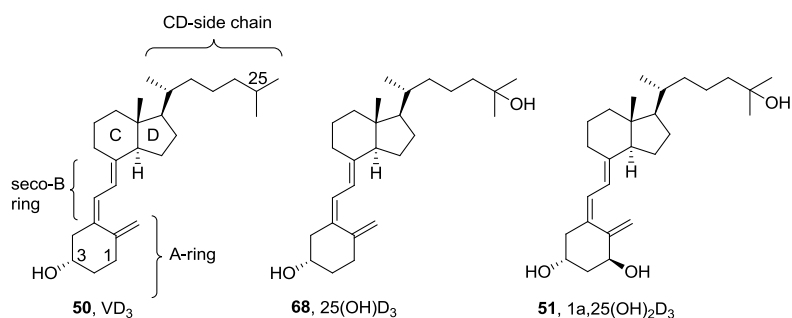
Figure 1. Structure of Vitamin D3 and related compounds.

A recent study demonstrated that vitamin D3 (VD3), a metabolic precursor to 1α,25-dihydroxyvitamin D3 [1α,25(OH)2D3, calcitriol], inhibits the Hh signaling pathway presumably by binding to Smo (Figure 1) [107]. Previous research into the potential preventative and therapeutic anti-cancer effects of the vitamin D class of sterols has focused on 1α,25(OH)$_2$D3, generally acknowledged as the hormonally active form of vitamin D. These anti-cancer effects are primarily mediated through the vitamin D receptor (VDR), a nuclear receptor that acts as a transcription factor to regulate apoptosis, proliferation, and differentiation [139]. The clinical usefulness of 1α,25(OH)$_2$D$_3$ and analogues has been limited by its tendency to promote hypercalcemia, an effect related to its VDR-mediated role in calcium regulation. Another recent publication detailing the anti-cancer effects of VD3 in murine models of basal cell carcinoma (BCC) suggested that VD3 holds promise as a therapeutic agent in Hh-dependent cancers; however, administration of VD3 resulted in significant VDR-mediated cellular effects [110].

The development of VD3 analogues that exert their anti-cancer effects through the Hh pathway inhibition would be less susceptible to hypercalcemic side-effects and represent an improved class of vitamin D-based anti-cancer chemotherapeutics. The studies described herein represent the first reported SAR studies for VD3 inhibition of Hh

signaling. Employing A-Ring analogues with varying 3' moieties, requirements for optimal Hh inhibition and suitability of *in vitro* assay systems were probed.

2. Design and synthesis of A-Ring analogues

2.1 Overview

(i) (CO)$_2$Cl$_2$, DMSO, TEA, 33%; (ii) NaH, MeI, 82%; (iii) TEA, MsCl; (iv) NaN$_3$, DMF, 25% over two steps; (v) PPh$_3$, H$_2$O, 50%; (vi) CCl$_3$COOH, DIAD, PBu$_3$, 45%; (vii) LiOH, H$_2$O,THF 55%.
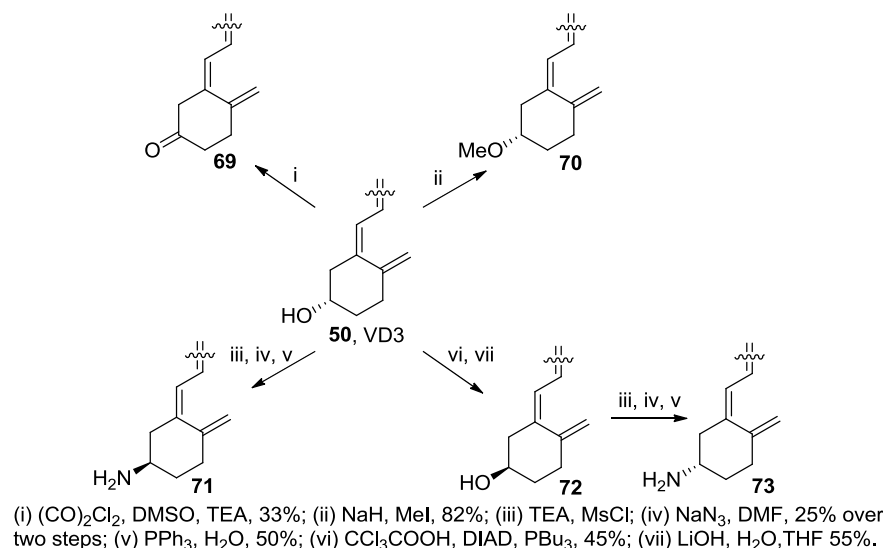
Scheme 1. Reaction conditions for synthesis of A-Ring analogues.

As the 3-(*S*)-hydroxyl of VD3 is the only non-carbon-hydrogen bond in the structure, our initial efforts of studying the structure-activity relationships for VD3 inhibition of Hh signaling began with straightforward modifications at this position (Scheme 1). These analogues were designed to probe the optimal configuration and hydrogen bonding characteristics at C-3. Standard attempts to oxidize the hydroxyl to the corresponding ketone (PDC, Dess-Martin periodinane) proved unsuccessful. Conversion to keto VD3 (**69**) in modest yield was achieved under the more strenuous Swern oxidation conditions [140]. Standard methylation provided the methoxy-VD3 derivative (**70**) in excellent yield. Mesylation of VD3, followed by substitution of the crude 3-(*S*)-OMs with sodium azide afforded the 3-(*R*)-N3 (25% yield over two steps). Conversion to the corresponding amine (**71**) proceeded in modest yield (50%) via standard Staudinger reduction conditions [141]. The inverted alcohol (**72**) was generated

through Mitsunobu conditions optimized for the VD3 scaffold [142]. Subsequent conversion of (**72**) to the 3-(*S*)-NH2 (**73**) proceeded in an analogues manner to that described above for the inverted amine.

2.2 Experimental protocols

(*Z*)-3-((*E*)-2-((1*R*,7a*R*)-7a-methyl-1-((*R*)-6-methylheptan-2-yl)hexahydro-1H-inden 4(2H)-ylidene)ethylidene)-4-methylenecyclohexanone (**69**). A solution of DMSO (1.85 mL, 26.0 mmol) in anhydrous CH_2Cl_2 (12 mL) was added dropwise to a stirred solution of oxalyl chloride (1.1 mL, 12.9 mmol) in CH_2Cl_2 (12 mL) at -78 °C under argon. This solution was stirred at -78 °C for 30 min at which time a solution of vitamin D3 (1 g, 2.6 mmol) in CH_2Cl_2 (15 mL) was added. This mixture was stirred at -78 °C for 20 min, triethylamine (9 mL, 65 mmol) was added, and the mixture was warmed to RT for 30 min. The mixture was diluted with CH_2Cl_2 (100 mL) and washed with H_2O (100 mL). The aqueous layer was removed, the organic layer washed with saturated NaCl (100 mL), dried (Na_2SO_4), and concentrated. Chromatography (SiO_2, 3:1, CH_2Cl_2:Hex) afforded **69** as a clear oil in moderate yield (33%). 1H NMR ($CDCl_3$, 500 MHz) δ 5.95 (s, 1H), 5.43 (s, 1H), 5.35 (s, 1H), 4.97 (t, *J* = 7.2 Hz, 1H), 3.18 (t, *J* = 7.5 Hz, 2H), 2.73 (m, *J* = 9.6, 5.4 Hz, 3H), 2.54 (m, *J* = 14.1, 7.7 Hz, 3H), 2.06 – 1.84 (m, 4H), 1.72 – 1.59 (m, 3H), 1.59 – 1.42 (m, 5H), 1.42 – 1.23 (m, 8H), 1.23 – 1.09 (m, 4H), 1.09 – 0.98 (m, 2H), 0.94 (d, *J* = 6.5 Hz, 3H), 0.89 (dd, *J* = 6.6, 2.3 Hz, 6H), 0.57 (s, 3H). 13C NMR ($CDCl_3$, 125 MHz) δ 199.8, 157.9, 142.5, 141.7, 126.7, 115.0, 114.9, 56.5, 55.7, 45.3, 40.4, 39.5, 37.8, 36.2, 36.1, 32.0, 30.9, 28.7, 28.0, 27.6, 23.9, 23.3, 22.9, 22.6, 22.2, 18.9, 11.9. IR (film) $υ_{max}$ 2925, 2827, 2378, 1725, 1663, 1450, 1439, 1375, 1258, 1195, 750, 699 cm^{-1}. ESI-HRMS *m/z* calculated for $C_{27}H_{44}O$ [M+H]$^+$ 383.3308, found 383.3314.

(1*S*,*Z*)-3-((*E*)-2-((1*R*,7a*R*)-7a-methyl-1-((*R*)-6-methylheptan-2-yl)hexahydro-1H inden-4(2H)-ylidene)ethylidene)-4-methylenecyclohexanol (**70**). A solution of vitamin

D3 (50 mg, 0.13 mmol) and sodium hydride (4.1 mg, 0.17 mmol) in anhydrous THF (3 mL) was cooled to 0°C and stirred for 15 min. Methyl iodide (36 mg, 0.26 mmol) was added dropwise and the solution warmed to 25°C and stirred for 12 hrs. The solution was diluted with EtOAc (10 mL) and washed with H_2O (10 mL). The aqueous layer was removed, the organic layer washed with saturated NaCl (10 mL), dried (Na_2SO_4), and concentrated. Chromatography (SiO_2, 20:1, Hex:EtOAc) afforded **70** as a clear oil in excellent yield (82%). 1H NMR ($CDCl_3$, 500 MHz) δ 6.25 (d, J = 11.2 Hz, 1H), 6.06 (d, J = 11.2 Hz, 1H), 5.06 (s, 1H), 4.84 (s, 1H), 3.43 (m, 1H), 3.37 (s, 3H), 2.90 – 2.81 (m, 1H), 2.60 (d, J = 13.1, 1H), 2.47 – 2.38 (m, 1H), 2.31 (m, 1H), 2.19 – 2.10 (m, 1H), 2.05 – 0.99 (m, 24H), 0.89 (dd, J = 6.6, 2.2 Hz, 6H), 0.58 (s, 3H). 13C NMR ($CDCl_3$, 125 MHz) δ 145.3, 141.7, 135.5, 121.8, 117.7, 112.2, 78.0, 56.6, 56.3, 55.8, 45.7, 42.4, 40.5, 39.4, 36.1 (2H), 32.2, 31.9, 28.0, 27.0, 27.6, 23.8, 23.5, 22.8, 22.5, 22.2, 18.8, 12.0. IR (film) v_{max} 3007, 2950, 2847, 1722, 1467, 1442, 1388, 1255, 1098, 748, 699 cm^{-1}. ESI-HRMS m/z calculated for $C_{28}H_{47}O$ [M+H]$^+$ 399.3621, found 399.3646.

General synthetic procedure for generating 71 and 73. The general synthesis of **71** and **73** followed a slight modification of the previously published procedure [141]. A solution of vitamin D3 (1 g, 2.6 mmol) and triethylamine (1 g, 10.4 mmol) in CH_2Cl_2 (15 mL) was cooled to 0°C and stirred for 5 mins. Methanesulfonyl chloride (595 mg, 5.2 mmol) was added dropwise and the solution warmed to 25°C over 20 min. The CH_2Cl_2 was removed and the mixture redissolved in EtOAc (10 mL) and saturated sodium bicarbonate (10 mL). The aqueous layer was removed, the organic layer was washed with H_2O (10 mL) and saturated NaCl (10 mL). The organic layer was dried (Na_2SO_4) and concentrated. The resulting crude mesylate (1 g, 2.2 mmol) and sodium azide (1.43 g, 22 mmol) in anhydrous DMF (15 mL) was stirred at 60°C for 12 hr. The mixture was diluted with EtOAc (50 mL) and H_2O (50 mL). The aqueous layer was removed, the organic layer washed with saturated NaCl (10 mL), dried (Na_2SO_4), and concentrated.

44

Chromatography (SiO_2, 1: 1, CH_2Cl_2: EtOAc) afforded the inverted azides as a yellow oil in modest yield (25% over two steps). Azide (100 mg, 0.24 mmol), triphenylphosphine (128 mg, 4.9 mmol), and H_2O (43 µL, 2.4 mmol) were stirred in THF (10 mL) under positive argon pressure at RT for 12 hr. The solution was concentrated and chromatography (SiO_2, 20:1:0.1, CH_2Cl_2: MeOH, NH_4OH) afforded the previously described amines as a yellow oil in modest yield (50%).

3. Biological evaluation

3.1 Experimental protocols

RT-PCR protocol: Following treatment and incubation, RNA was extracted with TRIZOL® Reagent following the manufacturer's instructions. cDNA synthesis was performed utilizing the High Capacity cDNA Reverse Transcription Kit (ABI) per the manufacturer's instructions on a BioRad MyCycler. Quantitative RT-PCR was performed on an ABI 7500 system using the following Taqman Gene Expression Assays: human GLI1, Hs00171790_m1; human Cyp24A1, Hs00167999_m1; human ActB, Hs99999903_ml; mouse GLI1, Mm00494645_m1; mouse Cyp24A1, Mm00487244_m1; mouse ActB, Mm00607939_s1. Relative gene expression levels were computed via the ΔΔCt method using GraphPad Prism.

Anti-proliferation protocol: Cells (3000/well, 100 µL) were seeded in 96-well plates and incubated overnight (37°C, 5% CO_2). Cells were treated in triplicate with DMSO, VD3, Cyc, or analogue at varying concentrations (1% DMSO final concentration). Following 72-hr incubation, viable cells were measured using CellTiter 96® aqueous Non-Radioactive Cell Proliferation Assay (Promega) per the manufacturer's instructions. Data was analyzed using GraphPad Prism and IC_{50} values represent mean ± SEM for at least three separate experiments.

3.2 Results & discussion

The Hh inhibitory activity of VD3 and **69**-**73** was initially examined through down-regulation of endogenous Gli1 mRNA in the Hh–dependent C3H10T1/2 cell line [46]. In this well-studied model system, the Hh pathway is silent under normal growth conditions and Gli1 expression is negligible. Incubation with oxysterols [20(S)- and 22(S)-hydroxycholesterol, 5 μM each] activates the pathway and results in significant (approximately 100-fold) up-regulation of Gli1 while co-administration with Hh pathway inhibitors prevents Gli1 up-regulation. For these studies, VD3 and **69**-**73** were evaluated at 5 μM and Gli1 mRNA expression levels were normalized to oxysterol controls (set as 100% expression). Several interesting SAR were observed from these assays (Table 1). First, removal of the hydrogen in analogues **69** and **70** resulted in a moderate to significant decrease in Hh inhibitory activity. In addition, both amine epimers, **71** and **73**, were 2-fold less active than VD3. Finally, inverting the stereochemistry at C-3 did not have an appreciable effect on Hh inhibition, suggesting the S-configuration of natural VD3 is not required for activity.

Table 1. *In vitro* activity of VD3 A-ring analogues.

Analogue	3-moiety	Relative Gli1 mRNA (%)[a]	Anti-proliferation IC$_{50}$ (μM)[b]	VDR Binding
Cyc	----	6.93 ±1.93	22.5 ± 0.5	----
VD3	3-(S)-OH	31.7 ± 0.7	29.7 ± 3.1	>100μM
69	3-keto	50.1 ± 6.4	50.6 ± 1.8	>100μM
70	3-(S)-OMe	72.2 ± 11	54.2 ± 6.2	>100μM
71	3-(R)-NH$_2$	68.0 ± 7.0	12.3 ± 0.5	>100μM
72	3-(R)-OH	25.0 ± 6.0	39.2 ± 1.5	>100μM
73	3-(S)-NH$_2$	62.7 ± 2.7	12.3 ± 0.1	>100μM

[a]Relative Gli1 mRNA levels in C3H10T1/2 when oxysterol treatment is equivalent to 100%.
[b]IC$_{50}$ values measured in U87MG cells (MTS assay).

In addition to evaluating the Hh inhibitory activity of VD3 and analogues, we sought to measure their anti-proliferative activities in human cancer cells. Recent studies

46

have suggested that the *in vivo* tumor microenvironment is required for proper Hh signaling and that cultured cancer cells may not function as an appropriate model system [12]. Nevertheless, Cyc treatment was previously shown to result in Gli1 down-regulation in the human glioblastoma cell line U87MG; therefore, we evaluated VD3 and analogues in this cellular model [143]. Interestingly, the two most active analogues in this assay were **71** and **73**, the 3-(*R*)- and 3-(*S*)-amines (IC_{50}s = 12.3 ± 0.1 and 12.3 ± 0.1, respectively). These results were in direct contrast with the Hh inhibitory activity of these compounds. The other compounds demonstrated modest anti-proliferation with IC_{50} values approximately 3-fold higher than **71** and **73**.
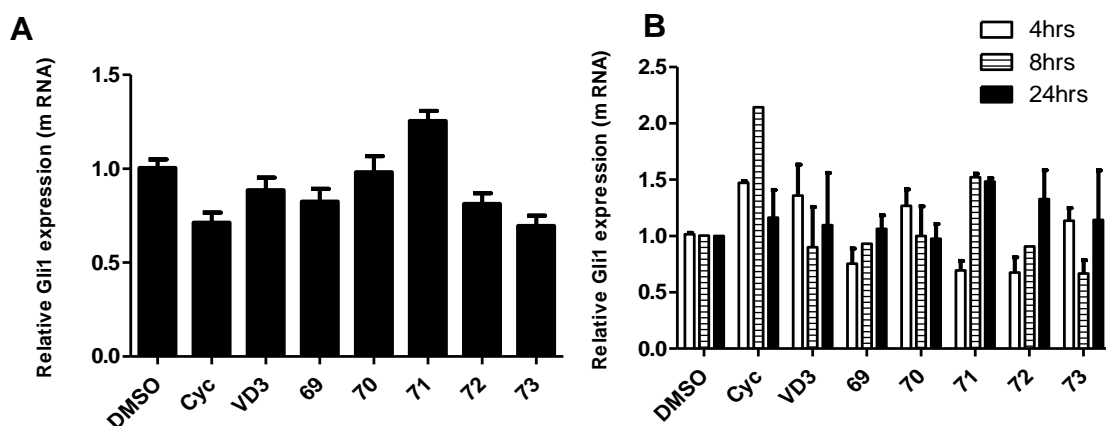
Figure 2. Relative Gli1 mRNA expression in U87MG cells.
(**A**) 5 µM treatment at 24 hr (**B**) Time-dependent Gli1 regulation with 10 µM compound.

The further analysis of VD3 and analogues included evaluating their ability to down-regulate Gli1 in U87MG cells. At 5 µM, none of the compounds evaluated significantly down-regulated Gli1 expression after 24 hrs (Figure 2A). As previous studies that demonstrated Cyc inhibits Hh signaling in U87MG cells measured Gli1 down-regulation following 4 hr incubation at 10 µM of the natural product, we evaluated each Hh inhibitor at this increased concentration and varying time points (Figure 2B) [143]. Under these conditions, none of the compounds tested demonstrated significant Gli1

47

down-regulation in this cell line. In fact, Cyc treatment resulted in a slight increase in Gli1 expression levels at 8 hr.

Based on these conflicting results and our ultimate goal of developing VD3 analogues that specifically target Smo and the Hh pathway, we evaluated each compound for its ability to regulate VDR signaling. VD3 and analogues were explored for their ability to bind VDR. For this assay, we utilized the PolarScreen™ VDR Competitor Assay, Red (Invitrogen) per the manufacturer's instructions. This assay is a fluorescence polarization-based competition assay that has been optimized for high-throughput applications and contains all the required components (including full length human VDR and a proprietary tight-binding fluorescent VDR ligand). Neither VD3 nor the A-ring analogues exhibited VDR binding at concentrations up to 100 µM, suggesting these compounds do not exhibit their biological activity through direct binding interactions with VDR (Table 1).
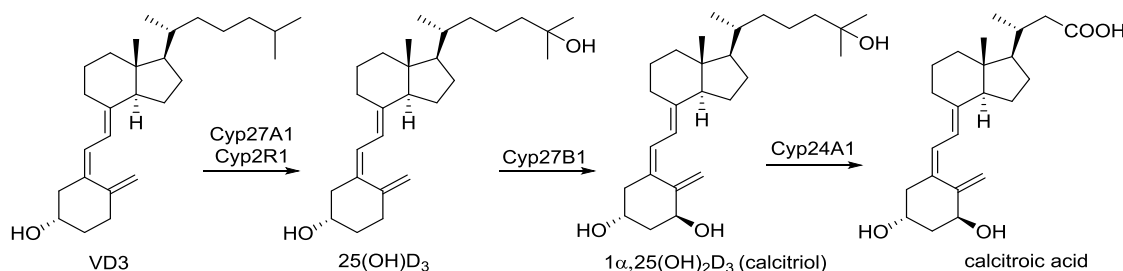
Figure 3. **Vitamin D metabolic pathway.**

Our next step towards understanding the cellular mechanisms responsible for the anti-proliferative activity of VD3 and **69-73** in U87MG cells was to evaluate their ability to activate VDR in cell culture. Primarily, VD3 is metabolized in liver and kidney by various Cyp450 enzymes to yield 25(OH)D3 and 1α,25(OH)$_2$D3 (Figure 3), forms of vitamin D which bind and activate VDR. Recent evidence has shown that various types of human cancers express increased levels of these metabolic enzymes [144-147]. While it remains

48

unclear whether the over-expression of these enzymes plays a role in the proliferation of human cancers, their presence outside the liver and kidney suggests that the possible metabolic transformation of VD3 and analogues in cancer cells may result in structures which activate VDR signaling [148]. With respect to VDR regulation, Cyp24A1 is responsible for converting $1\alpha,25(OH)_2D3$ into the physiologically inactive calcitroic acid. Cyp24A1 is elevated in response to VDR activation and serves as a natural feedback mechanism to regulate VDR signaling. For this reason, induction of Cyp24A1 is commonly used to monitor cellular activation of the VDR signaling. Incubation of U87MG cells with VD3 resulted in significant up-regulation of Cyp24A1 (~5-fold, Table 2). In addition, the VD3-epimer **72** demonstrated Cyp24A1 up-regulation comparable to VD3. Each amine exhibited modest VDR activation, while neither keto- nor methoxy-VD3 had a significant effect. In order to determine whether these effects were cell type dependent, we explored Cyp24A1 up-regulation in HT-29 cells, a colon cancer cell line known to produce a robust and reproducible Cyp24A1 response to $1\alpha,25(OH)_2D3$ administration [149, 150]. VD3, $1\alpha,25(OH)_2D3$ (0.1 µM), and **72** demonstrated significant up-regulation of Cyp24A1 in HT-29 cells. A recent study reported a modest increase in Cyp27A1 and Cyp27B1 expression upon administration of VD3 in HT-29 cells [151]. In this same study, significant up-regulation of Cyp24A1 following VD3 treatment was delayed compared to $1\alpha,25(OH)_2D3$ (24 hr and 4 hr, respectively), suggesting cellular conversion of VD3 to a more active form is necessary for VDR activation. By contrast, Cyc had no effects on Cyp24A1 in either cell line, confirming this effect as specific to the VD3 scaffold and not a general response related to Hh inhibition. Finally, we studied the ability of each compound to up-regulate Cyp24A1 in the C3H10T1/2 cell model. Similar to the results obtained in HT-29 cells, both VD3 and **72** resulted in significant Cyp24A1 up-regulation (Table 2). Of note, these results do not explain the anti-cancer activity for amines **71** and **73**. These two analogues were the most active in the anti-proliferative

49

assays; however, they are poor inhibitors of Hh signaling and do not activate VDR in cultured cells, suggesting their activity may be mediated by an as yet unidentified cellular signaling mechanism.

Table 2. Up-regulation of Cyp24A1 mRNA expression by VD3 and analogues.

Analogue[a]	U87MG	HT-29	C3H10T1/2
Cyc	1.6 ± 0.1[b]	0.9 ± 0.1	0.99 ± 0.1
VD3	4.9 ± 1.1	1063 ± 83	5786 ± 190
69	1.3 ± 0.02	0.9 ± 0.1	130 ± 33
70	1.0 ± 0.1	4.2 ± 0.1	1.1 ± 0.1
71	3.3 ± 0.4	6.1 ± 0.2	6.3 ± 2.2
72	6.9 ± 1.2	1654 ± 48	1444 ± 241
73	3.5 ± 0.3	6.4 ± 0.1	13.0 ± 3.6
$1\alpha,25(OH)_2D_3$	----	14160 ± 691	27890 ± 2774

[a]All compounds except $1\alpha,25(OH)2D3$ (0.1 µM) evaluated at 5 µM in C3H10T1/2 & 10 µM in HT-29 & U87MG
[b]Values represent Cyp24A1 mRNA expression level in cultured cells when DMSO set as 1.0.
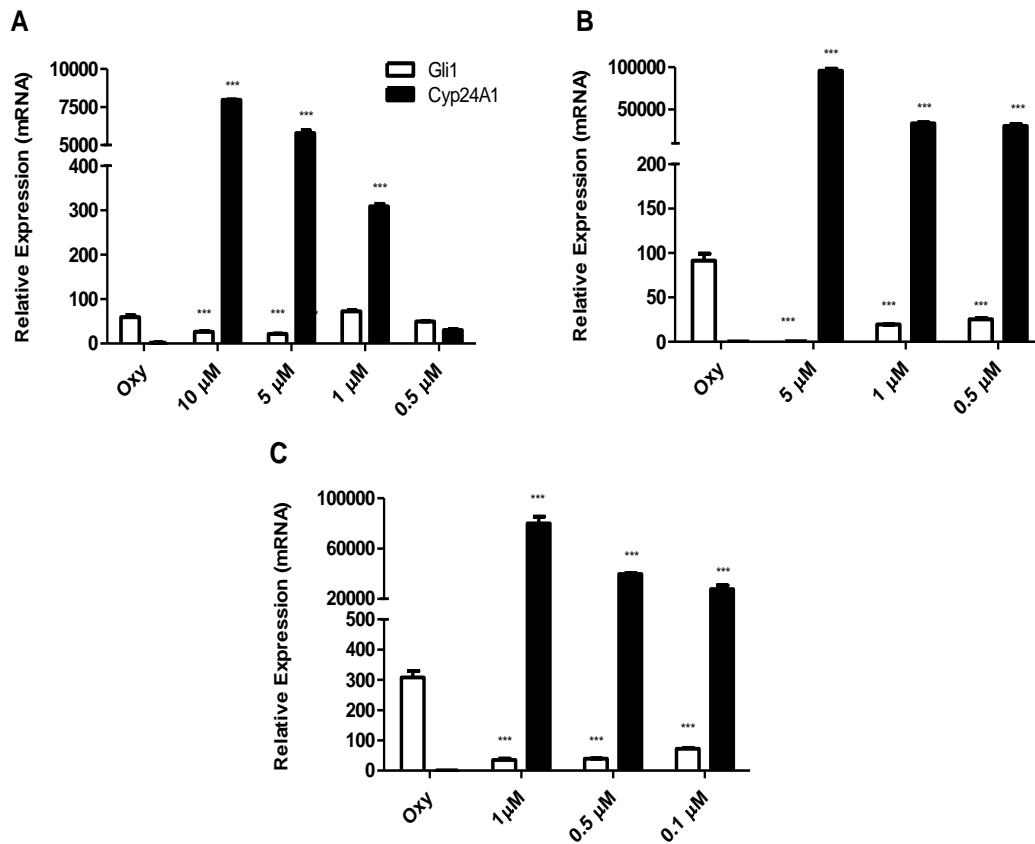
Figure 4. Relative Cyp24A1 mRNA levels in C3H10T1/2 cells.
VD3 (**A**), 25(OH)D3 (**B**), and $1\alpha,25(OH)_2D3$ (**C**) treatment (24hr).
DMSO was set as 1.0 and mRNA expression levels for treatments were calculated accordingly [p<0.0001].

50

The data for VD3 supports our hypothesis that its metabolism in cultured cancer cells results in a form that more readily activates VDR; however, these results also provide another source of potential confusion regarding VDR/Hh signaling. Recent studies exploring the relationships between VDR signaling and the Hh pathway have suggested that $1\alpha,25(OH)_2D3$ may directly regulate Hh signaling [152]. It is unclear whether these modulatory effects are mediated through direct inhibition of Hh signaling or as a downstream effect of VDR activation. In addition, minimal studies detailing the effects of $1\alpha,25(OH)_2D3$ in C3H10T1/2 cells have been reported. For these reasons, we sought to evaluate the dose-dependent effects on Hh and VDR signaling of VD3, $25(OH)_2D3$ and $1\alpha,25(OH)_2D3$ in this cell line (Figure 4). Not surprisingly, each vitamin D compound significantly up-regulated Cyp24A1 in a dose-dependent fashion. Of note, the lowest concentration of VD3 evaluated (0.5 µM) did not activate VDR signaling, while both $25(OH)_2D3$ and $1\alpha,25(OH)_2D3$ maintained robust Cyp24A1 up-regulation; lending further support to the hypothesis that these VD3 metabolites, and not VD3 itself, mediate the VDR response seen upon VD3 administration. In addition, both $25(OH)_2D3$ and $1\alpha,25(OH)_2D3$ significantly reduced GLI1 expression levels in this cell line.

4. Conclusion

Taken together, these results provide a better understanding of the necessary requirements for developing VD3 analogues as selective Hh pathway inhibitors. First, not only can VD3 analogues not directly interact with VDR, modifications to the scaffold must also yield structures that are not substrates for Cyp27A1 and Cyp2R1, enzymes that catalyze the metabolism of VD3 to 25(OH)2D3. Second, while both 25(OH)2D3 and $1\alpha,25(OH)2D3$ inhibit Hh signaling, they produce a robust VDR response in multiple cell lines and do not represent selective scaffolds for the development of Hh pathway inhibitors. Finally, as described above, there is no correlation between Hh inhibition in

C3H10T1/2 cells and Gli1 down-regulation in cultured epithelial cancer cells, supporting the recent findings that the *in vivo* tumor microenvironment is required for proper Hh signaling in human cancer.

CHAPTER III: Design, Synthesis and Evaluation of Hybrid Vitamin D3 Side Chain

Analogues as Hedgehog Pathway Inhibitors

1. Introduction

Previous studies undertaken in our lab revealed that VD3 mediated inhibition of Hh signaling *in vitro* is modest (IC_{50} = 4.1µM) and non-selective due to its ability to concurrently activate canonical VDR signaling [108, 113]. Thereafter, a medicinal chemistry approach was undertaken to design analogues of VD3 that selectively target Hh signaling. Initial attempts with analogues prepared by simple modifications of the 3'-hydroxyl functionality of the A-ring proved inadequate [108]. Next, as a part of our ongoing SAR studies to elucidate the pharmacophore of VD3 necessary for selective inhibition of Hh signaling, we adopted a deconstructive approach of studying analogues arising from each region of VD3 (Figure 1) [111]. The key observations of this study were that the truncated side chain analogues of VD3, **74**, Inhoffen Lythgoe diol, **75**, along with the 'southern' fragment of VD3, **76**, showed a considerable loss of activity. However, analogues with intact 'northern' regions of VD3 and VD2, **77** and **78**, retained Hh inhibitory activity comparable to VD3 albeit in a more selective fashion (Table 1). Therefore, probing the structural requirements of the CD-ring side chain region was the next warranted step. Studies described in this chapter were aimed at unraveling the optimum requirements for length and nature of VD3 side chain for potent and selective Hh inhibitory activity.
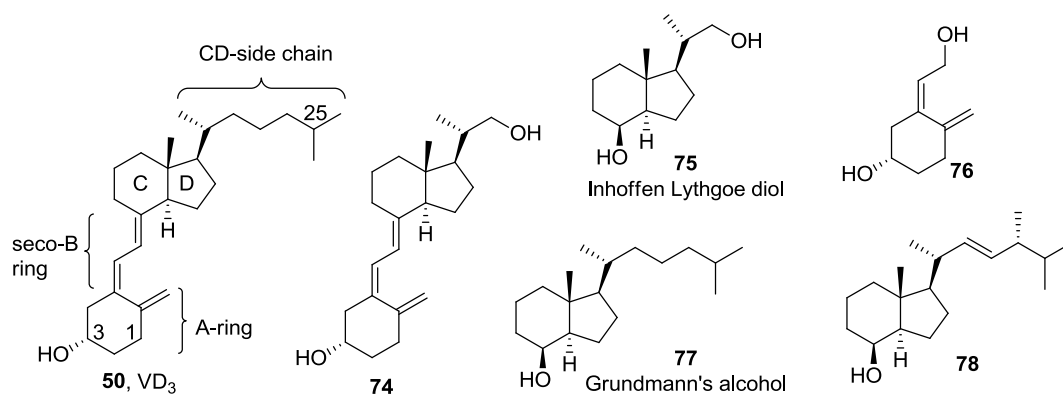
Figure 1. Structures of truncated VD3 analogues.

54

Table 1. Gli1 inhibitory activity and selectivity of truncated VD3 analogues.

Analogue	Relative Gli1 mRNA (%)[a]	Relative Cyp24A1 mRNA[b]
VD3	35.7 ± 0.3	8336 ± 38
74	80.0 ± 10.4	1354 ± 61
75	87.6 ± 1.2	4.1 ± 0.7
76	46.4 ±3.5	3.6 ± 0.5
77	80.9 ± 2.1	2.0 ± 0.2
78	32.1 ± 6.3	2.3 ± 1.2

[a]Relative Gli1 mRNA levels in C3H10T1/2 when oxysterol treatment is equivalent to 100%.
[b]Values represent Cyp24A1 mRNA expression in cultured cells relative to DMSO (1.0).

Initial attempts to prepare side chain derivatives proceeded with sulfur dioxide protection of the VD2 triene and protection of the 3' hydroxyl group as the silyl ether, followed by selective ozonolysis/reduction of the side chain olefin to provide TES-protected trans-VD3 alcohol **82** (Scheme 1) [153]. The next steps included tosylation of the resultant primary hydroxyl group and removal of the triene protecting group yielding the trans-VD3 derivative **84** [153, 154]. Subsequent photoisomerism led to precursor **85** required for the alkylation reaction via displacement of the primary tosylate using various commercially available Grignard reagents [153, 155]. Finally deprotection of the 3'-hydroxyl group afforded analogues with modified side chains **86**. This initial scheme to prepare VD3 analogues with side chain modifications proved challenging as several attempts to displace the tosyl functionality using a Grignard's reagent either failed or proceeded in extremely low yields (0% - 5%). Additionally, the inherent instability of the conjugated triene system of VD3 in solution due to thermal equilibrium between VD3 and pre-VD3 via a [1, 7]-sigmatropic hydrogen shift, posed general complications during synthetic manipulations of this structure [156]. Further biological evaluation of analogue **86** could not be carried out due to lack of necessary amounts of pure product required for complete chemical characterization and sample preparation for dosing cells.

55

www.manaraa.com
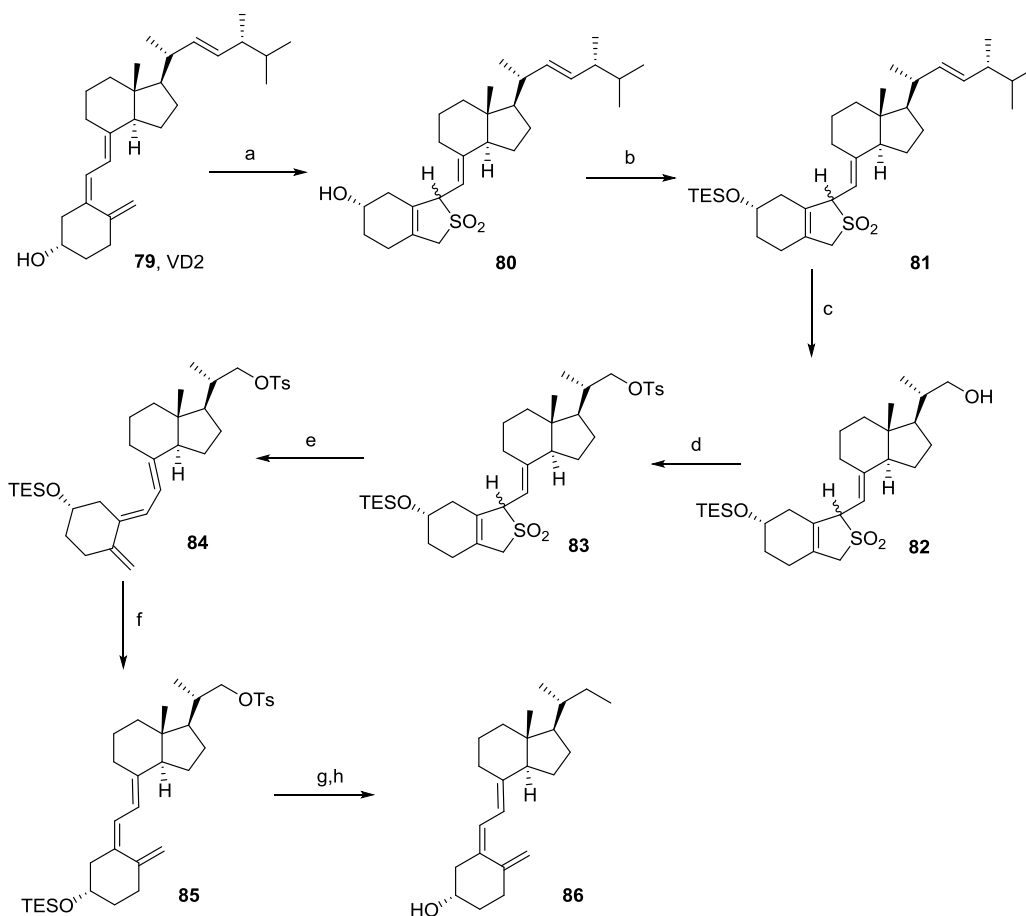
(a)H$_2$SO$_3$, benzene; (b) TESCl, Imidazole, anhydrous DCM, 90% over two steps; (c) O$_3$, pyridine, DCM:MeOH 3:1, NaBH$_4$, 75%; (d) TsCl, NEt$_3$, anhydrous DCM, 87%; (e) NaHCO$_3$, EtOH, reflux, 80%; (f) acridine (50 mol%), NEt$_3$, benzene, 365 nm, 90%; (g) CuI, MeMgBr, anhydrous THF, 0-5%; (h) TBAF, DCM, 70%.

Scheme 1. Synthetic route to VD3 side chain analogues.

In concurrent studies, the 'northern' region of VD3, also known as Grundmann's alcohol (**77**), was found to be equipotent to the parent VD3 scaffold (IC$_{50}$ values = 3.1 and 4.1 μM respectively) [111, 113]. Based on this finding, subsequent series of VD3 analogues designed to incorporate an aromatic A-ring isostere that maintains the approximate steric and hydrophobic features of the natural aliphatic A-ring into the seco-steroid scaffold identified compound **87** as a selective Hh inhibitor with enhanced activity (IC$_{50}$ = 0.74 μM) (Figure 2) [113]. Following the identification of improved Hh inhibitory scaffold **87**, we directed our efforts to incorporate the side chain modifications on this revised core structure. With this revision in design strategy, we aimed to fulfill analogue

optimization for enhanced potency and selectivity along with affording relative efficiency and ease in accessing hybrid side chain analogues.
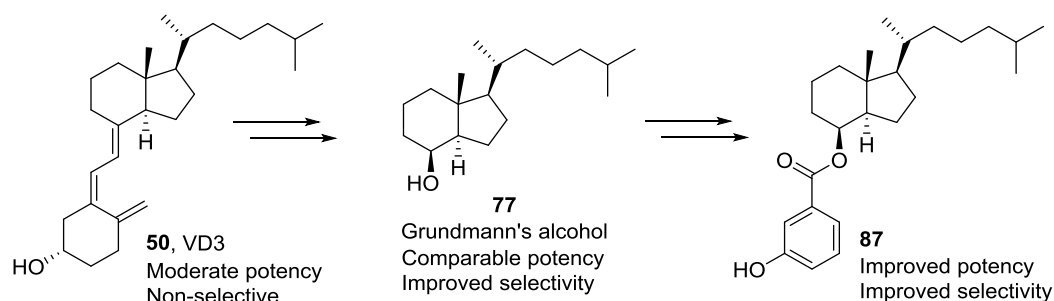
Figure 2. Development of hybrid VD3 as selective and potent Hh inhibitor.

2. Synthesis of hybrid side chain analogues of VD3

2.1 Overview

2.1.1 Route 1

Complete ozonolysis of VD2 and subsequent reduction of the resultant ozonide in a one-pot reaction generated the previously characterized Inhoffen Lythgoe diol, **75** (Scheme 2) [157]. The next step of preferential tosylation of the primary hydroxyl group in presence of another slightly hindered secondary hydroxyl group proceeded with modest yields leading to the preparation of key CD ring intermediate (**88**, Scheme 2) [158]. For the synthesis of the Ring-A aromatic mimic two consecutive protection/deprotection steps were carried out to prepare the carboxylate intermediate (**91**, Scheme 2) [159, 160]. With the necessary precursors in hand, the next step of esterification to prepare intermediate (**92**) proceeded with modest yields (Scheme 3) [113]. Syntheses of two linear (**93**, **94**), one branched alkyl (**95**) and one aromatic (**96**) side chain derivative were accomplished via displacement of the tosyl functional group from intermediate (**92**) using appropriate alkyl nucleophiles followed by a final deprotection step (Scheme 3). However, it became necessary to determine an alternate method due to the low yields and inconsistent reproducibility of the tosyl displacement step. Therefore, we sought to identify a viable

57

route to prepare additional analogues in an efficient manner using the current building blocks and available infrastructure.

(a) O_3,DCM:MeOH, $NaBH_4$, 40%; (b) TsCl,DMAP, Et_3N, anhydrous DCM, 85%; (c) MOMCl, DIPEA, anhydrous DCM, 98%; (d) 10% NaOH, MeOH, 76%
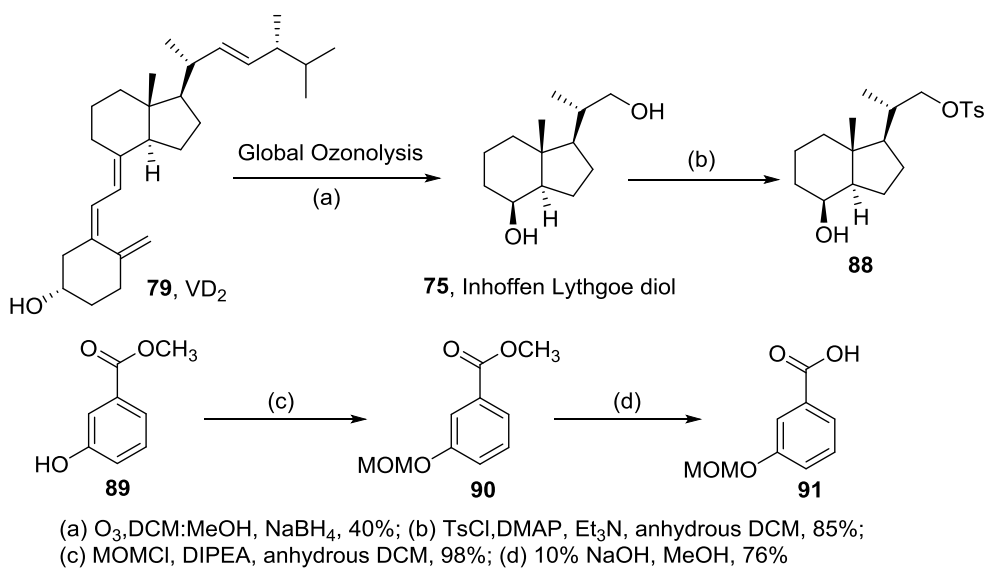
Scheme 2. Route 1: Synthesis of CD-ring and A-ring precursor.

Analogues prepared through Route 1

(a) DCC, DMAP, anhydrous DCM, 40%; (b) $NaBH_4$, DMSO, $150^{\circ}C$, 56%; (c) CuI, R'MgX, anhydrous THF, 10%; (d) TFA, DCM, 65%.
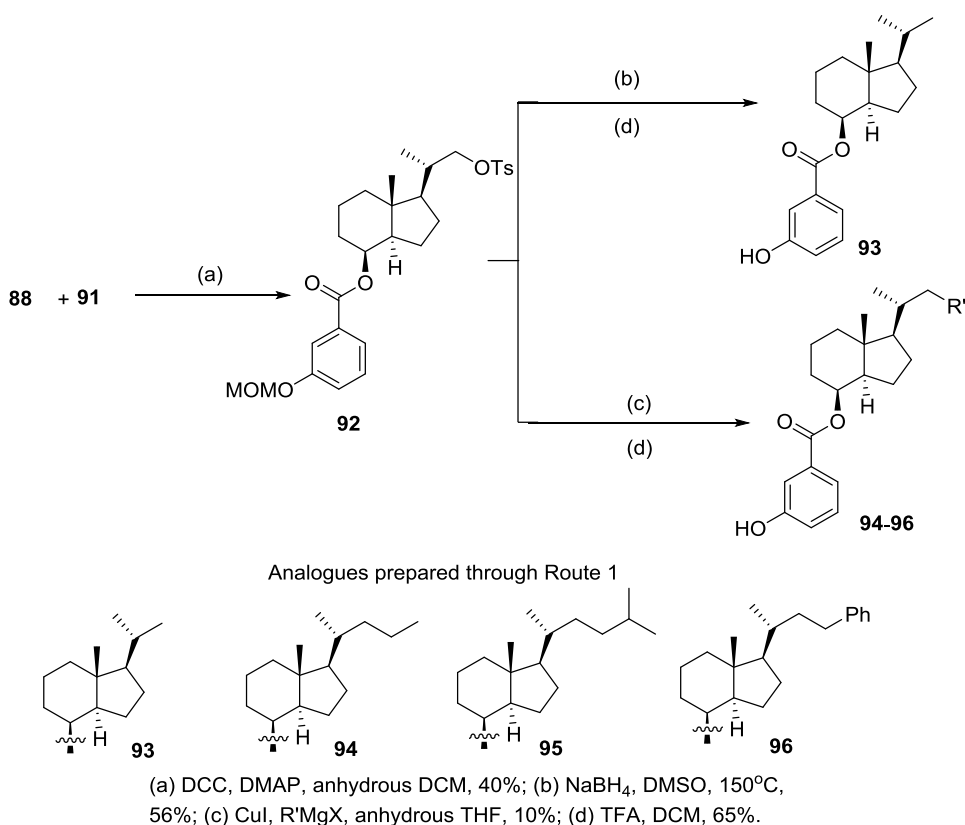
Scheme 3. Route 1: Preparation of hybrid side chain analogues.

2.1.2 Route 2

In this alternate route (Scheme 4), displacement of the tosyl moiety by relevant alkyl nucleophiles was carried out on intermediate (**88**) prior to the esterification step [155]. After installation of the necessary side chains on the CD-ring fragment to generate intermediate (**97**), previously described methods for esterification with intermediate (**91**) and unmasking of the 3' hydroxyl group of the aromatic A-ring mimic were carried out with improved yields. In this manner, a total of seven additional linear as well as branched alkyl chain analogues (**98 – 104**) were synthesized.
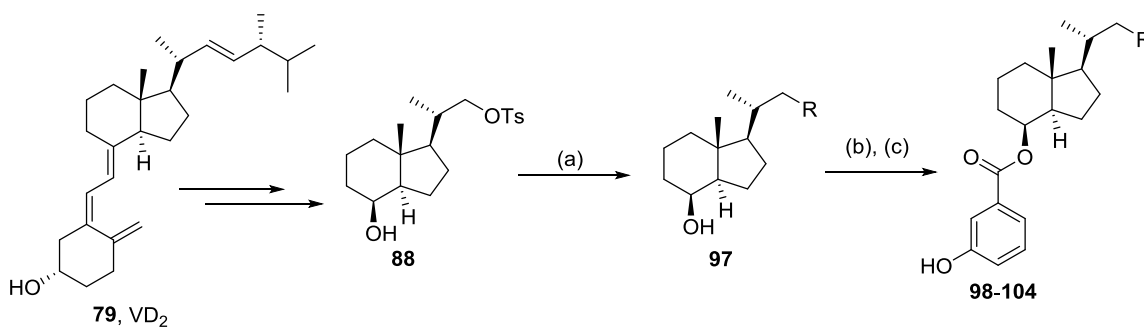
Analogues prepared through Route 2
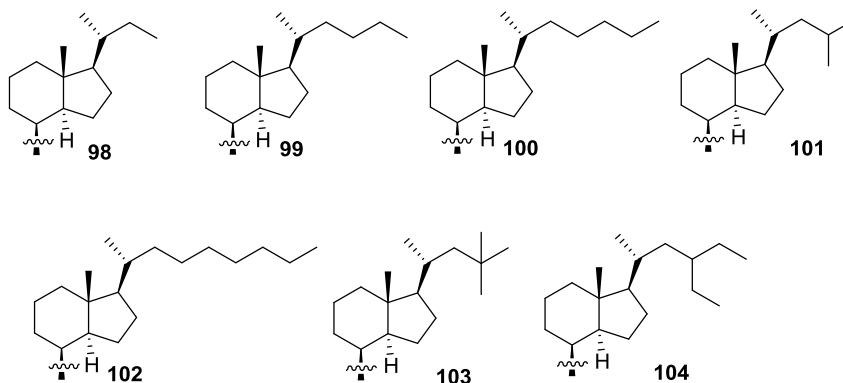
(a) RMgX, CuI, anhydrous THF, 40%; (b) **91**, DCC, DMAP, anhydrous DCM; (c) TFA, DCM, 65% two steps.

Scheme 4. Route 2: Preparation of hybrid side chain analogues.

2.1.3 Route 3

The preparation of additional hybrid VD3 side chain analogues was undertaken by adopting relevant modifications of the previously described routes. For instance,

naturally occurring unsaturated side chain precursor (**78**) was obtained from VD2 by oxidative cleavage of the VD2 triol (Scheme 5) [111]. By varying the nature of protecting groups used for masking A-ring phenolic moiety and hence the subsequent deprotection reactions required, two derivatives containing VD2-like side chains were accessible from **78** (Scheme 6). First, employing benzyl protected intermediate **106** in the esterification reaction followed by global deprotection and reduction afforded analogue **109** with relative ease. Alternately, coupling to A-ring mimic precursor **91** containing the methoxymethyl functionality led to the preparation of analogue **111** with an unsaturated side chain. Next, utilizing trimethylsilyl ether to mask the primary hydroxyl moiety of the Inhoffen Lythgoe diol, intermediate **107** was synthesized in the presence of a catalytic amount of DMAP [161]. Esterification of this intermediate succeeded by one-step removal of both protecting functional groups produced non-hydrocarbon side chain containing analogue **113** (Scheme 5 and 6).
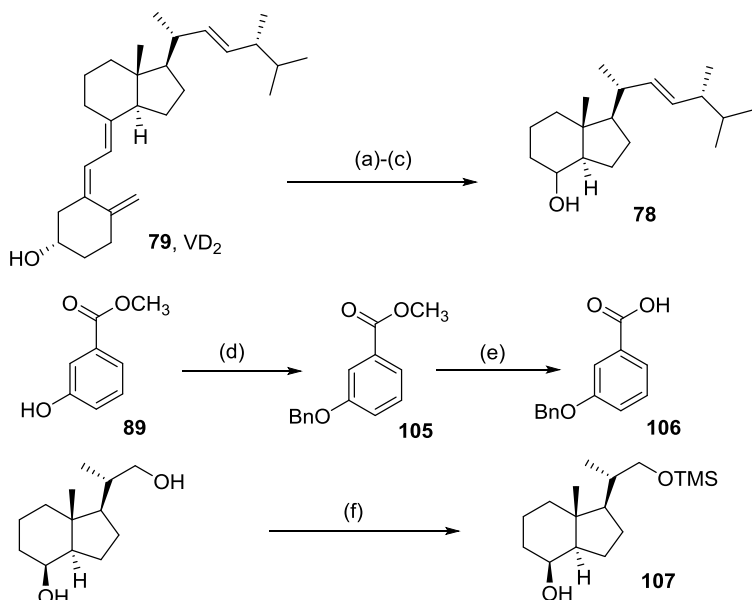
(a) KMnO$_4$, THF, H$_2$O (65%); (b) Pb(OAc)$_4$, DCM; (c) Vitride™, DCM, 69% two steps; (d) BnBr, K$_2$CO$_3$, acetone, 85%; (e) 20% KOH, THF, 75%; (f) TMSCl, TEA, DMAP, anhydrous DCM, 49%.

Scheme 5. Route 3: synthesis of CD-ring and A-ring precursor.
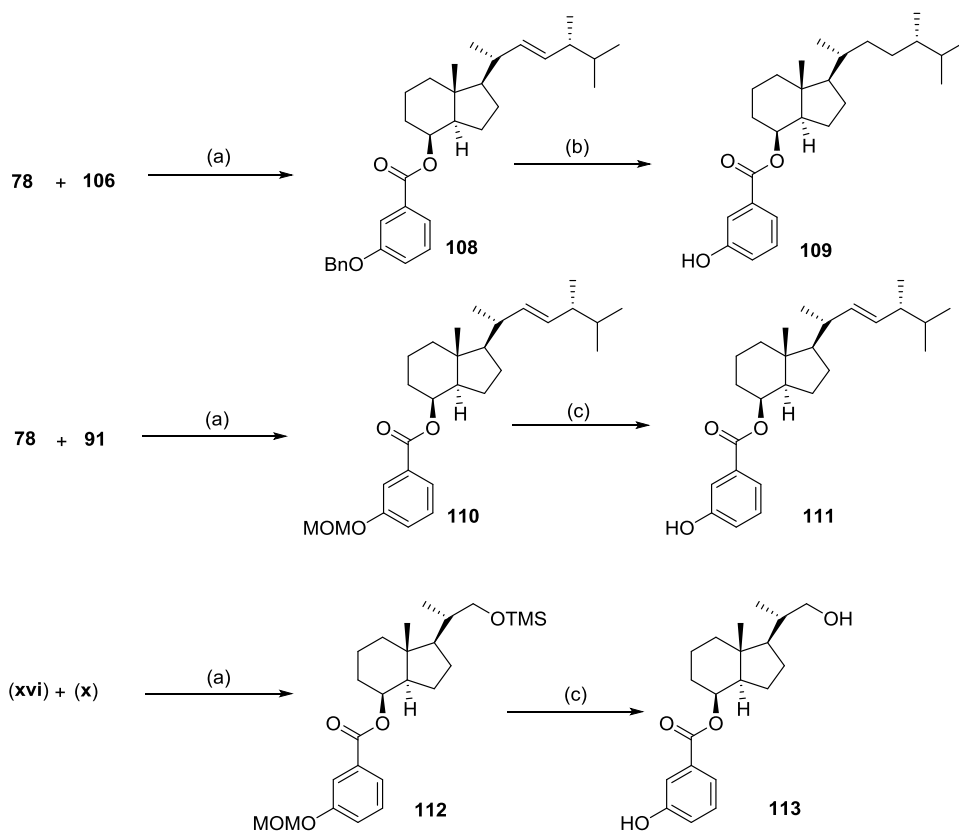
(a) DCC, DMAP, anhydrous DCM, 70%; (b) H$_2$/Pd(OH)$_2$, MeOH:THF, 75%; (c) TFA, DCM, 65%.

Scheme 6. Route 3: Access additional hybrid side chain analogues.

2.1.4   Synthetic strategy

The displacement of the tosyl functional group with a carbon based nucleophile obtained from relevant Grignard reagents represents the key transformation leading to the installation of various side arms on the hybrid VD3 scaffold. Initial attempts to carry out this reaction on relatively bulkier molecules such as intermediate **85** (Scheme 1) or intermediate **92** (Scheme 3) proved inadequate and inefficient. Not only were the reaction yields extremely poor (5%-10%), the reactions rarely proceeded to completion. Furthermore, methodical investigation of the effects of altering reaction parameters

including reaction time, temperature, solvent and copper catalyst did not offer reasonable improvement.
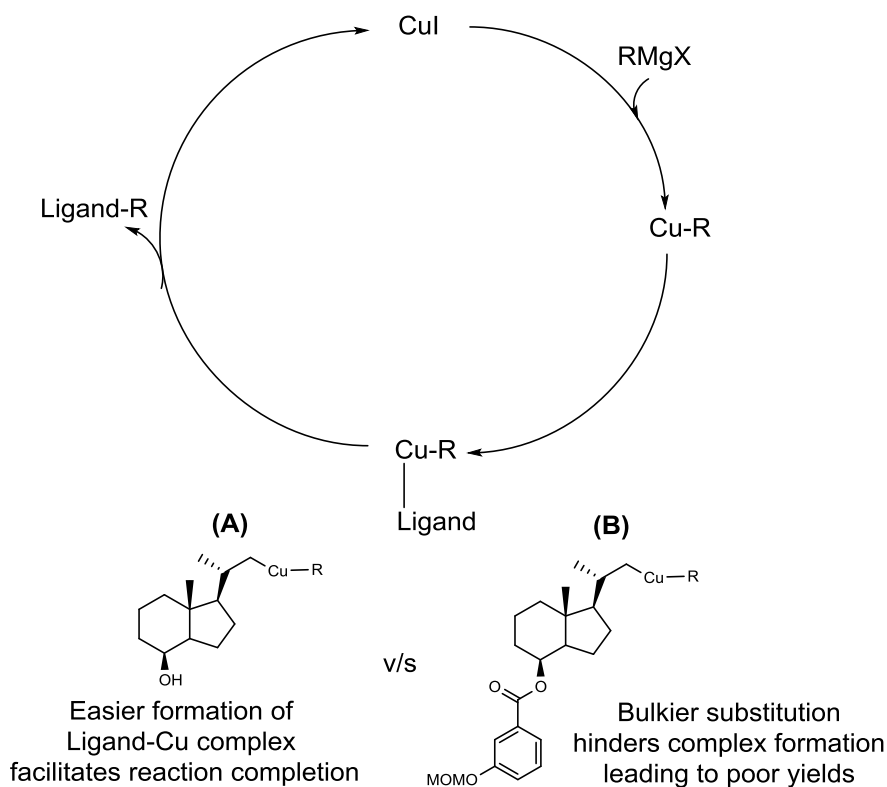
Figure 3. Comparison of intermediate structures during Ts displacement reaction.

Thereafter, the synthetic strategy was modified based on the hypothesis that less bulky substrates may facilitate effective completion of the rate determining step of complex formation with the copper catalyst (Figure 3). Guided by a previous literature report detailing successful displacement of the tosyl moiety from tosylated Inhofen Lythgoe diol **88** with Grignard reagents, a revised strategy (Route 2, Scheme 4) was adopted [162]. Although this shift in strategy lengthened the synthetic route to access the analogues, it afforded reaction reproducibility and improved yields.

2.2 Experimental protocols

Preparation of tosylated MOM-ester (92): Tosylated Inhoffen Lythgoe diol (**88**) (0.2 g, 0.55 mmol), dicyclohexylcarbodiimide (0.34 g, 1.65 mmol), and

www.manaraa.com

dimethylaminopyridine (0.2 g, 1.64 mmol) were dissolved in anhydrous CH_2Cl_2 (6-8 ml) in an oven-dried round bottom flask. Carboxylic acid (**91**) (0.3 g, 1.65 mmol) was added at 0° C, the reaction mixture was allowed to warm to RT and stirred for 12 h. The reaction mixture was diluted with CH_2Cl_2 (30 ml), washed with 0.1N HCl and brine, dried over Na_2SO_4 and concentrated under reduced pressure. The crude mixture was purified using column chromatography (SiO_2, 5-25% EtOAc in hexanes) to yield product as clear oil in 40% yield.

General procedure for Tosyl group displacement: Commercially purchased Grignard reagents (5 eq.) were added to an oven-dried round bottom flask containing CuI (1.6 eq.) in anhydrous THF (3-5 ml) under argon and stirred for 0.5 h at 0^oC. (**85**) (1 eq.) or (**92**) (1 eq.) or (**88**) (1 eq.) dissolved in anhydrous THF (1 ml) was added to the reaction mixture and stirred for 1 h at 0^oC. The reaction was quenched by addition of water, extracted with EtOAc (3X), washed with 0.1N HCl (3X), dried over Na_2SO_4 and concentrated under reduced pressure. The crude mixture was purified using column chromatography (SiO_2, 0-20% EtOAc in hexanes) to yield products as clear oils in 10-40% yield.

General procedure for removal of methoxymethyl (MOM) protecting group: To a solution of MOM-protected ester intermediate (20-25 mg, 1 eq.) in DCM (2 ml), excess of trifluoroacetic acid (10 eq.) was added. The reaction mixture was stirred at RT and reaction progress was monitored by thin layer chromatography. Upon completion, the reaction was neutralized using saturated Na_2CO_3 and washed with DCM. The combined organic layer was dried over Na_2SO_4, concentrated under reduced pressure and purified using column chromatography (SiO_2, 0-15% EtOAc in hexanes) to yield products as clear oils in 65% yield.

63

General procedure for esterification: (**97**), (**78**), or (**107**) (1 eq.), dicyclohexylcarbodiimide (3 eq.), and dimethylaminopyridine (3 eq.) were dissolved in anhydrous DCM (2-4 ml) in an oven-dried round bottom flask. Carboxylic acid (**91**) (3 eq.) dissolved in DCM was added at 0°C, the reaction mixture was allowed to warm to RT and stirred for 12 h. The reaction mixture was diluted with DCM (3x), washed with 0.1N HCl and brine, dried over Na_2SO_4 and concentrated under reduced pressure. The crude mixture was purified using column chromatography (SiO_2, 5-25% EtOAc in hexanes) to yield products as clear oils in 50-70% yield.

Preparation of benzyl protected methyl ester (105): To a stirred solution of 3-phenolic methyl ester **89** (1eq., 6.5 mmol) in acetone (30 mL), was added potassium carbonate (anhydrous, 6 eq., 39 mmoL) followed by benzyl bromide (1.2 eq., 7.9 mmol). The reaction mixture was refluxed until methyl ester was consumed (6h). The mixture was filtered over a celite pad, washed with EtOAC (30 mL), and concentrated. The crude residue was purified by column chromatography on silica gel (5% EtOAC in hexanes) to afford pure product as a clear oil in excellent yield (85%).

Preparation of benzyl protected 3' hydroxybenzoic acid (106): To a stirred solution of ester (**105**) (3.7 mmol) in THF (30 mL) was added potassium hydroxide (aq., 20%; 20 mL). The reaction mixture was stirred at room temperature for 12 hr at which time it was neutralized with portion-wise additions of 3N HCl and then the pH was reduced to ~1 using 1N HCl. The aqueous mixture was washed with EtOAc (3X100 mL). The combined organic fractions were dried (Na_2SO_4), filtered, and concentrated under reduced pressure. The crude residue was purified by column chromatography on silica gel (30-50% EtOAC in hexanes) to afford pure product as a white solid in good yield (70%).

Preparation of analogue 109: To a solution of benzyl-protected ester **108** (0.15 mmoL) in MeOH:THF (2:1, 6 mL) was added palladium hydroxide (10% on carbon; 10 mg). The mixture was sealed with a rubber septum, sequentially purged with argon and hydrogen, and stirred under positive hydrogen pressure (1 atm) at RT for 18 h. The mixture was filtered through a Celite pad, rinsed with EtOAC (10 mL) and concentrated under reduced pressure. The crude residue was purified using column chromatography (SiO$_2$, 10−40% EtOAc in hexanes) to yield **109** in 75% yield.

Preparation of TMS protected Inhoffen Lythgoe diol (107): To a solution of Inhoffen Lythgoe diol **75** (0.2 g, 0.9 mmol) in anhydrous DCM (10 ml), triethylamine (0.15 ml, 1.1 mmol), dimethylaminopyridine (0.004 g, 0.04 mmol) and TMSCl (0.127 ml, 0.99 mmol) were added and stirred overnight. The reaction mixture was diluted with DCM, washed with water, dried over Na$_2$SO$_4$ and concentrated under reduced pressure. Purification using column chromatography (SiO$_2$, EtOAc in hexanes) yielded pure product as clear oil in 49% yield.

(1*R*,3a*R*,4*S*,7a*R*)-1-isopropyl-7a-methyloctahydro-1H-inden-4-yl 3-hydroxybenzoate (93): ^{1}H NMR (500 MHz, CDCl$_3$) δ 7.65 (m, *J* = 7.8, 1.2 Hz, 1H), 7.58 (m, *J* = 2.6, 1.2 Hz, 1H), 7.35 (m, *J* = 7.9, 2.2 Hz, 1H), 7.07 (m, *J* = 8.1, 2.4, 1.0 Hz, 1H), 5.42 (m, *J* = 2.7 Hz, 1H), 5.36 (s, 1H), 2.13 − 2.04 (m, 2H), 2.01 (dd, *J* = 14.5, 3.8 Hz, 1H), 1.84 (m, *J* = 21.5, 18.5, 9.3, 5.3 Hz, 3H), 1.56 (m, *J* = 20.7, 14.0, 10.9, 7.3, 3.6 Hz, 7H), 1.50 − 1.38 (m, 1H), 1.36 − 1.30 (m, 1H), 1.26 − 1.18 (m, 1H), 1.06 (d, *J* = 2.2 Hz, 4H), 0.98 (dd, *J* = 6.5, 2.2 Hz, 3H), 0.88 (dd, *J* = 6.6, 2.2 Hz, 3H). ^{13}C NMR (126 MHz, CDCl$_3$) δ 166.5, 155.8, 132.4, 129.7, 122.0, 119.9, 116.3, 72.6, 58.5, 51.6, 41.9, 39.8, 30.7, 30.5, 29.7, 27.3, 23.0, 22.7, 22.4, 18.0, 13.7. IR (film) υ$_{max}$ 3430 (br s), 2956, 2939, 2868, 2858, 1700, 1684, 1601, 1589, 1294, 1217, 1160, 1110, 946, 756, 680, 669. DART -HRMS: m/z calculated for C$_{20}$H$_{28}$O$_3$NH$_4$: 334.2382 [M+NH$_4$]$^+$. Found: 334.2373.

(1R,3aR,4S,7aR)-7a-methyl-1-((R)-pentan-2-yl)octahydro-1H-inden-4-yl 3-hydroxy-benzoate (94): ^{1}H NMR (500 MHz, CDCl$_3$) δ 7.65 (m, J = 7.6, 2.9, 1.5 Hz, 1H), 7.59 (p, J = 1.9 Hz, 1H), 7.34 (m, J = 7.9, 2.0 Hz, 1H), 7.11 – 7.05 (m, 1H), 5.51 (s, 1H), 5.45 – 5.40 (m, 1H), 2.13 – 2.06 (m, 1H), 1.92 – 1.77 (m, 2H), 2.01 (m, J = 12.9, 5.1, 2.7 Hz, 1H), 1.69 – 1.50 (m, 5H), 1.50 – 1.34 (m, 3H), 1.29 (t, J = 2.3 Hz, 3H), 1.21 – 1.11 (m, 1H), 1.06 (p, J = 2.7 Hz, 4H), 0.95 (m, J = 6.5, 2.1 Hz, 3H), 0.93 – 0.87 (m, 3H). ^{13}C NMR (126 MHz, CDCl$_3$) δ 166.6, 155.9, 132.5, 129.8, 122.1, 120.1, 116.5, 72.8, 56.7, 51.8, 42.1, 40.1, 38.3, 35.4, 30.7, 29.9, 27.3, 22.9, 19.4, 18.8, 18.2, 13.8. IR (film) υ$_{max}$ 3400 (br s), 2976, 2947, 2867, 2866, 1684, 1600, 1579, 1296, 1215, 1145, 1110, 946, 756, 680, 659. DART-HRMS: m/z calculated for C$_{22}$H$_{32}$O$_3$NH$_4$: 362.2695 [M+NH$_4$]$^+$. Found: 362.2714.

(1R,3aR,4S,7aR)-7a-methyl-1-((R)-5-methylhexan-2-yl)octahydro-1H-inden-4-yl 3-hydroxybenzoate (95): ^{1}H NMR (500 MHz, CDCl$_3$) δ 7.65 (d, J = 7.5 Hz, 1H), 7.59 (d, J = 6.8 Hz, 1H), 7.35 (t, J = 8.0 Hz, 1H), 7.13 – 7.03 (m, 1H), 5.42 (m, J = 4.1, 2.2 Hz, 1H), 2.08 (m, J = 11.3, 3.9 Hz, 1H), 2.05 – 1.97 (m, 1H), 1.93 – 1.71 (m, 2H), 1.56 (m, J = 18.9, 12.5, 8.9, 4.5 Hz, 4H), 1.49 – 1.30 (m, 6H), 1.28 – 1.09 (m, 4H), 1.05 (s, 3H), 0.96 (d, J = 13.2, 6.2 Hz, 3H), 0.91 (dd, J = 6.6, 1.9 Hz, 6H). ^{13}C NMR (126 MHz, CDCl$_3$) δ 166.3, 155.7, 132.4, 129.7, 122.0, 119.9, 116.3, 72.6, 58.5, 51.6, 41.9, 39.8, 35.5, 31.9, 30.9, 30.7, 30.5, 29.7, 27.3, 23.0, 22.7, 22.4, 18.0, 13.7. IR (film) υ$_{max}$ 3385 (br s), 3019, 2951, 2935, 2868, 1689, 1599, 1589, 1466, 1453, 1366, 1344, 1295, 1215, 1157, 1106, 1075, 1062, 982, 946, 886, 755, 680, 668. DART-HRMS: m/z calculated for C$_{24}$H$_{36}$O$_3$NH$_4$: 391.2848 [M+NH$_4$]$^+$. Found: 391.2869.

(1R,3aR,4S,7aR)-7a-methyl-1-((R)-4-phenylbutan-2-yl)octahydro-1H-inden-4-yl 3-hydroxybenzoate (96): ^{1}H NMR (500 MHz, CDCl$_3$) δ 7.64 (d, J = 7.6 Hz, 1H),

66

7.60 – 7.57 (m, 1H), 7.33 (dd, *J* = 21.9, 7.9 Hz, 3H), 7.22 – 7.17 (m, 3H), 7.08 (dd, *J* = 8.1, 2.6 Hz, 1H), 5.57 (s, 1H), 5.42 (q, *J* = 2.7 Hz, 1H), 2.73 (m, *J* = 13.2, 11.2, 4.8 Hz, 1H), 2.50 (m, *J* = 13.4, 10.8, 6.0 Hz, 1H), 2.11 (m, *J* = 12.7, 3.5 Hz, 1H), 2.02 (m, *J* = 14.1, 2.5 Hz, 1H), 1.96 – 1.71 (m, 4H), 1.67 (q, *J* = 4.1 Hz, 1H), 1.64 – 1.45 (m, 4H), 1.44 – 1.33 (m, 1H), 1.29 (s, 2H), 1.24 (d, *J* = 7.3 Hz, 1H), 1.07 (d, *J* = 6.6 Hz, 3H), 1.05 (s, 3H). ^{13}C NMR (126 MHz, CDCl$_3$) δ 166.4, 155.8, 143.3, 132.3, 129.7, 128.4, 128.3, 125.5, 121.9, 120.0, 116.3, 72.6, 56.2, 51.6, 42.0, 40.0, 37.9, 35.3, 32.5, 30.5, 27.0, 22.7, 18.6, 18.0, 13.6. IR (film) υ$_{max}$ 3170, 2949, 2917, 2849, 1692, 1496, 1484, 1453, 1250, 1224, 756. DART-HRMS: m/z calculated for C$_{27}$H$_{33}$O$_3$: 405.2430 [M-H]$^+$. Found: 405.2437; calculated for C$_{27}$H$_{34}$O$_3$NH$_4$: 424.2852, [M+NH4]$^+$. Found: 424.2869.

(1*R*,3a*R*,4*S*,7a*R*)-1-((*R*)-sec-butyl)-7a-methyloctahydro-1H-inden-4-yl 3-hydroxy-benzoate (98): ^{1}H NMR (500 MHz, CDCl$_3$) δ 7.65 (m, *J* = 7.7, 1.2 Hz, 1H), 7.61 (dd, *J* = 2.6, 1.5 Hz, 1H), 7.38 – 7.31 (m, 1H), 7.08 (m, *J* = 8.1, 2.5, 1.0 Hz, 1H), 5.57 (s, 1H), 5.43 (q, *J* = 2.8 Hz, 1H), 2.12 – 2.06 (m, 1H), 2.05 – 1.98 (m, 1H), 1.91 – 1.77 (m, 2H), 1.64 – 1.43 (m, 6H), 1.41 – 1.30 (m, 2H), 1.25 (m, *J* = 7.9, 4.7, 2.6 Hz, 1H), 1.21 – 1.07 (m, 2H), 1.06 (s, 3H), 0.95 (d, *J* = 6.4 Hz, 3H), 0.89 – 0.83 (m, 3H). ^{13}C NMR (126 MHz, CDCl$_3$) δ 166.7, 156.0, 132.5, 129.9, 122.1, 120.2, 116.6, 72.9, 56.1, 51.8, 42.1, 40.1, 36.8, 30.7, 29.9, 28.3, 27.1, 22.2, 18.2, 18.2, 13.8. IR (film) υ$_{max}$ 3329 (br s), 3146, 3017, 2950, 2931, 2867, 1671, 1613, 1584, 1485, 1466, 1250, 1208, 1137, 1088, 1 061, 1032, 937, 917, 755, 702, 666. DART-HRMS: m/z calculated for C$_{21}$H$_{30}$O$_3$NH$_4$: 348.2539 [M+NH$_4$]$^+$. Found: 348.2564.

(1*R*,3a*R*,4*S*,7a*R*)-1-((*R*)-hexan-2-yl)-7a-methyloctahydro-1H-inden-4-yl 3-hydroxy-benzoate (99): ^{1}H NMR (500 MHz, CDCl$_3$) δ 7.65 (d, *J* = 7.6 Hz, 1H), 7.58 (d, *J* = 2.6 Hz, 1H), 7.39 – 7.31 (m, 1H), 7.12 – 7.04 (m, 1H), 5.43 (s, 1H), 5.41 – 5.31 (m, 1H), 2.14 – 2.05 (m, 1H), 2.05 – 1.96 (m, 1H), 1.92 – 1.75 (m, 2H), 1.74 – 1.51 (m, 5H), 1.51 –

1.30 (m, 4H), 1.29 – 1.08 (m, 9H), 1.06 (s, 3H), 1.02 – 0.96 (m, 3H), 0.89 (t, J = 3.9 Hz, 4H). ^{13}C NMR (126 MHz, CDCl$_3$) δ 166.4, 155.9, 132.5, 129.9, 122.2, 120.1, 116.5, 72.8, 58.7, 51.8, 42.1, 40.0, 30.9, 30.7, 29.9, 27.5, 23.2, 22.9, 22.6, 22.2, 18.2, 14.2, 13.9. IR (film) υ_{max} 3305 (br s), 3234, 2951, 2931, 2867, 2775, 1610, 1584, 1485, 1466, 1364, 1346, 1250, 1208, 1137, 1086, 1062, 1032, 937, 917, 755, 715, 656. DART-HRMS: m/z calculated for C$_{23}$H$_{34}$O$_3$NH$_4$: 376.2887 [M+NH$_4$]$^+$. Found: 376.2891

(1R,3aR,4S,7aR)-1-((R)-heptan-2-yl)-7a-methyloctahydro-1H-inden-4-yl 3-hydroxy-benzoate (100): ^{1}H NMR (500 MHz, CDCl$_3$) δ 7.65 (dd, J = 7.5, 1.6 Hz, 2H), 7.35 (t, J = 8.0 Hz, 1H), 7.13 – 7.03 (m, 1H), 5.79 (s, 1H), 5.42 (dd, J = 4.1, 2.2 Hz, 1H), 2.08 (m, J = 11.3, 3.9 Hz, 1H), 2.05 – 1.97 (m, 1H), 1.93 – 1.71 (m, 2H), 1.56 (m, J = 18.9, 12.5, 8.9, 4.5 Hz, 4H), 1.49 – 1.30 (m, 6H), 1.28 – 1.09 (m, 7H), 1.05 (s, 3H), 0.96 (dd, J = 13.2, 6.2 Hz, 3H), 0.91 (t, J = 7.1 Hz, 3H). ^{13}C NMR (126 MHz, CDCl$_3$) δ 166.7, 156.0, 132.4, 129.9, 122.1, 120.2, 116.6, 72.9, 56.6, 51.8, 42.1, 40.1, 35.8, 35.6, 32.5, 30.7, 27.2, 25.9, 22.9, 22.9, 18.8, 18.2, 14.3, 13.8. IR (film) υ_{max} 3375 (br s), 3138, 3011, 2951, 2931, 2867, 1613, 1584, 1485, 1466, 1364, 1346, 1250, 1208, 1137, 1086, 1062, 1032, 937, 917, 755, 704, 657. DART-HRMS: m/z calculated for C$_{24}$H$_{36}$O$_3$NH$_4$: 390.3008 [M+NH$_4$]$^+$. Found: 390.3045.

(1R,3aR,4S,7aR)-7a-methyl-1-((R)-4-methylpentan-2-yl)octahydro-1H-inden-4-yl 3-hydroxybenzoate (101): ^{1}H NMR (500 MHz, CDCl$_3$) δ 7.65 (d, J = 7.5 Hz, 1H), 7.59 (d, J = 6.8 Hz, 1H), 7.35 (q, J = 7.9, 7.3 Hz, 1H), 7.07 (d, J = 7.8 Hz, 1H), 5.42 (s, 2H), 2.17 – 2.08 (m, 1H), 2.02 (d, J = 14.7 Hz, 1H), 1.94 – 1.77 (m, 2H), 1.55 (m, J = 52.3, 39.8, 11.7, 6.8 Hz, 9H), 1.22 – 1.10 (m, 1H), 1.08 (s, 3H), 1.06 – 0.97 (m, 1H), 0.93 (d, J = 6.7 Hz, 3H), 0.90 (d, J = 7.3 Hz, 4H), 0.87 – 0.82 (m, 3H). ^{13}C NMR (126 MHz, CDCl$_3$) δ 166.5, 155.9, 132.5, 129.8, 122.1, 120.1, 116.5, 72.8, 57.6, 51.8, 45.7, 42.2, 40.2, 33.7, 30.7, 29.9, 27.5, 24.9, 22.9, 21.5, 18.8, 18.2, 13.8. IR (film) υ_{max} 3400 (br s), 3215, 2953,

68

2941, 2867, 2775, 1610, 1584, 1485, 1466, 1364, 1301, 1250, 1208, 1137, 1086, 1062, 1032, 937, 917, 715. DART-HRMS: m/z calculated for $C_{23}H_{34}O_3NH_4$: 376.2853 $[M+NH_4]^+$. Found: 376.2868.

(1R,3aR,4S,7aR)-7a-methyl-1-((R)-nonan-2-yl)octahydro-1H-inden-4-yl 3-hydroxybenzoate (102): ^{1}H NMR (500 MHz, CDCl$_3$) δ 7.65 (dd, J = 7.8, 1.3 Hz, 1H), 7.59 (dd, J = 2.6, 1.5 Hz, 1H), 7.34 (t, J = 7.9 Hz, 1H), 7.10 – 7.04 (m, 1H), 5.45 (s, 2H), 5.43 (s, 1H), 2.12 – 2.05 (m, 2H), 2.05 – 1.98 (m, 1H), 1.93 – 1.76 (m, 3H), 1.65 (s, 2H), 1.62 – 1.41 (m, 9H), 1.40 – 1.19 (m, 7H), 1.04 (d, J = 10.2 Hz, 3H), 0.99 (t, J = 6.9 Hz, 3H), 0.89 (dd, J = 6.8, 2.0 Hz, 3H). ^{13}C NMR (126 MHz, CDCl$_3$) δ 166.7, 156.1, 132.5, 129.8, 122.1, 120.2, 116.5, 72.9, 58.7, 51.8, 42.1, 40.0, 33.9, 30.9, 30.7, 30.3, 29.9, 29.8, 29.6, 27.5, 22.9, 22.6, 18.8, 18.2, 13.9, 13.8. IR (film) υ_{max} 3456 (br s), 2992, 2950, 2926, 2907, 1712, 1699, 1485, 1466, 1364, 1346, 1250, 1208, 1137, 1086, 1062, 1032, 937, 917, 715, 656. DART-HRMS: m/z calculated for $C_{26}H_{40}O_3NH_4$: 418.3982 $[M+NH_4]^+$. Found: 418.3301.

(1R,3aR,4S,7aR)-1-((R)-4,4-dimethylpentan-2-yl)-7a-methyloctahydro-1H-inden-4-yl 3-hydroxybenzoate (103): ^{1}H NMR (500 MHz, Chloroform-d) δ 7.79 – 7.54 (m, 2H), 7.44 – 7.31 (m, 1H), 7.18 – 6.99 (m, 1H), 5.80 (d, J = 12.1 Hz, 1H), 5.42 (s, 1H), 2.17 – 2.07 (m, 1H), 2.07 – 1.98 (m, 1H), 1.97 – 1.67 (m, 3H), 1.66 – 1.43 (m, 6H), 1.37 (dd, J = 14.4, 7.0 Hz, 2H), 1.25 (d, J = 10.1 Hz, 1H), 1.20 – 1.11 (m, 1H), 1.09 (d, J = 1.7 Hz, 1H), 1.06 – 0.99 (m, 1H), 0.99 – 0.85 (m, 11H). ^{13}C NMR (126 MHz, CDCl$_3$) δ 166.5, 155.8, 132.3, 129.7, 121.9, 120.0, 116.4, 72.8, 57.8, 51.7, 49.7, 42.0, 40.0, 32.4, 31.1, 30.5, 30.4, 30.4, 29.7, 27.7, 22.7, 22.6, 18.0, 13.4. IR (film) υ_{max} 3430 (br s), 3146, 3017, 2950, 2931, 2867, 1671, 1613, 1584, 1485, 1466, 1374, 1346, 1250, 1208, 1137, 1088, 1061, 1032, 937, 917, 755, 702, 666. DART-HRMS: m/z calculated for $C_{24}H_{36}O_3NH_4$: 390.3008 $[M+NH_4]^+$. Found: 390.3030.

(1*R*,3a*R*,4*S*,7a*R*)-1-((*R*)-4-ethylhexan-2-yl)-7a-methyloctahydro-1H-inden-4-yl 3-hydroxybenzoate (104): ¹H NMR (500 MHz, CDCl₃) δ 7.65 (m, *J* = 7.7, 1.1 Hz, 1H), 7.58 (dd, *J* = 2.7, 1.5 Hz, 1H), 7.35 (m, *J* = 7.9, 2.1 Hz, 1H), 7.07 (m, *J* = 8.1, 2.7, 1.1 Hz, 1H), 5.42 (q, *J* = 2.9 Hz, 1H), 5.29 (d, *J* = 4.4 Hz, 1H), 2.16 – 1.98 (m, 2H), 1.98 – 1.76 (m, 2H), 1.64 – 1.29 (m, 8H), 1.28 – 1.04 (m, 8H), 1.01 – 0.79 (m, 10H). ¹³C NMR (126 MHz, CDCl₃) δ 166.5, 155.8, 132.6, 129.84122.2, 120.0, 116.5, 72.8, 57.8, 51.8, 42.2, 39.8, 37.4, 33.6, 30.7, 29.9, 27.6, 26.8, 24.6, 22.9, 18.9, 18.2, 13.9, 11.5, 10.2. IR (film) υ$_{max}$ 3324 (br s), 3215, 2953, 2941, 2867, 2775, 1610, 1584, 1485, 1466, 1364, 1341, 1250, 1208, 1137, 1086, 1062, 1032, 937, 917, 715, 656. DART-HRMS: m/z calculated for $C_{25}H_{38}O_3NH_4$: 404.3208 [M+NH₄]⁺. Found: 404.3230.

(1*R*,3a*R*,4*S*,7a*R*)-1-((2*R*,5*R*)-5,6-dimethylheptan-2-yl)-7a-methyloctahydro-1H-inden-4-yl 3-hydroxybenzoate (109): ¹H NMR (500 MHz, CDCl₃) δ 7.62 (m, 1H), 7.58 (m, 1H), 7.32 (m, 1H), 7.05 (m, 1H), 5.58 (m, 1H), 5.39 (m, 1H), 2.05 (m, 1H), 1.98 (m, 1H), 1.81 (m, 2H), 1.65 (m, 1H), 1.53 (m, 5H), 1.40 (m, 4H), 1.29 (m, 8H), 1.02 (s, 3H), 0.93 (d, J = 6.6 Hz, 3H), 0.86 (d, J = 6.9 Hz, 3H), 0.78 (dd, J = 6.8, 3.4 Hz, 6H). 13C NMR (126 MHz, CDCl₃) δ 166.4, 155.7, 132.2, 129.6, 121.9, 119.9, 116.3, 72.6, 56.2, 51.5, 41.9, 39.8, 39.0, 35.8, 33.4, 31.4, 30.5, 30.4, 29.7, 27.0, 22.6, 20.5, 18.7, 18.0, 17.5, 15.4, 13.5. IR (film) υ$_{max}$ 3400, 2956, 2939, 2868, 2858, 1700, 1684, 1601, 1589, 1294, 1217, 1160, 1110, 946, 756, 680, 669. DART-HRMS: m/z calculated for $C_{26}H_{40}O_3NH_4$: 418.3321 [M+NH₄]⁺. Found: 418.3306.

(1*R*,3a*R*,4*S*,7a*R*)-1-((2*R*,5*S*,*E*)-5,6-dimethylhept-3-en-2-yl)-7a-methyloctahydro-1H-inden-4-yl 3-hydroxybenzoate (111): ¹H NMR (500 MHz, CDCl₃) δ 7.61 (m, 2H), 7.31 (m, 1H), 7.06 (m, 1H), 5.98 (br s, 1H), 5.39 (m, 1H), 5.18 (m, 2H), 2.01 (m, 3H), 1.81 (m, 2H), 1.68 (m, 1H), 1.49 (m, 6H), 1.24 (m, 4H), 1.15 (m, 1H), 1.04 (m, 3H), 1.02 (d, J = 6.5 Hz, 3H), 0.91 (d, J = 6.8 Hz, 3H), 0.73 (m, 6H). 13C NMR (126 MHz, CDCl₃) δ 162.0,

70

136.8, 127.9, 127.4, 125.1, 122.4, 120.7, 111.8, 108.2, 72.5, 69.4, 56.7, 56.5, 52.6, 51.6, 42.0, 41.8, 40.4, 39.9, 39.5, 39.4, 35.9, 35.9, 35.4, 35.2, 33.6, 30.6, 28.0, 27.1, 27.0, 23.8, 23.7, 22.8, 22.6, 22.5, 18.6, 18.5, 18.0, 17.4, 13.5, 13.4. IR (film) υ_{max} 3184, 3146, 3017, 2950, 2931, 2867, 1671, 1613, 1584, 1485, 1466, 1374, 1346, 1325, 1301, 1250, 1208, 1137, 1088, 1061, 1032, 937, 917, 883, 800, 755, 702, 666. DART-HRMS: m/z calculated for $C_{26}H_{38}O_3NH_4$: 416.3165 $[M+NH_4]^+$. Found: 416.3171.

(1R,3aR,4S,7aR)-1-((S)-1-hydroxypropan-2-yl)-7a-methyloctahydro-1H-inden-4-yl 3-hydroxybenzoate (113): ^{1}H NMR (500 MHz, CDCl$_3$) δ 7.63 (d, J = 7.6 Hz, 1H), 7.56 (d, J = 2.1 Hz, 1H), 7.34 (t, J = 7.8 Hz, 1H), 7.09 (dd, J = 8.2, 2.8 Hz, 1H), 5.66 (s, 1H), 5.39 (d, J = 3.3 Hz, 1H), 4.76 (s, 1H), 4.32 (dd, J = 10.8, 3.6 Hz, 1H), 4.12 (m, J = 17.6, 11.1, 5.6 Hz, 1H), 2.10 (m, J = 13.3, 3.4 Hz, 1H), 2.04 − 1.85 (m, 2H), 1.83 − 1.74 (m, 3H), 1.61 (m, J = 8.9, 5.0 Hz, 4H), 1.44 (m, J = 14.2, 6.1, 4.8 Hz, 2H), 1.14 (d, J = 6.6 Hz, 3H), 0.97 (d, J = 7.8 Hz, 3H). ^{13}C NMR (126 MHz, CDCl$_3$) δ 166.7, 156.1, 132.1, 129.8, 122.0, 120.3, 116.4, 74.768, 70.0, 53.1, 51.0, 42.2, 39.6, 35.8, 30.4, 26.2, 22.6, 17.6, 17.4, 13.0. IR (film) υ_{max} 3621, 3464, 3385 (br s), 3019, 2951, 2868, 1599, 1589, 1466, 1453, 1366, 1295, 1215, 1157, 1106, 1075, 1062, 982, 946, 886, 755, 680, 668. DART-HRMS: m/z calculated for $C_{20}H_{27}O_3$: 315.1960 $[M-OH]^+$, Found: 315.1983.

3. Biological evaluation

3.1 Experimental protocols

Cell line maintenance and general protocols: C3H10T1/2 cells were purchased from American Type Culture Collection (ATCC). ASZ001 cells were a generous gift of Dr. Ervin Epstein (Children's Hospital of Oakland Research Institute). Gibco by Life Technologies culture media was purchased from ABI. C3H10T1/2 cells were cultured in BME (Gibco) supplemented with 10% FBS (Atlanta Biologicals, Premium Select), 1% L-glutamine (Cellgro; 200 nM solution), and 0.5% penicillin/streptomycin (Cellgro; 10,000

71

l.U./mL penicillin, 10,000 µg/mL). ASZ001 cells were cultured in 154CF media, supplemented with 2% FBS (chelexed, heat-inactivated), 1.0% penicillin/streptomycin, and a final concentration of 0.05mM $CaCl_2$. Cells were maintained using the media described above (denoted "growth media"). Media denoted as "low FBS" contained 0.5% FBS and the same percentage of other supplements as specified for growth media ("low FBS" media with this percentage FBS was used for C3H10T1/2 cell assays). Following plating and 24 hr growth period, no FBS supplemented media was used for ASZ001 cell assays. All cells were grown in Corning Cell Culture, canted neck T75 or T150 flasks (Fisher Scientific) in an Autoflow IR water-jacketed CO_2 incubator (37°C, 5% CO_2). Experiments with C3H10T1/2 cells were performed in BD Falcon sterile 60 mm dishes. 500,000 cells at ~80% confluence were plated in 5 mL media. Experiments with ASZ001 cells were performed in BD Falcon 35 mm dishes or in 6-well, 35mm plates. For the ASZ001 line, 300,000 cells at ~80% confluence were plated in 2 mL media. DMSO was used as solvent to prepare all drug solutions and the final DMSO concentration did not exceed 0.3%. 20α-hydroxycholesterol, 22(*S*)-hydroxycholesterol (Oxysterol/Oxy) and VD3, for biological studies, were purchased from Sigma-Aldrich.

Analysis of Hh and VDR target gene expression in C3H10T1/2 cells: Cells were plated in growth media at ~80% confluence. Once cells reached confluence (approximately 24 hr), growth media was removed and replaced with low FBS media (5 mL). This was followed by addition of Oxy, Oxy and analogue, or DMSO (vehicle control). Cells were incubated (37°C, 5% CO_2) for 24 hr period and RNA was isolated and evaluated by qRT-PCR analysis as described previously in Chapter 2. Data was analyzed using GraphPad Prism 5 and IC_{50} values computed as mean ± SEM from at least three separate experiments performed in triplicate.

Analysis of Hh and VDR target gene expression in murine-derived BCC (ASZ001) cells: Cells were plated in growth media at ~80% confluence. After 24 hr, growth media was removed and replaced with no FBS media (2 mL). Cells were then incubated for an additional 24 hrs. After this time, addition of DMSO (vehicle control) or analogues was performed. Cells were incubated ($37°C$, 5% CO_2) for 48 hr and RNA was isolated and evaluated by qRT-PCR analysis as described previously. Data was analyzed using GraphPad Prism 5 and IC_{50} values computed as mean ± SEM from at least three separate experiments performed in triplicate.

3.2 Results & discussion
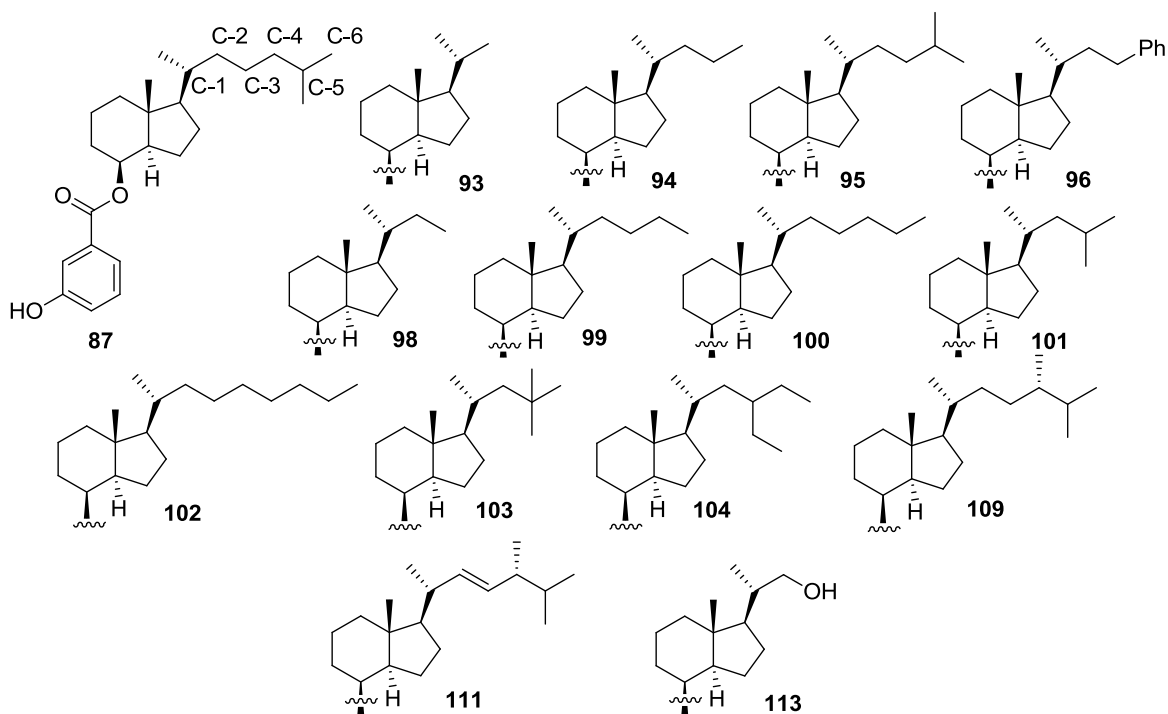
Figure 4. VD3 based hybrid side chain analogues.

This series of hybrid side chain analogues prepared for evaluation can be broadly categorized into two groups, i.e. hydrocarbon containing and non-hydrocarbon containing side chain analogues (Figure 4). Further, the first group has representatives

73

for linear alkyl side arms (**93**, **94**, **98**, **99**, **100** and **102**), branched alkyl chains (**95**, **101**, **103**, **104**, **109**) branched alkenyl side chains (**111**) as well as an aromatic side chain derivative (**96**). On the other hand, analogue (**113**) is the only non-hydrocarbon containing side chain analogue.

The initial evaluation of all hybrid VD3 side chain analogues as Hh pathway inhibitors was performed at a single dose (5 µM) by monitoring endogenous Gli1 mRNA levels in C3H10T1/2 cells following standard assay protocols [108, 111]. At this concentration, excluding **99**, **101**, **102**, and **103**, other derivatives maintained similar potency (0.5-10% Gli1 mRNA expression). Moreover, inhibitory activities of the latter were comparable to the previously identified VD3-based lead scaffold **87** and improved compared to that of VD3 (Table 1). Thereafter, relative mRNA expression levels of Gli1 were examined after treatment of C3H10T1/2 cells with a lower concentration (2.5 µM) (Table 1). At this dose, differences between assay readouts from treatments with different analogues were more pronounced and thus it was possible to identify analogues that maintained potent anti-Hh activity even at a lower concentration. Based on the data from treatments at two different doses, the optimum length of linear side chain proved to be critical in maintaining potent Gli1 inhibitory activity. Derivatives with shorter **93**, **94**, **98** and **99** or longer **102** chain lengths than the naturally occurring six-carbon side arm present in VD3 suffered losses in potency. In agreement with this general trend, **100** retained Hh antagonistic activity similar to the lead structure **87** in this cellular model. Several interesting effects on the inhibitory activity profile were observed on introduction of branched side chains. Analogues with very short branched chains **101** and **103** were less active than the parent scaffold. However, iso and ante-iso branching incorporated into five-carbon long side chain (**95** and **104** respectively) salvaged the loss in potency seen in the unbranched derivative with a comparable length side arm (**99**). In

74

terms of favorable features unraveled so far, **109** had a combination of extended six-carbon link primary chain along with terminal and non-terminal branching in the same molecule. Nonetheless, instead of the expected synergistic outcome of all these features incorporated in one derivative, deleterious effects on the level of Gli1 inhibition were observed. Interestingly, an additional unsaturation present in the side chain of this molecule helped to restore the diminished activity. Consequently, analogue **111** with comparatively rigid side arm exhibited slightly greater than two-fold improvement in activity as compared to relatively flexible analogue **109**. Finally, no improvement in activity was evident for the aromatic side chain containing derivative **96** or hydroxyl side chain analogue **113**. It is unclear whether the loss of activity in these cases can be attributed singularly to the planar/polar nature of these substituents respectively. Analysis of specific contributions of the length of the connecting carbon chains extending these functionalities spatially remains the subject of further investigation.

Table 2. Gli1 inhibitory activity in C3H10T1/2 cells.

Analogue	Relative Gli1 mRNA (%)[a]	
	5 µM treatment	2.5 µM treatment
VD3	31.7 ± 0.7	71.4 ± 2.1
87	1.9 ± 0.5	15 ± 2.0
93	1.31 ± 0.1	49.8 ± 1.8
94	7.7 ± 5.5	69.8 ± 27.2
95	2.9 ± 0.3	23.0 ± 4.3
96	7.2 ± 1.8	88.4 ± 55.4
98	0.7 ± 0.3	33.9 ± 13.1
99	38.4 ±4.15	52.3 ± 13.2
100	1.1 ± 0.3	17.3 ± 3.6
101	74.4 ± 0.7	90.1 ± 12.5
102	29.9 ± 16.1	54.4 ± 9.7
103	32.4 ± 28.93	49.1 ± 19.6
104	0.49 ± 0.2	17.4 ± 4.5
109	9.2 ± 6.1	40.4 ± 9.5
111	2.2 ± 0.5	15.6 ± 0.9
113	10.2 ± 6.1	56.9 ± 10.2

[a]Relative Gli1 mRNA levels when oxysterol treatment is equivalent to 100%.

اقرة للاستشارات

www.manaraa.com

After establishing the effects on Hh inhibitory activity by varying the nature of CD-ring appendages and thereby identifying favorable modifications, we directed our efforts towards assessing their effects on the selectivity profile of representative analogues. Previously, VD3 was shown to be a non-selective inhibitor of the Hh pathway, presumably due to its propensity to undergo metabolic transformation to form calcitriol and activate canonical VDR signaling [108]. It is noteworthy that as per the known route to such biotransformations, hydroxylations of the A-ring and the CD-ring side chain are required to yield ligands for VDR activation (Chapter 2, Figure 3). Since the modifications of A-ring led to improved selectivity for potent analogue **87**, we were interested in studying the repercussions of further altering the side chain region of this lead compound.

Table 3. VDR related activity mediated by hybrid side chain analogues.

Analogue	Relative Cyp24A1 mRNA[b]	VDR Binding Conc.
VD3	4004 ± 56	>100 µM
87	10.5 ± 2.1	>100 µM
93	0.7 ± 0.2	>100 µM
94	4.8 ± 0.9	>100 µM
95	2.8 ± 0.03	>100 µM
96	3.8 ± 0.1	>100 µM
98	1.1 ± 0.3	>100 µM
99	4.9 ± 0.5	>100 µM
100	4.4 ± 0.03	>100 µM
101	2.5 ± 1.0	>100 µM
102	3.8 ± 0.7	>100 µM
103	7.9 ± 1.4	>100 µM
104	0.6 ± 0.02	>100 µM
109	1.1 ± 0.02	>100 µM
111	6.8 ± 0.02	>100 µM
113	0.4 ± 0.1	>100 µM

[b]Values represent Cyp24A1 mRNA expression level in cultured cells when DMSO set as 1.0.

None of these derivatives directly bind to VDR as measured in the previously described *in vitro* VDR binding assay even at a high concentration of 100 µM (Table 3). Since C3H10T1/2 cells respond to VDR activation with robust up-regulation of Cyp24A1, a well-characterized target gene of canonical vitamin D signaling; we then studied off-

76

target effects mediated due to potential metabolism of VD3 analogues in this system (Table 3). Overall, every hybrid side chain analogue maintained the selectivity for Hh inhibition without concomitant activation of VDR signaling. Moreover, analogues such as **95**, **100**, **104** and **111** afforded slightly improved selectivity over **87** while maintaining better potency for Hh inhibition. Based on the fact that changing the side chain region didn't have drastic consequences on the selectivity profile, it can be hypothesized that optimum changes to the A-ring region can suffice to mitigate side effects of the original VD3 scaffold. However, additional fine tuning of selectivity can be achieved by above noted alterations to the side chain region.

Previous studies evaluating Hh pathway inhibition in cultured cancer cells have suggested that the majority of *in vitro* cancer cell lines do not appropriately model *in vivo* Hh signaling. With this in mind, we sought to characterize VD3 and related analogues in a cell line, ASZ001, which has shown initial promise as *in vitro* model of oncogenic Hh signaling. The ASZ001 cell line was developed from a visible BCC tumor isolated from a *Ptch1*^{+/-} mouse [163]. These cells demonstrate loss of the wildtype Ptch1 allele, high baseline expression of Gli1, and cellular morphology similar to Hh-dependent BCC tumors. In addition, treatment of these cells with either Cyc or VD3 resulting in Gli1 down-regulation has been previously reported [110, 163]. Previous studies performed in this cell line demonstrated that Gli1 down-regulation by VD3 in ASZ001 was more robust and reproducible following a 48 h compound incubation [110]. Preliminary evaluation in our lab was consistent with a 48 h incubation period resulting in reproducible Gli1 down-regulation induced by GDC-0449 or Cyc. For this reason, all data presented from this cell line were obtained at this time point.

77
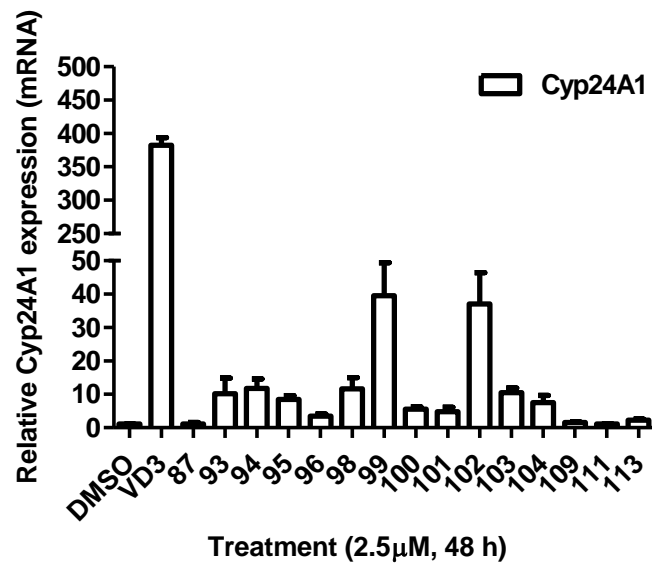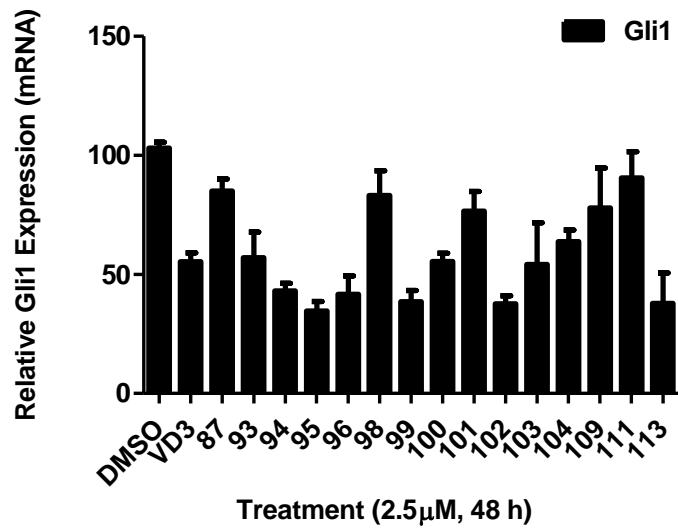
Figure 5. Hh specific activity of hybrid side chain analogues in ASZ001 cells.
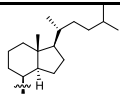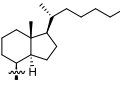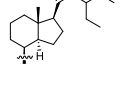
Initially, we evaluated the Hh specific activity of the hybrid side chain analogues in the ASZ001 cells at a single dose of 2.5 μM by quantifying relative mRNA expression levels of Hh responsive gene, Gli1, and VDR dependent gene, Cyp24A1, simultaneously (Figure 5). It had been previously established in our lab that the IC_{50} for VD3 down-regulation of Gli1 in ASZ001 cells correlated well with that obtained in the C3H10T1/2 fibroblasts, however; analogue **87** proves to be less effective in this model [113, 114].

78

Consistent with that observation, the extent of Gli1 downregulation in this cellular system by hybrid side chain derivatives was less than the levels observed in its MEF (C3H10T1/2) counterpart. The analogues demonstrating most prominent Hh inhibitory activity included **94**, **95**, **96**, **99**, **102** and **113**. While the selective and potent Hh antagonistic activity of **95** was consistent with its activity profile previously identified in C3H10T1/2 cells. It was intriguing to note that several of the more active analogues in ASZ001 cells such as linear side arm-containing analogues (**94**, **99** and **102**), hydroxylated side arm-containing analogue (**113**) and aromatic functional group containing (**96**) had demonstrated modest Hh inhibitory activities in C3H10T1/2 cells. Taking into account the comparatively higher Cyp24A1 expression mediated by **99** and **102**, the improved Hh inhibiton as a result of crosstalk between signaling cascades can be speculated. Next, although **96** and **113** did not demonstrate increased levels of Cyp24A1, these analogues caused excessive cell death at higher doses (5 μM and above) suggestive of additional non-specific mechanisms of toxicity. Nonetheless, the plausible reason for improved anti-Hh activity of **94** is unclear. Next, derivatives that maintained slightly less Gli1 inhibition than the above discussed analogues included **93**, **100**, **103** and **104**. While their Hh inhibitory activities were comparable to that of VD3, off-target effects via VDR signaling were minimal as depicted by low Cyp24A1 expression. Finally, analogues that failed to reduce Gli1 expression in ASZ001 included **98**, **101**, **109** and **111**. Once again, the drastic loss in activity of **111** in ASZ001 cells is in total contrast with its excellent potency observed in C3H10T1/2 cells. Taken together, there was a lack of definitive SAR trend in this cell based assay and further studies are required to corroborate the theories proposed to explain the discrepancies.

Based on the preliminary screening of active and specific Hh inhibitors, we decided to conduct further studies on analogues that exhibited an optimum

79

activity/selectivity ratio across both cellular systems. Therefore, we conducted concentration dependent analysis of Gli1 inhibitory potential of analogues **95**, **100** and **104** in both Hh signaling inducible MEF cells (C3H10T1/2) and murine BCC cells (ASZ001) (Figure 12). When tested in C3H10T1/2 cells, all three derivatives demonstrated low micromolar IC_{50} values for Gli1 downregulation. In ASZ001 cells, **95** maintained comparable low micromolar potency. Although, **100** and **104** retain Hh inhibitory activity, slightly higher IC_{50} values were recorded.

Table 4. Determination of IC_{50} values in C3H101/2 cells and ASZ001 cells.

Analogue	Structure	IC_{50} (µM)	
		C3H10T1/2	ASZ001
95		1.13 ± 0.56	1.61 ± 0.15
100		1.10 ± 0.37	6.57 ± 2.78
104		1.14 ± 0.45	4.98 ± 2.87

4. Conclusion

With the goal of identifying improved Hh antagonists, we studied the effects of modifying the side chain region of VD3. During the initial phase of this study, a VD3 based Hh selective lead compound (**87**, IC_{50} = 0.74 ± 0.1 µM) was identified in a parallel project. Subsequently, our investigation on side chain analogues of VD3 proceeded with altered CD-ring appendages installed on the novel VD3 based lead compound. A series of fourteen diverse side chain derivatives were prepared and evaluated in two different cellular models of Hh inhibition. Overall, linear or moderately branched hydrocarbon chains of five/six carbon links proved to be optimum for potent and selective anti-Hh

activity. Analogue **95** showed consistent improved performance in various cellular and other *in vitro* assays designed to determine Hh inhibition and VDR activation.

CHAPTER IV: Design, Synthesis and Evaluation of Itraconazole Analogues

Incorporating Modified Side Chains as Hedgehog Pathway Inhibitors

1. Introduction

One of the latest challenges to emerge in the discovery and development of safe and efficacious Hh inhibitors as anti-cancer agents is the retention of comparable activity against the drug-resistant forms of the hyperactive signaling cascade [89]. Recently identified as a potent inhibitor of the Hh pathway (IC_{50} approximately 800 nM) [116], itraconazole (ITZ) represents an extremely promising scaffold for the development of an improved class of Hh inhibitors for two important reasons. First, being a well-studied and widely used FDA approved antimycotic drug, the PK properties and safety profile of ITZ is very well documented [164]. Thus, the strategy of repurposing this previously approved drug will simplify and expedite the otherwise long-drawn process of drug discovery and clinical approval. Second, a recent study detailing the ability of ITZ to maintain potent inhibition of Hh signaling even in the presence of multiple mutant forms of Smo that confer resistance to either GDC-0449 or NVP-LDE225 was reported [101]. This finding is especially significant in the context of developing anti-Hh agents active against drug resistant cases of BCC and MB.

ITZ is a member of the triazole class of antifungal agents that exerts its antimycotic effects through potent inhibition of lanosterol 14α-demethylase (14LDM/ CYP51), a cytochrome P450 enzyme that catalyzes the oxidative conversion of lanosterol to ergosterol, a major component of fungal cell membranes [165]. The main structural regions of ITZ are a triazole-dioxolane portion, a central phenyl-piperizine-phenyl linker region and a side chain appended triazolone region (Figure 1). Further, the molecule possesses three chiral centers, two of which are on the dioxolane ring (2 and 4) while the third exists on the sec-butyl side chain (2'). Out of the eight possible stereoisomers, a mixture of four cis-isomers (1:1:1:1) is marketed as the antifungal drug. Previous investigations have confirmed that ITZ mediated Hh inhibition is unrelated to the 14-α-lanosterol demethylase inhibition accountable for its anti-fungal activity [116].

83

Following the identification of ITZ as Hh inhibitor, only a single report detailing SAR for ITZ inhibition of Hh signaling has been reported to date. These studies focused solely on incorporating modified alkyl substituents into the ITZ side chain [120].
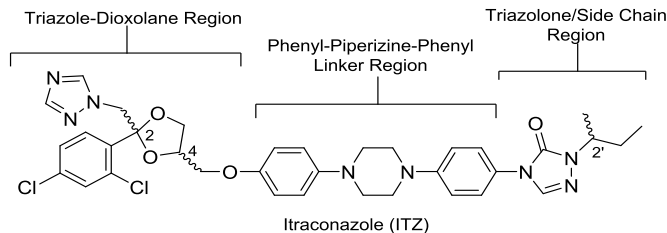
Figure 1. Structure, stereo-centers and regions of ITZ.

Despite the expected favorable outcomes of exploring the ITZ molecule for developing novel Hh inhbitors, several key tasks remain. Identifying the Hh inhibitory pharmacophore of ITZ is critical for guiding further modifications to suit the current purpose and enhance the potency and efficacy of the parent moiety by suitable modifications of the active core. Moreover, this knowledge will allow us to further improve the physicochemical features and bioavailability of second generation ITZ analogues which can be critical especially for clinical use in MB patients where blood-brain-barrier (BBB) penetration and accumulation is of utmost significance. Previous studies undertaken in Shh-Light II cells have indicated that other azole drugs (Ketoconazole, Fluconazole, Miconazole and Clotrimazole) that share structural features with ITZ and have comparable or better anti-fungal activities, exhibit decreased potencies as inhibitors of Smo [116]. To corroborate these findings, we evaluated several commercially available, structurally related triazole and imidazole anti-fungals for their ability to inhibit Hh signaling at 1 µM in the C3H10T1/2 murine fibroblast cell line when recombinant Sonic Hh protein was used to up-regulate Hh signaling (Figure 2, Table 1). We discovered that only Posaconazole (PSZ) maintained Hh inhibition comparable to ITZ in this assay. Interestingly, ITZ and PSZ share considerable structural and spatial similarity with certain differences in the triazole-dioxolane and triazolone side chain

84

regions of the molecules. Therefore, we were interested in studying the effects of integrating the structural features of PSZ with ITZ as hybrid second generation analogues. Keeping in mind the issues of poor water solubility and low bioavailability of ITZ [166], initial efforts were directed towards the generation of hydroxylated side chain containing ITZ derivatives to simultaneously achieve the goals of improving potency as well as physicochemical and pharmacokinetic attributes. A report of our current progress in identifying a suitable synthetic route to prepare ITZ derivatives with stereochemically defined hydroxylated side chains as mimics of the PSZ side arm and a brief description of preliminary biological evaluation is presented in this chapter.
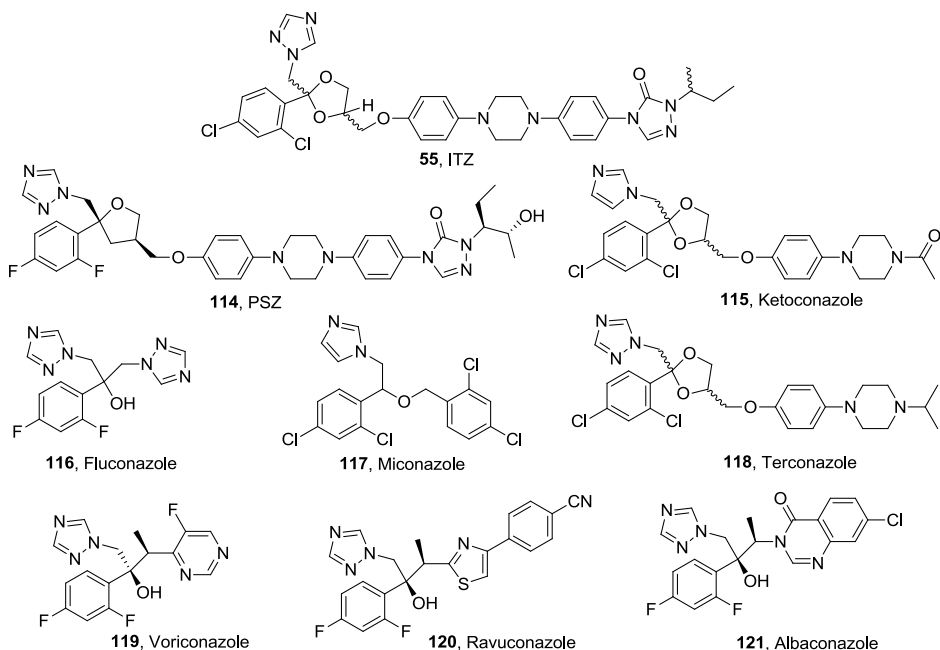
Figure 2. Structure of commercial azole antifungal drugs tested for Hh inhibition.

Table 1. Hh Inhibition for Commercially Available Azole Antifungals.

Compound	Relative Gli1 mRNA (%)	Compound	Relative Gli1 Mrna (%)
Recombinant SHh	100	Voriconazole	48.4 ± 7.4
ITZ	4.8 ± 2.1	Ravuconazole	35.2 ± 1.4
PSZ	5.1 ± 3.6	Albaconazole	44.5 ± 6.2
Fluconazole	75.3 ± 1.6	Terconazole	59.0 ± 10.6
Miconazole	63.2 ± 8.1	Ketoconazole	43.9 ± 0.3

[a]Relative Gli1 mRNA levels when SHh treatment is equivalent to 100%.

85

2. Synthesis of ITZ-PSZ hybrid analogues

2.1 Overview

Preparation of ITZ-PSZ hybrid analogues was accomplished through an optimized multistep route specifically planned for facile medicinal chemistry purposes of accessing stereochemically defined hydroxylated side chain derivatives of ITZ. The essential synthetic transformations can be classified as follows: (a) synthesis of hydroxylated side chain precursors (**A**), (b) synthesis of MOM-ITZ triazolone linker region intermediate (**B**), (c) alkylation of MOM-ITZ triazolone linker region intermediate (**C**) followed by deprotection to generate necessary phenolic intermediates (**D**), (d) synthesis of tosylated dioxolane intermediate (**E**) and (e) nucleophilic displacement of the tosyl moiety by phenolic precursors to generate final analogues (Scheme 1).
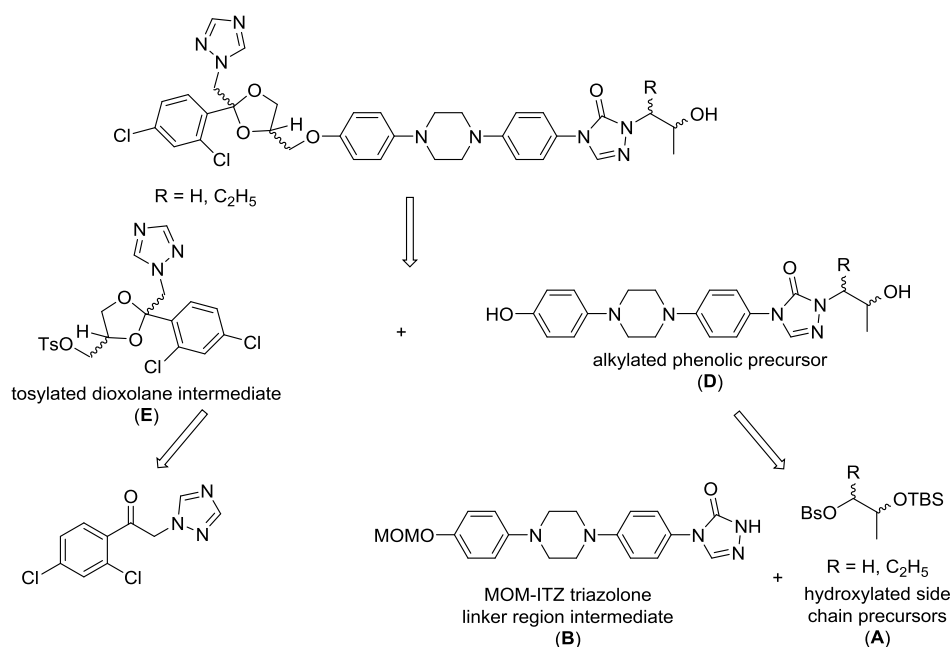
Scheme 1. Retrosynthesis of ITZ-PSZ hybrid analogues

Preparation of hydroxylated side chain precursors (**A**) was carried out using stereochemically defined starting materials methyl (*R*)-2-hydroxylpropanoate (**122**) or methyl (*S*)-2-hydroxylpropanoate (**123**). Masking the free hydroxyl groups as silyl ethers,

86

the resulting intermediates (**124**) and (**125**) were subjected to reduction by DIBAL-H to yield the corresponding aldehyde derivatives (**126**) and (**127**). Even with strictly controlled temperature of -78 ⁰C, some of the starting esters underwent complete reduction to form the corresponding alcohol derivatives (**128** and **129**) and selective generation of required aldehyde precursors proceeded with modest yields. Hence, attempts to reoxidize the hydroxylated derivative back to the aldehyde stage were made by utilizing PDC and Dess Martin Periodinane reagents respectively. While reaction with PDC led to the generation of partial oxidation product i.e. necessary aldehyde along with unwanted complete oxidation product (corresponding carboxylic acid), the reaction proceeded more successfully with the Dess Martin Periodinane conditions. Despite the success, these routes of recycling the alcohol derivatives back to the aldehyde precursors proved less favorable as there was unnecessarily addition to the overall steps required to generate final compounds. Therefore, we employed the previous strategy of 'selective' reduction with DIBAL-H on a larger scale reaction to prepare necessary amounts of intermediates (**126** and **127**) taking into consideration the expected reaction yields. These intermediates were then subjected to nucleophilic addition by ethylmagnesium bromide to prepare and isolate precursors (**130**-**133**). As expected, the presence of bulky silyl ether protecting group on the adjacent hydroxyl directed the addition following the Felkin Ahn model, generating the predominantly 'anti' derivatives with an overall yield of 60-72% in a 3:1 (anti:syn) ratio. Finally, the free hydroxyl moieties were converted to corresponding brosyl functionalities to yield intermediates (**A**: **134**-**139**) (Scheme 2).

87
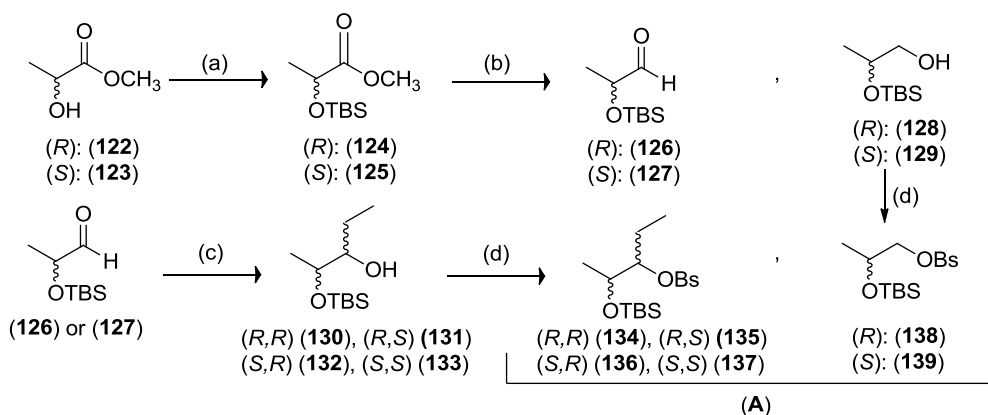
(a)TBSCl, Imidazole, anhydrous DCM, 95%; (b)DIBAL-H, anhydrous DCM, -78 °C, 30-40%; (c) C_2H_5MgBr, anhydrous THF, -78 °C, 60-72%; (d) Et$_3$N, DMAP, BsCl, anhydrous DCM, 0 °C, 65-80%.

Scheme 2. Synthesis of hydroxylated side chain precursors (A).

A previously reported literature protocol was followed for the synthesis of MOM-ITZ triazolone linker region (**B**: **144**) [120]. We proceeded by coupling commercially available *N*-(4-hydroxylphenyl)-piperazine (**140**) and 1-chloro-4-nitrobenzene (**141**) to yield *N*-(4-hydroxyphenyl)-*N'*-(4-nitrophenyl)-piperazine derivative. This crude product was directly used to react with methoxymethyl chloride to afford the MOM-protected intermediate (**142**). Subsequent reduction of the nitro group of (**142**) afforded the corresponding amine derivative precursor necessary for the synthesis of phenylcarbamate derivative (**143**). Ultimately, synthesis of the triazolone heterocycle was accomplished via formation of the semicarbazide intermediate from precursor (**143**) (Scheme 3).
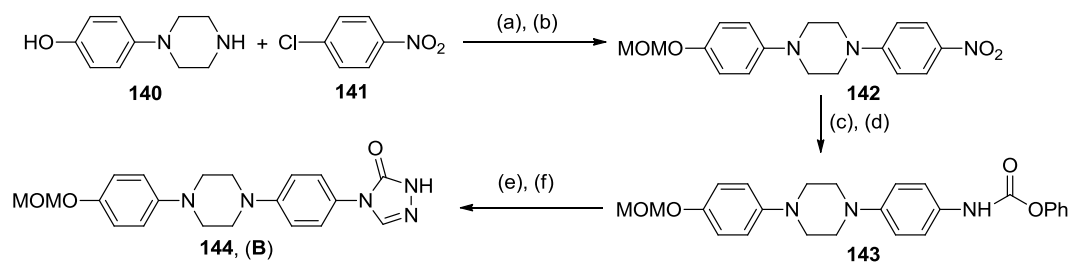
(a) DIPEA, NMP, 125° C; (b) MOMCl, Et$_3$N, 75%; (c) 10% Pd/C, NH$_2$NH$_2$·H$_2$O, EtOH, reflux, 99%; (d) Phenyl chloroformate, pyridine, CH$_3$CN; (e) NH$_2$NH$_2$·H$_2$O, 1,4-dioxane, reflux; (f) Formamidine acetate, 1-propanol, 110° C, 50%.

Scheme 3. Synthesis of MOM-ITZ triazolone linker region intermediate (B).

88

Next, alkylation of triazolone intermediate (**B**) was attempted by using Cs_2CO_3 in

the presence of 18-crown-6 at room temperature to generate the anion of (**B**) to facilitate

SN_2 displacement of the brosylate intermediates (**A**) [120]. However, with secondary

brosylates such as (**135**), the reaction failed to proceed under these conditions in either

DMF or DMSO (Table 2). Thereafter, the reaction was subjected to an elevated

temperature of 80 ºC affording better results [167]. Under these revised conditions, the

reactions proceeded to completion to form intermediates (**145**) and (**146**), however;

unreacted starting materials were recovered when using the sterically hindered

brosylates (**134**-**137**). Subsequently, the reaction mix was heated at 50 ºC with the base

(Cs_2CO_3) and the chelator (18-crown-6) to enhance the nucleophile formation before

addition of sterically crowded brosylate intermediates. Further, the reaction was heated

overnight at 80 ºC to facilitate the complete consumption of starting materials leading to

improved yields of (**C**: **147**-**150**). The final step to generate phenolic precursors (**D**: **151**-

156) was accomplished by global deprotection of methoxymethyl and silyl ether groups

using trifluoroacetic acid (Scheme 4).

	(C)	(D)
R = H, (R)	(145)	(151)
R = H, (S)	(146)	(152)
R = C₂H₅, (R,R)	(147)	(153)
R = C₂H₅, (R,S)	(148)	(154)
R = C₂H₅, (S,R)	(149)	(155)
R = C₂H₅, (S,S)	(150)	(156)
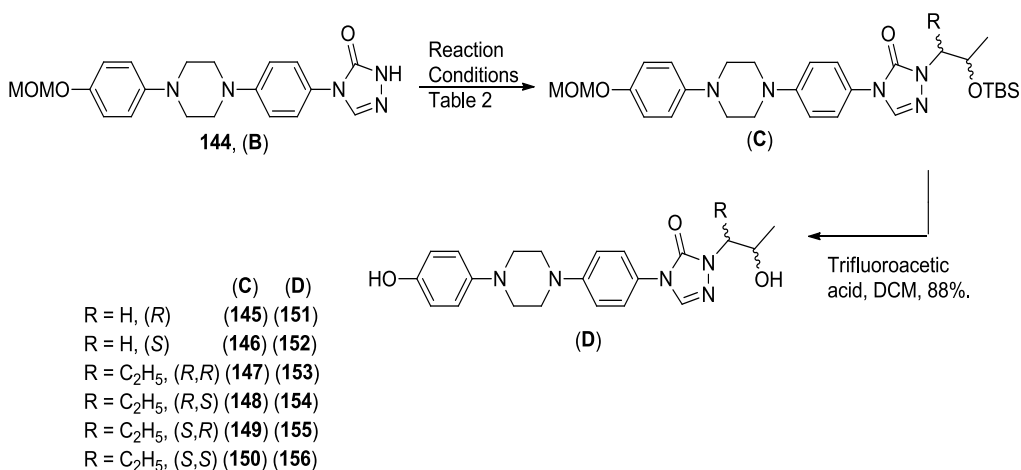
Scheme 4. Synthesis of phenolic precursors (D).

Table 2. Optimization of reaction conditions for alkylation of (B).

Reaction conditions	Observations	Reaction yields
CsCO$_3$, 18-crown-6, DMSO, rt, 1h; (**135**), rt 12h	No reaction	-
CsCO$_3$, 18-crown-6, DMF, rt, 1h; (**135**), rt 12h	No reaction	-
CsCO$_3$, 18-crown-6, DMF, rt, 1h; (**135**), 80ºC, 12h	Some unreacted starting material	30%
CsCO$_3$, 18-crown-6, DMF, 50 ºC, 1h; (**135**), 80ºC, 12h	Reaction complete	57%
CsCO$_3$, 18-crown-6, DMF, rt, 1h; (**138 /139**), 80ºC, 12h	Reaction complete	62%

Formerly reported literature methods for preparing the tosylated-dioxolane intermediate (**E**) were adopted with slight modifications to generate the intermediate as a mixture of both *cis* and *trans* isomers [168, 169]. Beginning with a protected glycerol intermediate (**157**), the free primary hydroxyl group was first transformed to the corresponding tosylate (**158**), followed by a deprotection step to yield mono-tosylated glycerol (**159**). In parallel, trichloroacetophenone (**160**) was utilized to facilitate substitution of chloro group with triazole functionality leading to precursor (**161**). Ultimately, triflic acid mediated ketalization using (**159**) proceeded to generate intermediate (**E**: **162**) as a mixture of *cis* (major product) and *trans* (minor product) isomers (Scheme 5).
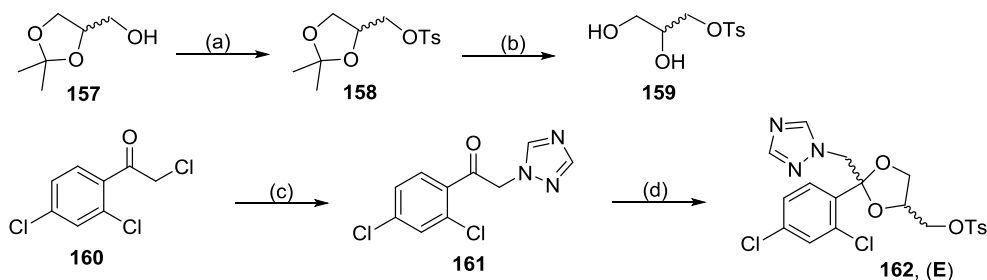
(a) TsCl, pyridine, DCM, 0ºC, 70%; (b) MeOH, HCl, reflux, 89%; (c) 1,2,4-triazole, NaHCO$_3$, toluene, 52%; (d) TfOH, toluene, (**159**), 36h, 60%.

Scheme 5. Synthesis of tosylated dioxolane intermediate (E).

The final step consisted of coupling the tosyl-dioxolane intermediate (**E**) with each of the phenolic precursors (**D**). Initial attempts of base assisted generation of the phenoxy nucleophile were performed using NaH in DMSO at elevated temperatures (50-90 ºC) [120, 170]. Adopting this protocol, final analogues (**163** and **164**) were synthesized in modest yields (Scheme 6). However, the purification steps of these analogues proved extremely challenging owing to the difficulties of removal of DMSO and several side products possibly formed due to the action of NaH in DMSO in the presence of free hydroxyl groups at elevated temperatures. Consequently, these analogues were isolated at 80-85% purity levels as determined by NMR spectral data. Thereafter, multiple efforts to couple tosyl-dioxolane intermediate (**E**) with phenolic precursors containing bulkier hydroxylated side appendages (**153**-**156**) failed. While, desired analogues were not detected in these reaction mixtures, the starting precursors had been consumed to form complex compounds of unknown structures. Based on the observations of typical color changes associated with ylide formation, it was hypothesized that under the aforementioned conditions, DMSO was participating in the reaction possibly through its activation to form sulfur ylides. As an alternate, DMF was employed as a solvent to successfully synthesize **165** with 20% yields (Scheme 6). This final coupling step is currently underway for other phenolic precursors.
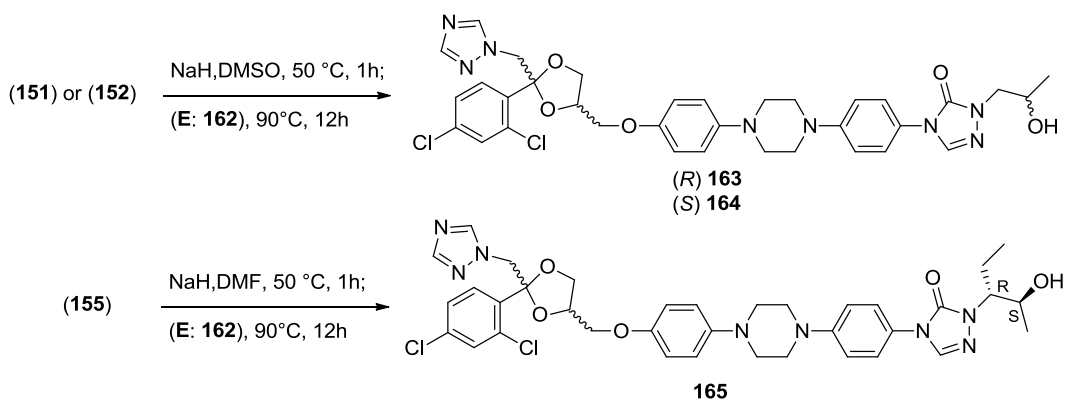
Scheme 6. Synthesis of ITZ-PSZ hybrid analogues.

91

2.2 Experimental protocols

General procedure for TBS protection: To a solution of methyl (*R*)-2-hydroxylpropanoate or methyl (*S*)-2-hydroxylpropanoate (5 g, 1 eq.) in anhydrous DCM (60 mL) was added imidazole (4.25 g, 1.3 eq.), and the mixture was stirred for 10 min at 0 °C. To this solution tert-butyldimethylsilyl chloride (8.68 g, 1.2 eq.) was added at 0 °C and the mixture was allowed to warm to RT and stirred overnight. After completion of the reaction, the mixture was diluted with water and extracted into DCM. The combined extract was washed with brine, dried over anhydrous Na_2SO_4 and concentrated under reduced pressure. The crude residue was purified by column chromatography (SiO_2, 0-5% EtOAc in hexanes) to give pure compounds (**124**) and (**125**) as colorless oils in 95 % yields.

General procedure for reduction to aldehyde: To a cooled (-78 °C), stirred solution of ester compounds (**124**) or (**125**) (5 g, 1 eq.) in anhydrous DCM (50 mL) was slowly added DIBAL-H (1.0 M, 2 eq.) and stirred for 2 h. The reaction was quenched with saturated sodium potassium tartarate (50 mL), stirred for 0.5 h and then filtered using excess DCM. The combined organic phases were separated, washed with brine, dried over anhydrous Na_2SO_4, and concentrated under reduced pressure. The crude product was purified by column chromatography (SiO_2, 0-5% EtOAc in hexanes) to give aldehydes (**126**) and (**127**) as a colorless liquids in 30-40 % yields.

General procedure for nucleophilic addition of Grignard reagents: Aldehyde (**126**) or (**127**) (1 g, 1 eq.) in anhydrous THF (20 mL) was added dropwise to ethylmagnesium bromide (3.0 M in anhydrous THF, 5 eq.) at -78 °C and the reaction mixture was stirred for 2 h. After completion, the reaction mixture was quenched with water and extracted into EtOAc. The combined organic layer was washed with 0.1N HCl, brine, dried over Na_2SO_4, and concentrated. The crude residue was purified by column

chromatography (SiO$_2$, 0-15% EtOAc in hexanes) to carefully separate the resulting isomers (**130-133**) as a colorless oils in good yields [**130** & **131**: 72% (1:3); **132** & **133**: 60% (3:1)].

General procedure for brosylation: To a solution of hydroxyl intermediate **128/129/130/131/132/133** (0.1- 0.12 g, 1 eq.) in anhydrous DCM (3-5 ml), triethylamine (2 eq.), dimethylaminopyridine (1 eq.) and 4-bromobenzene-1-sulfonyl chloride i.e. BsCl (1.3 eq.) were added at 0 °C. The reaction mixture was allowed to warm to RT while stirring overnight. On completion, the mixture was diluted with DCM, washed with water, dried over Na$_2$SO$_4$ and concentrated under reduced pressure. Purification using column chromatography (SiO$_2$, 0-10% EtOAc in hexanes) yielded intermediates (**A**: **134**-**139**) as clear oils in 65-80% yields.

General procedure for alkylation of linker region: To a solution of the linker region triazolone intermediate, (**C**), (1 eq.) in DMF was added Cs$_2$CO$_3$ (2 eq.) and 18-crown-6 (1 eq.). The resulting mixture was stirred at 50 ºC for 1 h followed by the addition of corresponding alkyl brosylates **A**: **134**-**139** (1.5 eq.). The reaction mixture was stirred overnight at 80 ºC. After cooling to room temperature, the reaction mixture was diluted with water and extracted with EtOAc. The combined organic layer was dried over Na$_2$SO$_4$, filtered, and concentrated to yield the crude product. Purification by column chromatography (SiO$_2$, 0-3% MeOH in DCM) afforded pure products (**C**: **145**-**150**) as a brown solid in 30-62% yields.

General procedure for coupling phenol intermediates (D) and tosylated dioxolane intermediate (E): To a solution of the phenol **D** (1 eq.) in DMF was added NaH (a 60% dispersion in mineral oil, 5 eq.). After the mixture was stirred at 50 °C under argon for 1 h, a solution of **E** (1.1 eq.) in DMF was added dropwise. After the addition,

93

the temperature was increased to 90 °C and the solution was stirred under argon overnight. The reaction was then quenched by the addition of a 50% aqueous NaCl solution, and the resulting mixture was extracted with CH_2Cl_2. The organic fractions were dried (Na_2SO_4), filtered, and concentrated under vacuum to yield the crude product, which was purified by column chromatography (SiO_2, 0-5% MeOH in DCM) to afford the desired products as white solids in 20% yields.

4-(4-(4-(4-((2-((1H-1,2,4-triazol-1-yl)methyl)-2-(3,5-dichlorophenyl)-1,3-dioxolan-4-yl)methoxy)phenyl)piperazin-1-yl)phenyl)-1-((R)-2-hydroxypropyl)-1H-1,2,4-triazol-5(4H)-one (163)

^{1}H NMR (500 MHz, CDCl$_3$) δ 8.31 – 8.15 (m, 1H), 8.01 – 7.85 (m, 1H), 7.66 – 7.54 (m, 1H), 7.54 – 7.38 (m, 1H), 7.25 – 7.02 (m, 1H), 6.97 (s, 5H), 6.95 – 6.78 (m, 3H), 4.81 (m, *J* = 25.3, 18.0, 9.1 Hz, 2H), 4.38 (m, *J* = 5.9 Hz, 1H), 4.26 – 3.97 (m, 1H), 3.93 (q, *J* = 7.6 Hz, 1H), 3.82 (m, *J* = 14.6, 6.7, 3.8 Hz, 2H), 3.53 (m, *J* = 9.6, 4.7 Hz, 1H), 3.33 – 3.16 (m, 8H), 1.64 (s, 1H), 1.27 (s, 1H).

4-(4-(4-(4-((2-((1H-1,2,4-triazol-1-yl)methyl)-2-(3,5-dichlorophenyl)-1,3-dioxolan-4-yl)methoxy)phenyl)piperazin-1-yl)phenyl)-1-((S)-2-hydroxypropyl)-1H-1,2,4-triazol-5(4H)-one (164)

^{1}H NMR (500 MHz, CDCl$_3$) δ 8.29 – 8.19 (m, 1H), 7.97 – 7.85 (m, 1H), 7.64 – 7.55 (m, 1H), 7.49 (d, *J* = 2.0 Hz, 1H), 7.14 (d, *J* = 8.2 Hz, 1H), 6.97 (s, 4H), 6.90 – 6.74 (m, 5H), 4.81 (m, *J* = 25.3, 18.0, 9.1 Hz, 2H), 4.38 (p, *J* = 5.9 Hz, 1H), 4.25 – 3.99 (m, 1H), 3.93 (q, *J* = 7.6 Hz, 1H), 3.82 (m, *J* = 14.8, 6.6, 3.7 Hz, 2H), 3.53 (m, *J* = 9.6, 4.7 Hz, 1H), 3.34 – 3.16 (m, 8H), 1.64 (s, 1H), 1.27 (s, 1H).

4-(4-(4-(4-((2-((1H-1,2,4-triazol-1-yl)methyl)-2-(3,5-dichlorophenyl)-1,3-dioxolan-4-yl)methoxy)phenyl)piperazin-1-yl)phenyl)-1-((2S,3R)-2-hydroxypentan-3-yl)-1H-1,2,4-triazol-5(4H)-one (165)

^{1}H NMR (500 MHz, CDCl$_3$) δ 8.23 (s, 1H), 8.15 (s, 1H), 7.98 (s, 1H), 7.92 (s, 1H), 7.67 (s, 1H), 7.60 (dd, J = 8.4, 2.5 Hz, 2H), 7.50 (t, J = 1.9 Hz, 1H), 7.48 – 7.42 (m, 2H), 7.28 – 7.25 (m, 1H), 7.15 (d, J = 8.2 Hz, 1H), 7.09 – 7.02 (m, 2H), 7.00 – 6.93 (m, 2H), 6.86 – 6.79 (m, 3H), 4.87 (d, J = 14.7 Hz, 1H), 4.81 – 4.74 (m, 2H), 4.39 (tt, J = 6.5, 4.9 Hz, 1H), 4.26 – 4.14 (m, 2H), 4.09 (m, J = 11.0, 3.5 Hz, 2H), 4.02 – 3.79 (m, 4H), 3.76 – 3.67 (m, 1H), 3.52 (dd, J = 9.7, 6.3 Hz, 1H), 3.44 – 3.35 (m, 5H), 3.30 – 3.23 (m, 5H), 2.05 (m, J = 14.6, 11.0, 7.3 Hz, 1H), 1.90 (m, J = 14.7, 7.4, 3.6 Hz, 1H), 1.64 (d, J = 8.3 Hz, 6H), 1.28 (d, J = 6.5 Hz, 5H), 0.94 (t, J = 7.4 Hz, 3H). ^{13}C NMR (126 MHz, CDCl$_3$) δ 153.0, 152.7, 151.4, 150.8, 146.0, 136.1, 134.3, 134.3, 133.0, 131.4, 129.6, 127.3, 127.3, 123.7 (2C), 118.5 (2C), 116.6 (2C), 115.3 (2C), 107.6, 107.2, 74.7, 70.3, 67.5, 66.2, 61.6, 53.5, 50.6 (2C), 49.2 (2C), 31.6, 22.7, 19.5, 14.1, 10.8. IR (film) υ$_{max}$ 3436, 3181, 2933, 1646, 1511, 1456, 1385, 1348, 1277. DART-HRMS: m/z calculated for C$_{38}$H$_{43}$Cl$_2$N$_6$O$_5$: 735.2577 [M+H]$^{+}$, Found: 735.2548.

3. Biological evaluation

3.1 Experimental protocols

Analysis of Hh target gene expression: Cells were plated and grown according to cell line specific protocols described in Chapter 3. Recombinant SHh protein (200 ng/ ml) was used to activate Hh signaling in C3H10T1/2 cells. RNA isolation and evaluation by qRT-PCR analysis was performed as described in previous chapters. Data was analyzed using GraphPad Prism 5 and IC$_{50}$ values computed as mean ± SEM from at least three separate experiments performed in triplicate.

3.2 Results

Table 3. Preliminary evaluation of hybrid ITZ analogues.

163

164
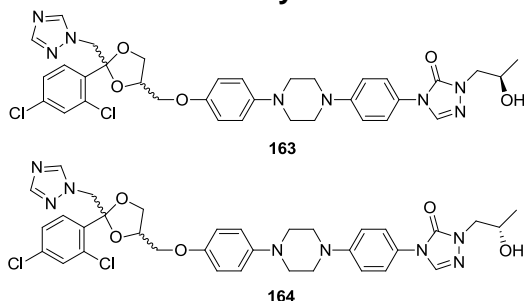
Analogue	Gli1 mRNA IC$_{50}$ Values (µM)	
	C3H10T1/2 cells	ASZ cells
ITZ	0.074 ± 0.02	0.14 ± 0.02
PSZ	0.01 ± 0.005	0.54 ± 0.05
163	0.45 ± 0.09	0.15 ± 0.01
164	0.18 ± 0.02	0.10 ± 0.01

Preliminary evaluation conducted in C3H10T/12 cells revealed that both ITZ hybrid analogues maintain potent inhibition of Gli1 mRNA expression (180-450 nM). Overall, the (*R*) hydroxyl containing analogue i.e. **163** showed two-fold loss of activity as compared to the (*S*) hydroxyl derivative **164** in this cellular assay. The biological activity profile of these analogues showed similar trends when studied in the ASZ cells. Both derivatives strongly inhibited Gli1 mRNA expression in these cells as well (Table 3).

4. Conclusion

Discovery of potent Hh inhibitory activity mediated by ITZ opened new avenues for drug discovery explorations based on this scaffold. A comparative analysis of Hh inhibitory activities of various members from the azole class of antifungal drugs revealed PSZ to be an equipotent inhibitor of the Hh signaling cascade. This finding guided the design and development of next generation ITZ-PSZ hybrid analogues. However, the task of preparing such chimeric molecules entailed a challenging multi-step synthetic

96

route. Aiming to simplify this synthetic route for the purpose of easy and efficient medicinal chemistry investigations, necessary modifications to the existing synthetic strategy were planned and successfully executed. Preliminary evaluation of two new derivatives indicated that these hydroxylated side chain derivatives of ITZ maintain potent Hh inhibitory activity *in vitro*. Taken together, an optimized methodology for rapid synthesis of chirally defined hydroxylated side chain derivatives has led to the synthesis of active Hh inhibitors and will prove to be advantageous for the future production of related molecules.

97

CHAPTER V: Future Directions in the Development of Small Molecule Inhibitors of

the Hh Pathway

1. Contributions of VD3 project

The identification of aberrant Hh pathway signaling in a variety of human cancers led to a surge in research projects that focused on the development of pathway inhibitors as anti-cancer agents. Many of these initial drug discovery efforts focused on the development of small molecules that target Smo, the most druggable target within the pathway. Further, the FDA approval of GDC-0449 in early 2012 validated the clinical efficacy of treating Hh-dependent cancers with a Smo antagonist. Our initial efforts towards identifying improved Hh inhibitors began with studies based on VD3. To date, the molecular target for VD3 in the context of Hh signaling has not been confirmed. Therefore, *in silico* modeling or structure based drug designing was not feasible. Due to this challenge, a chemical-biology approach was adopted and implemented in order to successfully fulfill the goals of this project. Preliminary results suggesting that the metabolic conversion of VD3 to its physiologically active form, calcitriol, activates VDR signaling further led to the aim of repurposing the VD3 scaffold for selective Hh modulation. The knowledge gathered from probing *in vitro* biological models with VD3 and its early analogues guided the design and discovery of improved next generation derivatives. One of the most significant outcomes of these studies was a better understanding of the structural requirements of VD3 for potent and selective Hh inhibition (Figure 1). The CD-ring region of VD3 was determined to be the necessary pharmacophore for Hh pathway inhibition. It was established that modifications of the A-ring, seco B-ring and CD-ring side chain afforded greater selectivity for Hh modulation thereby diminishing the detrimental effects of concomitant VDR activation. Taking into account these key SAR findings, new VD3 based Hh antagonists were designed, prepared and evaluated. Among these novel analogues, **95**, **100** and **104** afforded approximately four-fold improvement in Hh inhibitory activity while gaining greater than 1000-fold selectivity for Hh signaling over the VDR pathway.

99
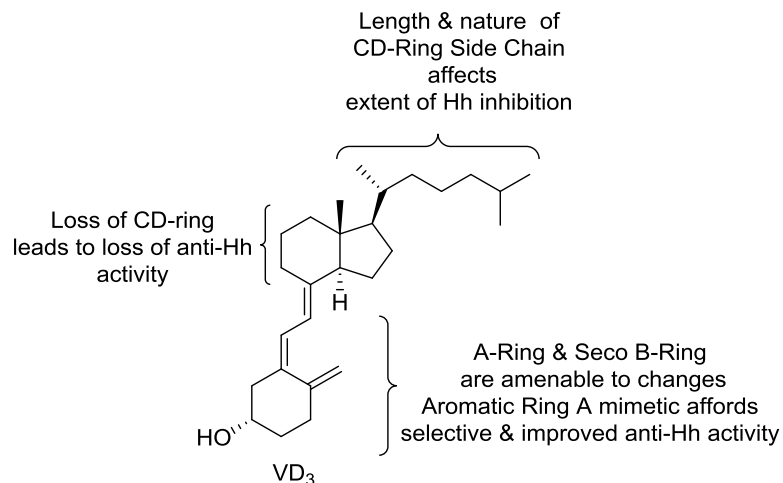
Figure 1. SAR of VD3 for potent and selective Hh pathway inhibition.

Another important contribution of this project was towards the optimization of *in vitro* assay systems for expedited evaluation of Hh inhibitors. Developing reliable cell based assays for monitoring endogenous Hh activity in cancer cell lines has proven to be a significant challenge. According to the generally accepted notion, the tumor microenvironment allowing cross talk with surrounding stromal cells is crucial for proper Hh signaling in several forms of cancer. Therefore, accurate *in vitro* evaluation of biological activities of potential Hh antagonists has been difficult owing to the lack of paracrine mode of Hh signaling in cultured epithelial tumor cells. This shortcoming was corroborated while working with human glioblastoma cell line U87MG to test A-ring analogues of VD3. Thereafter, a qRT-PCR based assay using MEFs such as C3H10T1/2 has been routinely employed for evaluating Hh inhibitors. Relatively higher time and resources consumed in this assay, which arises from using low RNA yielding MEF cells prompted us to search for suitable modifications to the assay protocol with the intention of developing a higher throughput assay. Consequently, the assay was optimized for a 96 or 24-well format to facilitate efficient screening of analogues with reliability and reproducibility directly from the cell lysate using commercially available Cells-to-CT kit (Life Technologies).

Since esterase enzymes are abundant in *in vitro* and *in vivo* systems, ester bonds are generally susceptible to metabolic cleavage under such environment. Thus, to avert metabolic liabilities, ester linkages are typically avoided in a drug molecule except when formulating a 'pro-drug'. With these caveats in mind, we continued our exploration of VD3 SAR employing this class of ester linked analogues for a few different reasons. First, from a chemistry point of view, access to this group of analogues proved to be quick and efficient allowing expedited synthesis and investigation of biological activities. Next, based on distinct SAR trends it was established that observed activity is through the intact ester-linked scaffold and not the resulting metabolites [113, 114]. Prior to conducting *in vivo* studies, it will be essential to identify and incorporate a linker less susceptible to metabolism while maintaining potent and selective Hh inhibition. Functional moieties such as amide, carbamate or ureido which are generally 'drug like' linker groups are proposed for this purpose and are being prepared currently by other researchers in the Hadden lab.

A comprehensive understanding of the subcellular components that interact with VD3 is essential to developing VD3 analogues that exert their biological effects through selective inhibition of Hh signaling. Ongoing studies designed to explore the cellular mechanisms through which VD3 and its analogue **87** inhibit Hh signaling have focused on the two cellular receptors previously associated with VD3 i.e. VDR and Smo. Previously, tritiated analogue of VD3 was shown to selectively bind yeast cultures in which expression of human Smo had been chemically induced [107]. In addition, this binding was antagonized by the addition of Cyc. On the contrary, results from our binding experiments suggest that neither VD3 nor **87** bind Smo in the Cyc binding pocket; however, this data does not preclude binding to another region of Smo [114]. Preliminary analysis of VDR-mediated Hh inhibition for VD3 and **87** suggested that VDR

101

is required for the anti-Hh effects of VD3 but not for calcitriol or analogue **87**. The inability of VD3 to maintain Hh inhibition in the presence of VDR knockdown was surprising for several reasons. First, similar studies performed in ASZ cells utilizing VDR-specific shRNA demonstrated that VDR knockdown did not affect the ability of VD3 to down-regulate Gli1 mRNA expression [110]. In addition, as demonstrated by our lab [108] and others, [171] calcitriol inhibits Hh signaling *in vitro* and *in vivo* and these anti-Hh effects of calcitriol were not abrogated in Vdr $^{-/-}$ fibroblasts [171]. More specifically, the ability of calcitriol to inhibit Hh signaling *in vitro* has been localized to a step downstream of Ptch, suggesting its effects may also be mediated via Smo. As our assays (C3H10T1/2) and those previously reported (ASZ and fibroblasts) were performed in different cell lines, it is clear that cellular context is essential for determining the mechanisms through which VD3, calcitriol, and their analogues inhibit Hh signaling. Therefore, the development of chemical probes that can definitively identify binding interactions will be necessary to further our understanding of whether the anti-Hh effects of these sterols are mediated via direct binding to Smo, or another, as yet unidentified, mechanism.

2. Contributions of ITZ project

Following the identification of ITZ as a potent Hh/Smo antagonist, several new clinical trials have been initiated to assess the implications of repurposing this antifungal drug for the treatment of Hh-driven cancers. Along with promising initial results from these studies, an additional factor in favor of ITZ is its potent anti-Hh activity against the known drug resistant forms of the signaling cascade [101, 117]. Irrespective of the final consequences of current clinical trials, the ITZ scaffold is certainly a promising new drug lead for the development of Hh inhibitors. Therefore, we examined possible design strategies to develop ITZ based analogues for the inhibition of Hh signaling.

102

During a comparative analysis of several azole antimycotic drugs, it was revealed that PSZ exhibits potent Hh inhibition similar to ITZ. Hence, we prepared three analogues that incorporate stereochemically defined hydroxylated side chains reminiscent of the PSZ side chain to determine whether this enhanced Hh inhibitory activity is mediated through the side arm region. Also, these analogues were designed with the objective of enhancing water solubility of the otherwise poorly soluble ITZ molecule. After several rounds of optimization with respect to previously reported synthetic routes to either ITZ or PSZ, rapid access to this class of compounds was accomplished.

With a protocol in place for the synthesis of chimeric ITZ-PSZ analogues, future efforts can be directed towards preparing related analogues (Figure 2). This class of analogues will provide SAR inferences regarding the effects of defined stereochemistry of the side chain on Hh inhibition. Further, evaluation of potent analogues against drug resistant forms of Smo will aid the identification of ideal candidates for advanced development.
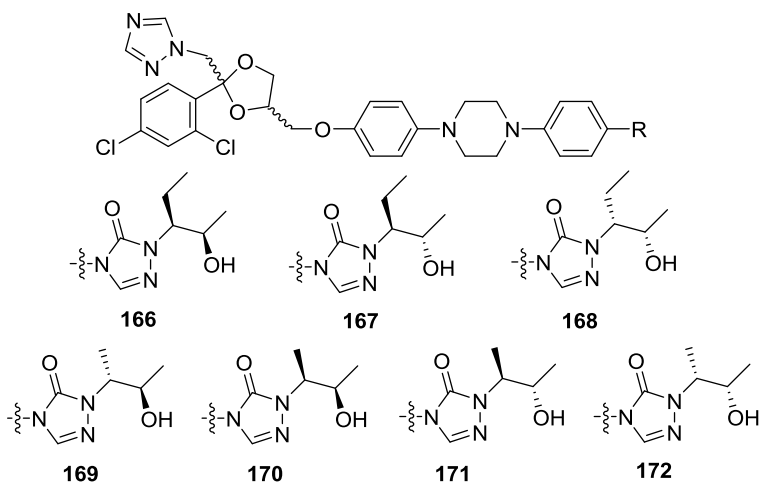
Figure 2. Additional side chain analogues of ITZ.

103

3. Future outlook for the discovery and development of Hh pathway inhibitors

The recent identification of multiple mechanisms that can result in resistance to Smo antagonists has led numerous researchers to target additional pathway components. The general consensus has been that small molecules acting on targets downstream of Smo, particularly at the level of the Gli transcription factors or on distinct binding sites of Smo, hold more promise for resistant forms of Hh-dependent cancers. Several research groups have identified pathway inhibitors that function through inhibition of Gli function; however, the majority of these have only demonstrated modest inhibitory activity in vitro and in-depth SAR, mechanism of action, and in vivo studies for these compounds have not been reported. The last year has seen numerous structural reports detailing several distinct small-molecule binding sites on Smo. Understanding key molecular interactions between Smo antagonists and these binding sites may also facilitate the design of small molecules with enhanced potency against resistant forms of Smo. Meanwhile, a combination therapy approach has shown reasonable success in inhibiting resistant forms of Hh signaling in human cancer. For instance co-administration with verapamil, an inhibitor of P-gp, restored the anti-Hh activity of IPI-926 in murine MB that had developed resistance due to IPI-926-induced overexpression of P-gp [37]. In a separate study, co-administration of NVP-LDE225 with either the PI3K inhibitor NVP-BKM120 or the dual PI3K-mTOR inhibitor NVP-BEZ235 significantly delayed the development of resistance and enhanced MB tumor regression in animal models [35]. Similarly, small molecule inhibitors of Aurora kinase or Polo-like kinase demonstrated potent anti-tumor effects *in vitro* and *in vivo* in murine *Ptch*$^{-/-}$ MB both alone and in combination with NVP-LDE225 [172]. A related combination approach that utilized two pathway inhibitors that act through diverse mechanisms has also proven effective. Combined oral administration of ITZ and ATO in a subcutaneous allograft of SmoD477G-driven MB demonstrated potent inhibition of both Hh signaling and tumor

104

growth [101]. While these combination studies have proven effective in a preclinical setting, their advancement into clinical trials is necessary to definitively evaluate their ability to inhibit resistant forms of Hh signaling in human cancer.

In addition to the issues associated with acquired resistance to Smo antagonists, another limitation associated with the development of pathway inhibitors is related to their general application across a wide-range of human cancers. While aberrant Hh signaling has been implicated in various forms of human cancer, the scope of using Smo antagonists as a monotherapy has proven limited. To date, only BCC and MB, malignancies that are driven by specific mutations in *Ptch*, *Smo*, or *Sufu* have proven amenable to this type of therapeutic intervention. IPI-926 was withdrawn from several Phase II trials for failing to meet its endpoint against cancers that are not generally considered to be strictly Hh-dependent. In addition, the anti-cancer activity of pathway inhibitors *in vitro* and *in vivo* in non-Hh-dependent cancers is often not correlative with their anti-Hh effects [12, 108]. Again, there have been increasing reports in which a Smo antagonist used in combination with another small molecule has demonstrated promising preclinical or clinical activity. Specific examples include the clinical studies of notch inhibitor RO4929097 combined with GDC-0449 in treating advanced or metastatic sarcoma based on the fact that both of these signaling mechanisms are responsible for sustaining sarcoma tumors [173]. Similarly, promising results have been reported in combining GDC-0449 with gemcitabine and nab-paclitaxel against advanced pancreatic cancer [174].

As a whole, these results clearly highlight the anti-cancer potential of Hh pathway inhibitors in Hh-dependent cancers, as well as the potential of combination regimens in resistant or non-Hh-dependent cancer. Moreover, they also emphasize the need for continued development to ensure there will be effective treatments for future patients

who experience detrimental side effects or are not responsive to the compounds currently under development.

106

REFERENCES

1. Ingham, P. W.; McMahon, A. P. Hedgehog signaling in animal development: paradigms and principles. *Genes Dev.* **2001**, *15,* 3059-3087.

2. Hadden, M. K. Hedgehog pathway agonism: Therapeutic potential and small-molecule development. *ChemMedChem* **2014**, *9,* 27-37.

3. Sekulic, A.; Migden, M. R.; Oro, A. E.; Dirix, L.; Lewis, K. D.; Hainsworth, J. D.; Solomon, J. A.; Yoo, S.; Arron, S. T.; Friedlander, P. A.; Marmur, E.; Rudin, C. M.; Chang, A. L. S.; Low, J. A.; Mackey, H. M.; Yauch, R. L.; Graham, R. A.; Reddy, J. C.; Hauschild, A. Efficacy and safety of Vismodegib in advanced basal-cell carcinoma. *N. Engl. J. Med.* **2012**, *366,* 2171-2179.

4. Solar ultraviolet radiation: Global burden of disease from solar ultraviolet radiation. *http://www.who.int/uv/health/solaruvradfull_180706.pdf*.

5. Ling, G.; Ahmadian, A.; Persson, A.; Unden, A. B.; Afink, G.; Williams, C.; Uhlen, M.; Toftgard, R.; Lundeberg, J.; Ponten, F. PATCHED and p53 gene alterations in sporadic and hereditary basal cell cancer. *Oncogene* **2001**, *20,* 7770-7778.

6. Reifenberger, J.; Wolter, M.; Knobbe, C. B.; Koehler, B.; Schoenicke, A.; Scharwaechter, C.; Kumar, K.; Blaschke, B.; Ruzicka, T.; Reifenberger, G. Somatic mutations in the PTCH, SMOH, SUFUH and TP53 genes in sporadic basal cell carcinomas. *Br. J. Dermatol.* **2005**, *152,* 43-51.

7. Raffel, C.; Jenkins, R. B.; Frederick, L.; Hebrink, D.; Alderete, B.; Fults, D. W.; James, C. D. Sporadic medulloblastomas contain PTCH mutations. *Cancer Res.* **1997**, *57,* 842-845.

8. Taylor, M. D.; Liu, L.; Raffel, C.; Hui, C.; Mainprize, T. G.; Zhang, X.; Agatep, R.; Chiappa, S.; Gao, L.; Lowrance, A.; Hao, A.; Goldstein, A. M.; Stavrou, T.; Scherer, S. W.; Dura, W. T.; Wainwright, B.; Squire, J. A.; Rutka, J. T.; Hogg, D. Mutations in SUFU predispose to medulloblastoma. *Nat. Genet.* **2002**, *31,* 306-310.

9. Tostar, U.; Malm, C. J.; Meis-Kindblom, J. M.; Kindblom, L.; Toftgaerd, R.; Unden, A. B. Deregulation of the Hedgehog signalling pathway: a possible role for the PTCH and SUFU genes in human rhabdomyoma and rhabdomyosarcoma development. *J. Pathol.* **2006**, *208,* 17-25.

10. Zibat, A.; Missiaglia, E.; Rosenberger, A.; Pritchard-Jones, K.; Shipley, J.; Hahn, H.; Fulda, S. Activation of the hedgehog pathway confers a poor prognosis in embryonal and fusion gene-negative alveolar rhabdomyosarcoma. *Oncogene* **2010**, *29,* 6323-6330.

11. Thayer, S. P.; Pasca di Magliano, M.; Heiser, P. W.; Nielsen, C. M.; Roberts, D. J.; Lauwers, G. Y.; Qi, Y. P.; Gysin, S.; Fernandez-del Castillo, C.; Yajnik, V.; Antoniu, B.; McMahon, M.; Warshaw, A. L.; Hebrok, M. Hedgehog is an early and late mediator of pancreatic cancer tumorigenesis. *Nature* **2003**, *425,* 851-856.

107

12. Yauch, R. L.; Gould, S. E.; Scales, S. J.; Tang, T.; Tian, H.; Ahn, C. P.; Marshall, D.; Fu, L.; Januario, T.; Kallop, D.; Nannini-Pepe, M.; Kotkow, K.; Marsters, J. C.; Rubin, L. L.; de Sauvage, F. J. A paracrine requirement for Hedgehog signalling in cancer. *Nature* **2008**, *455,* 406-410.

13. Tian, H.; Callahan, C. A.; DuPree, K. J.; Darbonne, W. C.; Ahn, C. P.; Scales, S. J.; de Sauvage, F. J. Hedgehog signaling is restricted to the stromal compartment during pancreatic carcinogenesis. *Proc. Natl. Acad. Sci.* **2009**, *106,* 4254-4259.

14. Berman, D. M.; Karhadkar, S. S.; Maitra, A.; Montes De, O. R.; Gerstenblith, M. R.; Briggs, K.; Parker, A. R.; Shimada, Y.; Eshleman, J. R.; Watkins, D. N.; Beachy, P. A. Widespread requirement for Hedgehog ligand stimulation in growth of digestive tract tumours. *Nature* **2003**, *425,* 846-851.

15. Karhadkar, S. S.; Bova, G. S.; Abdallah, N.; Dhara, S.; Gardner, D.; Maitra, A.; Isaacs, J. T.; Berman, D. M.; Beachy, P. A. Hedgehog signalling in prostate regeneration, neoplasia and metastasis. *Nature* **2004**, *431,* 707-712.

16. Sanchez, P.; Hernandez, A. M.; Stecca, B.; Kahler, A. J.; DeGueme, A. M.; Barrett, A.; Beyna, M.; Datta, M. W.; Datta, S.; Ruiz i Altaba, A. Inhibition of prostate cancer proliferation by interference with SONIC HEDGEHOG-GLI1 signaling. *Proc. Natl. Acad. Sci. U. S. A.* **2004**, *101,* 12561-12566.

17. Fan, L.; Pepicelli, C. V.; Dibble, C. C.; Catbagan, W.; Zarycki, J. L.; Laciak, R.; Gipp, J.; Shaw, A.; Lamm, M. L. G.; Munoz, A.; Lipinski, R.; Thrasher, J. B.; Bushman, W. Hedgehog signaling promotes prostate xenograft tumor growth. *Endocrinology* **2004**, *145,* 3961-3970.

18. Kubo, M.; Nakamura, M.; Tasaki, A.; Yamanaka, N.; Nakashima, H.; Nomura, M.; Kuroki, S.; Katano, M. Hedgehog signaling pathway is a new therapeutic target for patients with breast cancer. *Cancer Res.* **2004**, *64,* 6071-6074.

19. Mukherjee, S.; Frolova, N.; Sadlonova, A.; Novak, Z.; Steg, A.; Page, G. P.; Welch, D. R.; Lobo-Ruppert, S. M.; Ruppert, J. M.; Johnson, M. R.; Frost, A. R. Hedgehog signaling and response to cyclopamine differ in epithelial and stromal cells in benign breast and breast cancer. *Cancer Biol. Ther.* **2006**, *5,* 674-683.

20. Oniscu, A.; James, R. M.; Morris, R. G.; Bader, S.; Malcomson, R. D. G.; Harrison, D. J. Expression of Sonic Hedgehog pathway genes is altered in colonic neoplasia. *J. Pathol.* **2004**, *203,* 909-917.

21. Monzo, M.; Moreno, I.; Artells, R.; Ibeas, R.; Navarro, A.; Moreno, J.; Hernandez, R.; Granell, M.; Pie, J. Sonic hedgehog mRNA expression by real-time quantitative PCR in normal and tumor tissues from colorectal cancer patients. *Cancer Lett. (Amsterdam, Neth.)* **2006**, *233,* 117-123.

22. Chatel, G.; Ganeff, C.; Boussif, N.; Delacroix, L.; Briquet, A.; Nolens, G.; Winkler, R. Hedgehog signaling pathway is inactive in colorectal cancer cell lines. *Int. J. Cancer* **2007**, *121,* 2622-2627.

23. Dierks, C.; Grbic, J.; Zirlik, K.; Beigi, R.; Englund, N. P.; Guo, G.; Veelken, H.; Engelhardt, M.; Mertelsmann, R.; Kelleher, J. F.; Schultz, P.; Warmuth, M. Essential role of stromally induced hedgehog signaling in B-cell malignancies. *Nat. Med.* **2007**, *13,* 944-951.

24. Hegde, G. V.; Peterson, K. J.; Emanuel, K.; Mittal, A. K.; Joshi, A. D.; Dickinson, J. D.; Kollessery, G. J.; Bociek, R. G.; Bierman, P.; Vose, J. M.; Weisenburger, D. D.; Joshi, S. S. Hedgehog-induced survival of B-cell Chronic Lymphocytic Leukemia cells in a stromal cell microenvironment: A potential new therapeutic target. *Mol. Cancer Res.* **2008**, *6,* 1928-1936.

25. Amakye, D.; Jagani, Z.; Dorsch, M. Unraveling the therapeutic potential of the Hedgehog pathway in cancer. *Nat. Med. (N. Y. , NY, U. S.)* **2013**, *19,* 1410-1422.

26. Ng, J. M. Y.; Curran, T. The Hedgehog's tale: Developing strategies for targeting cancer. *Nat. Rev. Cancer* **2011**, *11,* 493-501.

27. Merchant, A. A.; Matsui, W. Targeting Hedgehog - a cancer stem cell pathway. *Clin. Cancer Res.* **2010**, *16,* 3130-3140.

28. Magee, J. A.; Piskounova, E.; Morrison, S. J. Cancer stem cells: Impact, heterogeneity, and uncertainty. *Cancer Cell* **2012**, *21,* 283-296.

29. Clevers, H. The cancer stem cell: premises, promises and challenges. *Nat. Med. (N. Y. , NY, U. S.)* **2011**, *17,* 313-319.

30. Coni, S.; Infante, P.; Gulino, A. Control of stem cells and cancer stem cells by hedgehog signaling: Pharmacologic clues from pathway dissection. *Biochem. Pharmacol. (Amsterdam, Neth.)* **2013**, *85,* 623-628.

31. *http://www.cancer.gov/cancertopics/druginfo/fda-vismodegib*.

32. Rudin, C. M.; Hann, C. L.; Laterra, J.; Yauch, R. L.; Callahan, C. A.; Fu, L.; Holcomb, T.; Stinson, J.; Gould, S. E.; Coleman, B.; LoRusso, P. M.; Von Hoff, D. D.; de Sauvage, F. J.; Low, J. A. Treatment of medulloblastoma with Hedgehog pathway inhibitor GDC-0449. *N. Engl. J. Med.* **2009**, *361,* 1173-1178.

33. Dijkgraaf, G. J. P.; Alicke, B.; Weinmann, L.; Januario, T.; West, K.; Modrusan, Z.; Burdick, D.; Goldsmith, R.; Robarge, K.; Sutherlin, D.; Scales, S. J.; Gould, S. E.; Yauch, R. L.; de Sauvage, F. J. Small-molecule inhibition of GDC-0449 refractory Smoothened mutants and downstream mechanisms of drug resistance. *Cancer Res.* **2011**, *71,* 435-444.

34. Yauch, R. L.; Dijkgraaf, G. J. P.; Alicke, B.; Januario, T.; Ahn, C. P.; Holcomb, T.; Pujara, K.; Stinson, J.; Callahan, C. A.; Tang, T.; Bazan, J. F.; Kan, Z.; Seshagiri, S.; Hann, C. L.; Gould, S. E.; Low, J. A.; Rudin, C. M.; de Sauvage, F. J. Smoothened mutation confers resistance to a Hedgehog pathway inhibitor in Medulloblastoma. *Science* **2009**, *326,* 572-574.

109

35. Buonamici, S.; Williams, J.; Morriessey, M.; Wang, A.; Guo, R.; Vattay, A.; Hsiao, K.; Yuan, J.; Green, J.; Ospina, B.; Yu, Q.; Ostrom, L.; Fordjour, P.; Anderson, D. L.; Monahan, J. E.; Kelleher, J. F.; Peukert, S.; Pan, S.; Wu, X.; Maira, S.; Garcia-Echeverria, C.; Briggs, K. J.; Watkins, D. N.; Yao, Y.; Lengauer, C.; Warmuth, M.; Sellers, W. R.; Dorsch, M. Interfering with resistance to smoothened antagonists by inhibition of the PI3K pathway in medulloblastoma. *Sci. Transl. Med.* **2010**, *2,* 51ra70.

36. Chang Anne, L. S.; Oro, A. E. Initial assessment of tumor regrowth after Vismodegib in advanced basal cell carcinoma. *Arch Dermatol* **2012**, *148,* 1324-1325.

37. Lee, M. J.; Hatton, B. A.; Villavicencio, E. H.; Khanna, P. C.; Friedman, S. D.; Ditzler, S.; Pullar, B.; Robison, K.; White, K. F.; Tunkey, C.; LeBlanc, M.; Randolph-Habecker, J.; Knoblaugh, S. E.; Hansen, S.; Richards, A.; Wainwright, B. J.; McGovern, K.; Olson, J. M. Hedgehog pathway inhibitor saridegib (IPI-926) increases lifespan in a mouse medulloblastoma model. *Proc. Natl. Acad. Sci. U. S. A.* **2012**, *109,* 7859-7864.

38. Riobo, N. A.; Lu, K.; Ai, X.; Haines, G. M.; Emerson, C. P.,Jr Phosphoinositide 3-kinase and Akt are essential for Sonic Hedgehog signaling. *Proc. Natl. Acad. Sci. U. S. A.* **2006**, *103,* 4505-4510.

39. Wang, Y.; Ding, Q.; Yen, C.; Xia, W.; Izzo, J. G.; Lang, J.; Li, C.; Hsu, J. L.; Miller, S. A.; Wang, X.; Lee, D.; Hsu, J.; Huo, L.; LaBaff, A. M.; Liu, D.; Huang, T.; Lai, C.; Tsai, F.; Chang, W.; Chen, C.; Wu, T.; Buttar, N. S.; Wang, K. K.; Wu, Y.; Wang, H.; Ajani, J.; Hung, M. The crosstalk of mTOR/S6K1 and Hedgehog pathways. *Cancer Cell* **2012**, *21,* 374-387.

40. Das, S.; Samant, R. S.; Shevde, L. A. Nonclassical activation of Hedgehog signaling enhances multidrug resistance and makes cancer cells refractory to Smoothened-targeting Hedgehog Inhibition. *J. Biol. Chem.* **2013**, *288,* 11824-11833.

41. Robarge, K. D.; Brunton, S. A.; Castanedo, G. M.; Cui, Y.; Dina, M. S.; Goldsmith, R.; Gould, S. E.; Guichert, O.; Gunzner, J. L.; Halladay, J.; Jia, W.; Khojasteh, C.; Koehler, M. F. T.; Kotkow, K.; La, H.; La Londe, R. L.; Lau, K.; Lee, L.; Marshall, D.; Marsters, J. C.; Murray, L. J.; Qian, C.; Rubin, L. L.; Salphati, L.; Stanley, M. S.; Stibbard, J. H. A.; Sutherlin, D. P.; Ubhayaker, S.; Wang, S.; Wong, S.; Xie, M. GDC-0449-A potent inhibitor of the Hedgehog pathway. *Bioorg. Med. Chem. Lett.* **2009**, *19,* 5576-5581.

42. Rudin, C. M. Vismodegib. *Clin. Cancer Res.* **2012**, *18,* 3218-3222.

43. Pan, S.; Wu, X.; Jiang, J.; Gao, W.; Wan, Y.; Cheng, D.; Han, D.; Liu, J.; Englund, N. P.; Wang, Y.; Peukert, S.; Miller-Moslin, K.; Yuan, J.; Guo, R.; Matsumoto, M.; Vattay, A.; Jiang, Y.; Tsao, J.; Sun, F.; Pferdekamper, A. C.; Dodd, S.; Tuntland, T.; Maniara, W.; Kelleher, J. F.,III; Yao, Y.; Warmuth, M.; Williams, J.; Dorsch, M. Discovery of NVP-LDE225, a potent and selective Smoothened antagonist. *ACS Med. Chem. Lett.* **2010**, *1,* 130-134.

44. Taipale, J.; Chen, J. K.; Cooper, M. K.; Wang, B.; Mann, R. K.; Milenkovic, L.; Scotts, M. P.; Beachy, P. A. Effects of oncogenic mutations in Smoothened and Patched can be reversed by cyclopamine. *Nature (London)* **2000**, *406,* 1005-1009.

45. Rominger, C. M.; Bee, W. T.; Copeland, R. A.; Davenport, E. A.; Gilmartin, A.; Gontarek, R.; Hornberger, K. R.; Kallal, L. A.; Lai, Z.; Lawrie, K.; Lu, Q.; McMillan, L.; Truong, M.; Tummino, P. J.; Turunen, B.; Will, M.; Zuercher, W. J.; Rominger, D. H. Evidence for allosteric interactions of antagonist binding to the Smoothened receptor. *J. Pharmacol. Exp. Ther.* **2009**, *329,* 995-1005.

46. Chen, J. K.; Taipale, J.; Cooper, M. K.; Beachy, P. A. Inhibition of hedgehog signaling by direct binding of cyclopamine to smoothened. *Genes Dev.* **2002**, *16,* 2743-2748.

47. Zhang, J.; Garrossian, M.; Gardner, D.; Garrossian, A.; Chang, Y.; Kim, Y. K.; Chang, C. T. Synthesis and anticancer activity studies of cyclopamine derivatives. *Bioorg. Med. Chem. Lett.* **2008**, *18,* 1359-1363.

48. Winkler, J. D.; Isaacs, A.; Holderbaum, L.; Tatard, V.; Dahmane, N. Design and synthesis of inhibitors of Hedgehog signaling based on the alkaloid cyclopamine. *Org Lett* **2009**, *11,* 2824-2827.

49. Feldmann, G.; Fendrich, V.; McGovern, K.; Bedja, D.; Bisht, S.; Alvarez, H.; Koorstra, J. M.; Habbe, N.; Karikari, C.; Mullendore, M.; Gabrielson, K. L.; Sharma, R.; Matsui, W.; Maitra, A. An orally bioavailable small-molecule inhibitor of Hedgehog signaling inhibits tumor initiation and metastasis in pancreatic cancer. *Mol. Cancer Ther.* **2008**, *7,* 2725-2735.

50. Tremblay, M. R.; Lescarbeau, A.; Grogan, M. J.; Tan, E.; Lin, G.; Austad, B. C.; Yu, L.; Behnke, M. L.; Nair, S. J.; Hagel, M.; White, K.; Conley, J.; Manna, J. D.; Alvarez-Diez, T. M.; Hoyt, J.; Woodward, C. N.; Sydor, J. R.; Pink, M.; MacDougall, J.; Campbell, M. J.; Cushing, J.; Ferguson, J.; Curtis, M. S.; McGovern, K.; Read, M. A.; Palombella, V. J.; Adams, J.; Castro, A. C. Discovery of a potent and orally active Hedgehog pathway antagonist (IPI-926). *J Med Chem* **2009**, *52,* 4400-4418.

51. Wagner, A. H. P.; Okuno, S.; Eriksson, M.; Shreyaskumar, P.; Ferrari, S.; Casali, P.; Chawla, S.; Woehr, M.; Ross, R.; O'Keeffe, J.; Hillock, A.; Demetri, G.; Reichardt, P. In *In Results from a phase 2 randomized, placebo-controlled, double blind study of the hedgehog (HH) pathway antagonist IPI-926 in patients (PTS) with advanced chondrosarcoma (CS).* Connective Tissue Oncology Society 18th Annual Meeting; 2013; .

52. Winkler, J. D.; Isaacs, A. K.; Xiang, C.; Baubet, V.; Dahmane, N. Design, synthesis, and biological evaluation of estrone-derived Hedgehog signaling inhibitors. *Tetrahedron* **2011**, *67,* 10261-10266.

53. Heretsch, P.; Buettner, A.; Tzagkaroulaki, L.; Zahn, S.; Kirchner, B.; Giannis, A. Exo-Cyclopamine - a stable and potent inhibitor of hedgehog-signaling. *Chem. Commun. (Cambridge, U. K.)* **2011**, *47,* 7362-7364.

54. Moschner, J.; Chentsova, A.; Eilert, N.; Rovardi, I.; Giannis, A.; Heretsch, P. Cyclopamine analogs bearing exocyclic methylenes are highly potent and acid-stable inhibitors of hedgehog signaling. *Beilstein J Org Chem* **2013**, *9,* 2328-2335.

55. Heretsch, P.; Tzgkaroulaki, L.; Giannis, A. Cyclopamine and Hedgehog signaling: Chemistry, biology, medical perspectives. *Angew. Chem. , Int. Ed.* **2010**, *49,* 3418-3427.

56. Munchhof, M. J.; Li, Q.; Shavnya, A.; Borzillo, G. V.; Boyden, T. L.; Jones, C. S.; LaGreca, S. D.; Martinez-Alsina, L.; Patel, N.; Pelletier, K.; Reiter, L. A.; Robbins, M. D.; Tkalcevic, G. T. Discovery of PF-04449913, a potent and orally bioavailable inhibitor of Smoothened. *ACS Med. Chem. Lett.* **2012**, *3,* 106-111.

57. Rohner, A.; Spilker, M. E.; Lam, J. L.; Pascual, B.; Bartkowski, D.; Li, Q. J.; Yang, A. H.; Stevens, G.; Xu, M.; Wells, P. A.; Planken, S.; Nair, S.; Sun, S. Effective targeting of Hedgehog signaling in a Medulloblastoma model with PF-5274857, a potent and selective Smoothened antagonist that penetrates the blood-brain barrier. *Mol. Cancer Ther.* **2012**, *11,* 57-65.

58. Miller-Moslin, K.; Peukert, S.; Jain, R. K.; McEwan, M. A.; Karki, R.; Llamas, L.; Yusuff, N.; He, F.; Li, Y.; Sun, Y.; Dai, M.; Perez, L.; Michael, W.; Sheng, T.; Lei, H.; Zhang, R.; Williams, J.; Bourret, A.; Ramamurthy, A.; Yuan, J.; Guo, R.; Matsumoto, M.; Vattay, A.; Maniara, W.; Amaral, A.; Dorsch, M.; Kelleher, J. F.,III 1-Amino-4-benzylphthalazines as orally bioavailable Smoothened antagonists with antitumor activity. *J. Med. Chem.* **2009**, *52,* 3954-3968.

59. Peukert, S.; He, F.; Dai, M.; Zhang, R.; Sun, Y.; Miller-Moslin, K.; McEwan, M.; Lagu, B.; Wang, K.; Yusuff, N.; Bourret, A.; Ramamurthy, A.; Maniara, W.; Amaral, A.; Vattay, A.; Wang, A.; Guo, R.; Yuan, J.; Green, J.; Williams, J.; Buonamici, S.; Kelleher, J. F.; Dorsch, M. Discovery of NVP-LEQ506, a second-generation inhibitor of Smoothened. *ChemMedChem* **2013**, *8,* 1261-1265.

60. Ohashi, T.; Oguro, Y.; Tanaka, T.; Shiokawa, Z.; Shibata, S.; Sato, Y.; Yamakawa, H.; Hattori, H.; Yamamoto, Y.; Kondo, S.; Miyamoto, M.; Tojo, H.; Baba, A.; Sasaki, S. Discovery of pyrrolo[3,2-c]quinoline-4-one derivatives as novel Hedgehog signaling inhibitors. *Bioorg. Med. Chem.* **2012**, *20,* 5496-5506.

61. Ohashi, T.; Oguro, Y.; Tanaka, T.; Shiokawa, Z.; Tanaka, Y.; Shibata, S.; Sato, Y.; Yamakawa, H.; Hattori, H.; Yamamoto, Y.; Kondo, S.; Miyamoto, M.; Nishihara, M.; Ishimura, Y.; Tojo, H.; Baba, A.; Sasaki, S. Discovery of the investigational drug TAK-441, a pyrrolo[3,2-c]pyridine derivative, as a highly potent and orally active Hedgehog signaling inhibitor: Modification of the core skeleton for improved solubility. *Bioorg. Med. Chem.* **2012**, *20,* 5507-5517.

62. Ishii, T.; Shimizu, Y.; Nakashima, K.; Kondo, S.; Ogawa, K.; Sasaki, S.; Matsui, H. Inhibition mechanism exploration of investigational drug TAK-441 as inhibitor against Vismodegib-resistant Smoothened mutant. *Eur. J. Pharmacol.* **2014**, *723,* 305-313.

63. *http://www.takeda.com/research/files/pipeline_20130204_en.pdf*.

64. Ibuki, N.; Ghaffari, M.; Pandey, M.; Iu, I.; Fazli, L.; Kashiwagi, M.; Tojo, H.; Nakanishi, O.; Gleave, M. E.; Cox, M. E. TAK-441, a novel investigational smoothened antagonist, delays castration-resistant progression in prostate cancer by disrupting paracrine hedgehog signaling. *Int. J. Cancer* **2013**, *133,* 1955-1966.

65. Hipskind, P. A.; Takakuwa, T. US Patent WO2009134574, **2009**.

66. Bender, M. H.; Hipskind, P. A.; Capen, A. R.; Cockman, M.; Credille, K. M.; Gao, H.; Bastian, J. A.; Clay, J. M.; Lobb, K. L.; Sall, D. J.; Thompson, M. L.; Wilson, T.; Wishart, G. N.; Patel, B. K. R. Identification and characterization of a novel smoothened antagonist for the treatment of cancer with deregulated hedgehog signaling. *Cancer Res.* **2011**, *71,* Suppl 1-Abstract 2819.

67. Gendreau, S. B.; Hawkins, D.; Ho, C.; Lewin, A.; Lin, T.; Merchant, A.; Rowley, R. B.; Wang, Q.; Matsui, W.; Fargnoli, J. Preclinical characterization of BMS-833923 (XL139), a hedgehog (HH) pathway inhibitor in early clinical development. *Mol Cancer Ther* **2009**, *8,* Meeting Abstract Supplement.

68. Malancona, S.; Altamura, S.; Filocamo, G.; Kinzel, O.; Hernando, J. I. M.; Rowley, M.; Scarpelli, R.; Steinkuehler, C.; Jones, P. Identification of MK-5710 ((8aS)-8a-methyl-1,3-dioxo-2-[(1S,2R)-2-phenylcyclopropyl]-N-(1-phenyl-1H-pyrazol-5-yl)hexahydroimidazo[1,5-a]pyrazine-7(1H)-carboxamide), a potent smoothened antagonist for use in Hedgehog pathway dependent malignancies, Part 1. *Bioorg. Med. Chem. Lett.* **2011**, *21,* 4422-4428.

69. Kinzel, O.; Alfieri, A.; Altamura, S.; Brunetti, M.; Bufali, S.; Colaceci, F.; Ferrigno, F.; Filocamo, G.; Fonsi, M.; Gallinari, P.; Malancona, S.; Hernando, J. I. M.; Monteagudo, E.; Orsale, M. V.; Palumbi, M. C.; Pucci, V.; Rowley, M.; Sasso, R.; Scarpelli, R.; Steinkuehler, C.; Jones, P. Identification of MK-5710 ((8aS)-8a-methyl-1,3-dioxo-2-[(1S,2R)-2-phenylcyclo- propyl]-N-(1-phenyl-1H-pyrazol-5-yl)hexahydro-imidazo[1,5-a]pyrazine-7(1H)-carboxamide), a potent smoothened antagonist for use in Hedgehog pathway dependent malignancies, Part 2. *Bioorg. Med. Chem. Lett.* **2011**, *21,* 4429-4435.

70. Ontoria, J. M.; Bufi, L. L.; Torrisi, C.; Bresciani, A.; Giomini, C.; Rowley, M.; Serafini, S.; Bin, H.; Hao, W.; Steinkuehler, C.; Jones, P. Identification of a series of 4-[3-(quinolin-2-yl)-1,2,4-oxadiazol-5-yl]piperazinyl ureas as potent Smoothened antagonist Hedgehog pathway inhibitors. *Bioorg. Med. Chem. Lett.* **2011**, *21,* 5274-5282.

71. Muraglia, E.; Ontoria, J. M.; Branca, D.; Dessole, G.; Bresciani, A.; Fonsi, M.; Giuliano, C.; Llauger Bufi, L.; Monteagudo, E.; Palumbi, M. C.; Torrisi, C.; Rowley, M.; Steinkuehler, C.; Jones, P. N-(2-alkylaminoethyl)-4-(1,2,4-oxadiazol-5-yl)piperazine-1-carboxamides as highly potent smoothened antagonists. *Bioorg. Med. Chem. Lett.* **2011**, *21,* 5283-5288.

72. Tao, H.; Jin, Q.; Koo, D.; Liao, X.; Englund, N. P.; Wang, Y.; Ramamurthy, A.; Schultz, P. G.; Dorsch, M.; Kelleher, J.; Wu, X. Small molecule antagonists in distinct binding modes Inhibit drug-resistant mutant of Smoothened. *Chem. Biol. (Cambridge, MA, U. S.)* **2011**, *18,* 432-437.

73. Strand, M. F.; Wilson, S. R.; Dembinski, J. L.; Holsworth, D. D.; Khvat, A.; Okun, I.; Petersen, D.; Krauss, S. A novel synthetic Smoothened antagonist transiently inhibits pancreatic adenocarcinoma xenografts in a mouse model. *PLoS One* **2011**, *6,* e19904.

74. Peukert, S.; Jain, R. K.; Geisser, A.; Sun, Y.; Zhang, R.; Bourret, A.; Carlson, A.; DaSilva, J.; Ramamurthy, A.; Kelleher, J. F. Identification and structure-activity relationships of ortho-biphenyl carboxamides as potent Smoothened antagonists inhibiting the Hedgehog signaling pathway. *Bioorg. Med. Chem. Lett.* **2009**, *19,* 328-331.

75. Wang, Y.; Arvanites, A. C.; Davidow, L.; Blanchard, J.; Lam, K.; Yoo, J. W.; Coy, S.; Rubin, L. L.; McMahon, A. P. Selective identification of Hedgehog pathway antagonists by direct analysis of Smoothened ciliary translocation. *ACS Chem. Biol.* **2012**, *7,* 1040-1048.

76. Wu, V. M.; Chen, S. C.; Arkin, M. R.; Reiter, J. F. Small molecule inhibitors of Smoothened ciliary localization and ciliogenesis. *Proc. Natl. Acad. Sci. U. S. A.* **2012**, *109,* 13644-13649.

77. Manetti, F.; Faure, H.; Roudaut, H.; Gorojankina, T.; Traiffort, E.; Schoenfelder, A.; Mann, A.; Solinas, A.; Taddei, M.; Ruat, M. Virtual screening-based discovery and mechanistic characterization of the acylthiourea MRT-10 family as smoothened antagonists. *Mol. Pharmacol.* **2010**, *78,* 658-665.

78. Solinas, A.; Faure, H.; Roudaut, H.; Traiffort, E.; Schoenfelder, A.; Mann, A.; Manetti, F.; Taddei, M.; Ruat, M. Acylthiourea, acylurea, and acylguanidine derivatives with potent Hedgehog inhibiting activity. *J. Med. Chem.* **2012**, *55,* 1559-1571.

79. Xin, M.; Wen, J.; Tang, F.; Tu, C.; Shen, H.; Zhao, X. The discovery of novel N-(2-pyrimidinylamino) benzamide derivatives as potent hedgehog signaling pathway inhibitors. *Bioorg. Med. Chem. Lett.* **2013**, *23,* 6777-6783.

80. Xin, M.; Wen, J.; Tang, F.; Tu, C.; Huang, W.; Shen, H.; Zhao, X.; Cheng, L.; Wang, M.; Zhang, L. Synthesis and evaluation of 4-(2-pyrimidinylamino) benzamides inhibitors of Hedgehog signaling pathway. *Bioorg. Med. Chem. Lett.* **2014**, *24,* 983-988.

81. Xin, M.; Zhang, L.; Tang, F.; Tu, C.; Wen, J.; Zhao, X.; Liu, Z.; Cheng, L.; Shen, H. Design, synthesis, and evaluation of pyrrolo[2,1-f][1,2,4]triazine derivatives as novel Hedgehog signaling pathway inhibitors. *Bioorg. Med. Chem.* **2014**, *22,* 1429-1440.

82. Nedelcu, D.; Liu, J.; Xu, Y.; Jao, C.; Salic, A. Oxysterol binding to the extracellular domain of Smoothened in Hedgehog signaling. *Nat. Chem. Biol.* **2013**, *9,* 557-564.

83. Wang, Y.; Davidow, L.; Arvanites, A. C.; Blanchard, J.; Lam, K.; Xu, K.; Oza, V.; Yoo, J. W.; Ng, J. M. Y.; Curran, T.; Rubin, L. L.; McMahon, A. P. Glucocorticoid compounds modify Smoothened localization and Hedgehog pathway activity. *Chem. Biol.* **2012**, *19,* 972-982.

84. Nachtergaele, S.; Whalen, D. M.; Mydock, L. K.; Zhao, Z.; Malinauskas, T.; Krishnan, K.; Ingham, P. W.; Covey, D. F.; Siebold, C.; Rohatgi, R. Structure and function of the Smoothened extracellular domain in vertebrate Hedgehog signaling. *Elife* **2013**, *2,* e01340.

85. Myers, B. R.; Sever, N.; Chong, Y. C.; Kim, J.; Belani, J. D.; Rychnovsky, S.; Bazan, J. F.; Beachy, P. A. Hedgehog Pathway modulation by multiple lipid binding sites on the Smoothened effector of signal response. *Dev. Cell* **2013**, *26,* 346-357.

86. Rana, R.; Carroll, C. E.; Lee, H.; Bao, J.; Marada, S.; Grace, C. R. R.; Guibao, C. D.; Ogden, S. K.; Zheng, J. J. Structural insights into the role of the Smoothened cysteine-rich domain in Hedgehog signalling. *Nat. Commun.* **2013**, *4,* 3965/1-3965/9.

87. Wang, C.; Wu, H.; Katritch, V.; Han, G. W.; Huang, X.; Liu, W.; Siu, F. Y.; Roth, B. L.; Cherezov, V.; Stevens, R. C. Structure of the human Smoothened receptor bound to an antitumour agent. *Nature (London, U. K.)* **2013**, *497,* 338-343.

88. Weierstall, U.; James, D.; Wang, C.; White, T. A.; Wang, D.; Liu, W.; Spence, J. C. H.; Doak, R. B.; Nelson, G.; Fromme, P.; Fromme, R.; Grotjohann, I.; Kupitz, C.; Zatsepin, N. A.; Liu, H.; Basu, S.; Wacker, D.; Han, G. W.; Katritch, V.; Boutet, S.; Messerschmidt, M.; Williams, G.; Koglin, J. E.; Seibert, M. M.; Klinker, M.; Gati, C.; Shoeman, R. L.; Barty, A.; Chapman, H. N.; Kirian, R. A.; Beyerlein, K. R.; Stevens, R. C.; Li, D.; Shah, S. T. A.; Howe, N.; Caffrey, M.; Cherezov, V. Lipidic cubic phase injector facilitates membrane protein serial femtosecond crystallography. *Nat. Commun.* **2014**, *5,* 4309/1-4307/6.

89. Metcalfe, C.; de Sauvage, F. J. Hedgehog fights back: Mechanisms of acquired resistance against Smoothened antagonists. *Cancer Res.* **2011**, *71,* 5057-5061.

90. Chamoun, Z.; Mann, R. K.; Nellen, D.; von Kessler, D. P.; Bellotto, M.; Beachy, P. A.; Basler, K. Skinny hedgehog, an acyltransferase required for palmitoylation and activity of the hedgehog signal. *Science (Washington, DC, U. S.)* **2001**, *293,* 2080-2084.

91. Petrova, E.; Rios-Esteves, J.; Ouerfelli, O.; Glickman, J. F.; Resh, M. D. Inhibitors of Hedgehog acyltransferase block Sonic Hedgehog signaling. *Nat. Chem. Biol.* **2013**, *9,* 247-249.

92. Stanton, B. Z.; Peng, L. F.; Maloof, N.; Nakai, K.; Wang, X.; Duffner, J. L.; Taveras, K. M.; Hyman, J. M.; Lee, S. W.; Koehler, A. N.; Chen, J. K.; Fox, J. L.; Mandinova, A.; Schreiber, S. L. A small molecule that binds Hedgehog and blocks its signaling in human cells. *Nat. Chem. Biol.* **2009**, *5,* 154-156.

93. Dockendorff, C.; Nagiec, M. M.; Weiwer, M.; Buhrlage, S.; Ting, A.; Nag, P. P.; Germain, A.; Kim, H.; Youngsaye, W.; Scherer, C.; Bennion, M.; Xue, L.; Stanton, B. Z.; Lewis, T. A.; MacPherson, L.; Palmer, M.; Foley, M. A.; Perez, J. R.; Schreiber, S. L. Macrocyclic Hedgehog pathway inhibitors: Optimization of cellular activity and mode of action studies. *ACS Med. Chem. Lett.* **2012**, *3,* 808-813.

94. Hwang, S.; Thangapandian, S.; Lee, Y.; Sakkiah, S.; John, S.; Lee, K. W. Discovery and evaluation of potential Sonic Hedgehog signaling pathway inhibitors using pharmacophore modeling and molecular dyanamics simulations. *J. Bioinf. Comput. Biol.* **2011**, *9,* 15-35.

95. Hwang, S.; Thangapandian, S.; Lee, K. W. Molecular dynamics simulations of sonic hedgehog-receptor and inhibitor complexes and their applications for potential anticancer agent discovery. *PLoS One* **2013**, *8,* e68271.

96. Lauth, M.; Bergstroem, A.; Shimokawa, T.; Toftgard, R. Inhibition of GLI-mediated transcription and tumor cell growth by small-molecule antagonists. *Proc. Natl. Acad. Sci. U. S. A.* **2007**, *104,* 8455-8460.

97. Bosco-Clement, G.; Zhang, F.; Chen, Z.; Zhou, H. -.; Li, H.; Mikami, I.; Hirata, T.; Yagui-Beltran, A.; Lui, N.; Do, H. T.; Cheng, T.; Tseng, H. -.; Choi, H.; Fang, L. -.; Kim, I. -.; Yue, D.; Wang, C.; Zheng, Q.; Fujii, N.; Mann, M.; Jablons, D. M.; He, B. Targeting Gli transcription activation by small molecule suppresses tumor growth. *Oncogene* **2014**, *33,* 2087-2097.

98. Mahindroo, N.; Connelly, M. C.; Punchihewa, C.; Kimura, H.; Smeltzer, M. P.; Wu, S.; Fujii, N. Structure-Activity Relationships and cancer-cell selective toxicity of novel inhibitors of glioma-associated oncogene homologue 1 (Gli1) mediated transcription. *J. Med. Chem.* **2009**, *52,* 4277-4287.

99. Zhang, P. The use of arsenic trioxide (As2O3) in the treatment of acute promyelocytic leukemia. *J. Biol. Regul. Homeostatic Agents* **1999**, *13,* 195-200.

100. Kim, J.; Lee, J. J.; Kim, J.; Gardner, D.; Beachy, P. A. Arsenic antagonizes the Hedgehog pathway by preventing ciliary accumulation and reducing stability of the Gli2 transcriptional effector. *Proc. Natl. Acad. Sci. U. S. A. , Early Ed.* **2010**, *107,* 13432-13437.

101. Kim, J.; Aftab, B. T.; Tang, J. Y.; Kim, D.; Lee, A. H.; Rezaee, M.; Kim, J.; Chen, B.; King, E. M.; Borodovsky, A.; Riggins, G. J.; Epstein, E. H.; Beachy, P. A.; Rudin, C. M. Itraconazole and Arsenic Trioxide inhibit Hedgehog pathway activation and tumor growth associated with acquired resistance to Smoothened antagonists. *Cancer Cell* **2013**, *23,* 23-34.

102. Beauchamp, E. M.; Ringer, L.; Bulut, G.; Sajwan, K. P.; Hall, M. D.; Lee, Y.; Peaceman, D.; Ozdemirli, M.; Rodriguez, O.; MacDonald, T. J.; Albanese, C.; Toretsky, J. A.; Uren, A. Arsenic trioxide inhibits human cancer cell growth and tumor development in mice by blocking Hedgehog/GLI pathway. *J. Clin. Invest.* **2011**, *121,* 148-160.

103. Hyman, J. M.; Firestone, A. J.; Heine, V. M.; Zhao, Y.; Ocasio, C. A.; Han, K.; Sun, M.; Rack, P. G.; Sinha, S.; Wu, J. J.; Solow-Cordero, D. E.; Jiang, J.; Rowitch, D. H.; Chen, J. K. Small-molecule inhibitors reveal multiple strategies for hedgehog pathway blockade. *Proc. Natl. Acad. Sci. U. S. A.* **2009**, *106,* 14132-14137.

104. Chenna, V.; Hu, C.; Pramanik, D.; Aftab, B. T.; Karikari, C.; Campbell, N. R.; Hong, S.; Zhao, M.; Rudek, M. A.; Khan, S. R.; Rudin, C. M.; Maitra, A. A polymeric nanoparticle encapsulated small-molecule Inhibitor of Hedgehog Signaling (NanoHHI) bypasses secondary mutational resistance to Smoothened antagonists. *Mol. Cancer Ther.* **2012**, *11,* 165-173.

105. Xu, Y.; Chenna, V.; Hu, C.; Sun, H.; Khan, M.; Bai, H.; Yang, X.; Zhu, Q.; Sun, Y.; Maitra, A.; Fan, J.; Anders, R. A. Polymeric nanoparticle-encapsulated Hedgehog pathway Inhibitor HPI-1 (NanoHHI) Inhibits systemic metastases in an orthotopic model of human hepatocellular carcinoma. *Clin. Cancer Res.* **2012**, *18,* 1291-1302.

106. Rifai, Y.; Arai, M. A.; Sadhu, S. K.; Ahmed, F.; Ishibashi, M. New Hedgehog/GLI signaling inhibitors from Excoecaria agallocha. *Bioorg. Med. Chem. Lett.* **2011**, *21,* 718-722.

107. Bijlsma, M. F.; Spek, C. A.; Zivkovic, D.; van de Water, S.; Rezaee, F.; Peppelenbosch, M. P. Repression of smoothened by patched-dependent (pro-)vitamin D3 secretion. *PLoS Biol.* **2006**, *4,* 1397-1410.

108. Banerjee, U.; Ghosh, M.; Kyle Hadden, M. Evaluation of vitamin D3 A-ring analogues as Hedgehog pathway inhibitors. *Bioorg. Med. Chem. Lett.* **2012**, *22,* 1330-1334.

109. Lois, W. B.; Karla, C. S. Q.; Khatera, Z.; Amber van Straaten; C. Arnold Spek; Maarten F Bijlsma Assessing the efficacy of the hedgehog pathway inhibitor vitamin D3 in a murine xenograft model for pancreatic cancer. *Cancer Biol. & Therapy* **2010**, *10,* 79-88.

110. Tang, J. Y.; Xiao, T. Z.; Oda, Y.; Chang, K. S.; Shpall, E.; Wu, A.; So, P.; Hebert, J.; Bikle, D.; Epstein, E. H.,Jr Vitamin D3 inhibits hedgehog signaling and proliferation in murine basal cell carcinomas. *Cancer Prev. Res.* **2011**, *4,* 744-751.

111. DeBerardinis, A. M.; Banerjee, U.; Miller, M.; Lemieux, S.; Hadden, M. K. Probing the structural requirements for vitamin D3 inhibition of the hedgehog signaling pathway. *Bioorg. Med. Chem. Lett.* **2012**, *22,* 4859-4863.

112. Albert, B.; Hahn, H. Interaction of Hedgehog and Vitamin D signaling pathways in basal cell carcinomas. In *Sunlight, Vitamin D and Skin Cancer;* Reichrath, J., Ed.; Landes Biosciences & Springer Science: Austin, TX, 2014; pp 329.

113. DeBerardinis, A. M.; Banerjee, U.; Hadden, M. K. Identification of Vitamin D3-based Hedgehog pathway inhibitors that Incorporate an aromatic A-ring isostere. *ACS Med. Chem. Lett.* **2013**, *4,* 590-595.

114. DeBerardinis, A. M.; Madden, D.; Banerjee, U.; Sail, V.; Raccuia, D. S.; De Carlo, D.; Lemieux, S.; Meares, A.; Hadden, M. K. Structure-Activity Relationships for Vitamin D3-based aromatic A-Ring analogues as Hedgehog pathway inhibitors. *J. Med. Chem.* **2014**, *57,* 3724-3736.

115. Guerlet, G.; Spangenberg, T.; Mann, A.; Faure, H.; Ruat, M. Synthesis and biological evaluation of desmethylveramiline, a micromolar Hedgehog inhibitor. *Bioorg. Med. Chem. Lett.* **2011**, *21,* 3608-3612.

116. Kim, J.; Tang, J. Y.; Gong, R.; Kim, J.; Lee, J. J.; Clemons, K. V.; Chong, C. R.; Chang, K. S.; Fereshteh, M.; Gardner, D.; Reya, T.; Liu, J. O.; Epstein, E. H.; Stevens,

D. A.; Beachy, P. A. Itraconazole, a commonly used antifungal that inhibits hedgehog pathway activity and cancer growth. *Cancer Cell* **2010**, *17,* 388-399.

117. Kim, D. J.; Kim, J.; Spaunhurst, K.; Montoya, J.; Khodosh, R.; Chandra, K.; Fu, T.; Gilliam, A.; Molgo, M.; Beachy, P. A.; Tang, J. Y. Open-label, exploratory phase II trial of oral Itraconazole for the treatment of Basal Cell Carcinoma. *J Clin Oncol* **2014**, *32,* 745-751.

118. Chong, C. R.; Xu, J.; Lu, J.; Bhat, S.; Sullivan, D. J., Jr.; Liu, J. O. Inhibition of angiogenesis by the antifungal drug itraconazole. *ACS Chem. Biol.* **2007**, *2,* 263-270.

119. Aftab, B. T.; Dobromilskaya, I.; Liu, J. O.; Rudin, C. M. Itraconazole Inhibits angiogenesis and tumor growth in Non-Small Cell Lung cancer. *Cancer Res.* **2011**, *71,* 6764-6772.

120. Shi, W.; Nacev, B. A.; Aftab, B. T.; Head, S.; Rudin, C. M.; Liu, J. O. Itraconazole side chain analogues: Structure-activity relationship studies for Inhibition of endothelial cell proliferation, vascular endothelial Growth Factor Receptor 2 (VEGFR2) glycosylation, and Hedgehog signaling. *J. Med. Chem.* **2011**, *54,* 7363-7374.

121. Schaefer, G. I.; Perez, J. R.; Duvall, J. R.; Stanton, B. Z.; Shamji, A. F.; Schreiber, S. L. Discovery of small-molecule modulators of the Sonic Hedgehog pathway. *J. Am. Chem. Soc.* **2013**, *135,* 9675-9680.

122. Bassilana, F.; Carlson, A.; Da Silva, J. A.; Grosshans, B.; Vidal, S.; Beck, V.; Wilmeringwetter, B.; Llamas, L. A.; Showalter, T. B.; Rigollier, P.; Bourret, A.; Ramamurthy, A.; Wu, X.; Harbinski, F.; Plonsky, S.; Lee, L.; Ruffner, H.; Grandi, P.; Schirle, M.; Jenkins, J.; Sailer, A. W.; Bouwmeester, T.; Porter, J. A.; Myer, V.; Finan, P. M.; Tallarico, J. A.; Kelleher, J. F.,III; Seuwen, K.; Jain, R. K.; Luchansky, S. J. Target identification for a Hedgehog pathway inhibitor reveals the receptor GPR39. *Nat. Chem. Biol.* **2014**, *10,* 343-349.

123. Arai, M. A.; Tateno, C.; Hosoya, T.; Koyano, T.; Kowithayakorn, T.; Ishibashi, M. Hedgehog/GLI-mediated transcriptional inhibitors from *Zizyphus cambodiana*. *Bioorg. Med. Chem.* **2008**, *16,* 9420-9424.

124. Eichenmueller, M.; Hemmerlein, B.; von Schweinitz, D.; Kappler, R. Betulinic acid induces apoptosis and inhibits hedgehog signalling in rhabdomyosarcoma. *Br. J. Cancer* **2010**, *103,* 43-51.

125. Tan, Y.; Yu, R.; Pezzuto, J. M. Betulinic acid-induced programmed cell death in human melanoma cells involves mitogen-activated protein kinase activation. *Clin. Cancer Res.* **2003**, *9,* 2866-2875.

126. Kim, W.; Meliton, V.; Park, K. W.; Hong, C.; Tontonoz, P.; Niewiadomski, P.; Waschek, J. A.; Tetradis, S.; Parhami, F. Negative regulation of Hedgehog signaling by liver X receptors. *Mol. Endocrinol.* **2009**, *23,* 1532-1543.

127. Bei, Y.; Chen, X.; Liu, Y.; Xu, J.; Wang, W.; Gu, Z.; Xing, K.; Zhu, A.; Chen, W.; Shi, L.; Wang, Q.; Zhang, X.; Zhang, Q. Novel norcantharidin-loaded liver targeting chitosan nanoparticles to enhance intestinal absorption. *Int. J. Nanomed.* **2012**, *7,* 1819-1827.

128. Chen, Y.; Kuo, C.; Chen, S.; Chen, W.; Huang, W.; Chao, K. S. C.; Liao, H. Small-molecule synthetic compound norcantharidin reverses multi-drug resistance by regulating Sonic hedgehog signaling in human breast cancer cells. *PLoS One* **2012**, *7,* e37006.

129. Zhang, L.; Ji, Q.; Liu, X.; Chen, X.; Chen, Z.; Qiu, Y.; Sun, J.; Cai, J.; Zhu, H.; Li, Q. Norcantharidin inhibits tumor angiogenesis via blocking VEGFR2/MEK/ERK signaling pathways. *Cancer Sci.* **2013**, *104,* 604-610.

130. Lee, J.; Wu, X.; Pasca di Magliano, M.; Peters, E. C.; Wang, Y.; Hong, J.; Hebrok, M.; Ding, S.; Cho, C. Y.; Schultz, P. G. A small-molecule antagonist of the Hedgehog signaling pathway. *ChemBioChem* **2007**, *8,* 1916-1919.

131. Cupido, T.; Rack, P. G.; Firestone, A. J.; Hyman, J. M.; Han, K.; Sinha, S.; Ocasio, C. A.; Chen, J. K. The imidazopyridine derivative JK184 reveals dual roles for microtubules in Hedgehog signaling. *Angew Chem Int Ed Engl* **2009**, *48,* 2321-2324.

132. Ericson, J.; Morton, S.; Kawakami, A.; Roelink, H.; Jessell, T. M. Two critical periods of sonic hedgehog signaling required for the specification of motor neuron identity. *Cell (Cambridge, Mass.)* **1996**, *87,* 661-673.

133. Maun, H. R.; Wen, X.; Lingel, A.; de Sauvage, F. J.; Lazarus, R. A.; Scales, S. J.; Hymowitz, S. G. Hedgehog pathway antagonist 5E1 binds Hedgehog at the pseudo-active site. *J. Biol. Chem.* **2010**, *285,* 26570-26580.

134. Michaud, N. R.; Wang, Y.; McEachern, K. A.; Jordan, J. J.; Mazzola, A. M.; Hernandez, A.; Jalla, S.; Chesebrough, J. W.; Hynes, M. J.; Belmonte, M. A.; Wang, L.; Kang, J. S.; Jovanovic, J.; Laing, N.; Jenkins, D. W.; Hurt, E.; Liang, M.; Frantz, C.; Hollingsworth, R. E.; Simeone, D. M.; Blakey, D. C.; Bedian, V. Novel neutralizing Hedgehog antibody MEDI-5304 exhibits antitumor activity by inhibiting paracrine Hedgehog signaling. *Mol. Cancer Ther.* **2014**, *13,* 386-398.

135. Bailey, J. M.; Mohr, A. M.; Hollingsworth, M. A. Sonic hedgehog paracrine signaling regulates metastasis and lymphangiogenesis in pancreatic cancer. *Oncogene* **2009**, *28,* 3513-3525.

136. Chang, Q.; Foltz, W. D.; Chaudary, N.; Hill, R. P.; Hedley, D. W. Tumor-stroma interaction in orthotopic primary pancreatic cancer xenografts during hedgehog pathway inhibition. *Int. J. Cancer* **2013**, *133,* 225-234.

137. Coon, V.; Laukert, T.; Pedone, C. A.; Laterra, J.; Kim, K. J.; Fults, D. W. Molecular therapy targeting Sonic hedgehog and hepatocyte Growth Factor signaling in a mouse model of medulloblastoma. *Mol. Cancer Ther.* **2010**, *9,* 2627-2636.

138. Jenkins, D.; Kang, J. S.; Laing, N.; Michaud, N. WO2010032061, 2010.

139. Deeb, K. K.; Trump, D. L.; Johnson, C. S. Vitamin D signalling pathways in cancer: potential for anticancer therapeutics. *Nat. Rev. Cancer* **2007**, *7,* 684-700.

140. Kornmayer, S. C.; Rominger, F.; Gleiter, R. Synthesis of 11,12-didehydrodibenzo[a,e]cycloocten-5(6H)-one: a strained eight-membered alkyne. *Synthesis* **2009**, 2547-2552.

141. Loibner, H.; Zbiral, E. Synthesis of 3-deoxy-3-aminovitamin D3 and 3-deoxy-3-epiamino-vitamin D3 and D2. *Tetrahedron* **1978**, *34,* 713-716.

142. DeBerardinis, A. M.; Hadden, M. K. *Tetrahedron Lett.* **2011**, submitted.

143. Clement, V.; Sanchez, P.; de Tribolet, N.; Radovanovic, I.; Ruiz i Altaba, A. HEDGEHOG-GLI1 signaling regulates human glioma growth, cancer stem cell self-renewal, and tumorigenicity. *Curr. Biol.* **2007**, *17,* 165-172.

144. Cross, H. S.; Bareis, P.; Hofer, H.; Bischof, M. G.; Bajna, E.; Kriwanek, S.; Bonner, E.; Peterlik, M. 25-Hydroxyvitamin D3-1Î±-hydroxylase and vitamin D receptor gene expression in human colonic mucosa is elevated during early cancerogenesis. *Steroids* **2001**, *66,* 287-292.

145. McCarthy, K.; Laban, C.; Bustin, S. A.; Ogunkolade, W.; Khalaf, S.; Carpenter, R.; Jenkins, P. J. Expression of 25-hydroxyvitamin D-1-alpha-hydroxylase, and vitamin D receptor mRNA in normal and malignant breast tissue. *Anticancer Res* **2009**, *29,* 155-157.

146. Matusiak, D.; Benya, R. V. CYP27A1 and CYP24 expression as a function of malignant transformation in the colon. *J. Histochem. Cytochem.* **2007**, *55,* 1257-1264.

147. Downie, D.; McFadyen, M. C. E.; Rooney, P. H.; Cruickshank, M. E.; Parkin, D. E.; Miller, I. D.; Telfer, C.; Melvin, W. T.; Murray, G. I. Profiling cytochrome P450 expression in ovarian cancer: Identification of prognostic markers. *Clin. Cancer Res.* **2005**, *11,* 7369-7375.

148. Matusiak, D.; Murillo, G.; Carroll, R. E.; Mehta, R. G.; Benya, R. V. Expression of vitamin D receptor and 25-hydroxyvitamin D3-1Î±-hydroxylase in normal and malignant human colon. *Cancer Epidemiol. , Biomarkers Prev.* **2005**, *14,* 2370-2376.

149. Kane, K. F.; Langman, M. J. S.; Williams, G. R. Antiproliferative responses of two human colon cancer cell lines to vitamin D3 are differentially modified by 9-cis-retinoic acid. *Cancer Res.* **1996**, *56,* 623-632.

150. Kumagai, T.; O'Kelly, J.; Said, J. W.; Koeffler, H. P. Vitamin D2 analog 19-nor-1,25-dihydroxyvitamin D2: Antitumor activity against leukemia, myeloma, and colon cancer cells. *J. Natl. Cancer Inst.* **2003**, *95,* 896-905.

151. Murillo, G.; Nagpal, V.; Tiwari, N.; Benya, R. V.; Mehta, R. G. Actions of vitamin D are mediated by the TLR4 pathway in inflammation-induced colon cancer. *J. Steroid Biochem. Mol. Biol.* **2010**, *121,* 403-407.

120

152. Teichert, A. E.; Elalieh, H.; Elias, P. M.; Welsh, J.; Bikle, D. D. Overexpression of hedgehog signaling is associated with epidermal tumor formation in vitamin D receptor-null mice. *J Invest Dermatol* **2011**, *131,* 2289-2297.

153. Andrews, D. R.; Barton, D. H. R.; Hesse, R. H.; Pechet, M. M. Synthesis of 25-hydroxy- and 1Î±,25-dihydroxy vitamin D3 from vitamin D2 (calciferol). *J. Org. Chem.* **1986**, *51,* 4819-4828.

154. DeBerardinis, A. M.; Banerjee, U.; Miller, M.; Lemieux, S.; Hadden, M. K. Probing the structural requirements for vitamin D3 inhibition of the hedgehog signaling pathway. *Bioorg. Med. Chem. Lett.* **2012**, *22,* 4859-4863.

155. Okamura, W. H.; Shen, G. Y.; Barrack, S. A.; Henry, H. L. Vitamin D analogs: potential inhibitors of vitamin D metabolism. *Proc. Workshop Vitam. D* **1988**, *7th,* 12-21.

156. Okamura, W. H.; Midland, M. M.; Hammond, M. W.; Abd, R. N.; Dormanen, M. C.; Nemere, I.; Norman, A. W. Chemistry and conformation of vitamin D molecules. *J Steroid Biochem Mol Biol* **1995**, *53,* 603-613.

157. Zhu, G.; Okamura, W. H. Synthesis of Vitamin D (Calciferol). *Chem. Rev. (Washington, D. C.)* **1995**, *95,* 1877-1952.

158. Deluca, H. F.; Grzywacz, P.; Plum, L. A.; Clagett-Dame, M. Patent Application Country: Application: US; US; Priority Application Country: US Patent US20070066566, 2007.

159. Gant, T. G.; Sarshar, S. US2008/300316, **2008**.

160. Winkle, M. R.; Ronald, R. C. Regioselective metalation reactions of some substituted (methoxymethoxy)arenes. *J. Org. Chem.* **1982**, *47,* 2101-2108.

161. Chaudhary, S. K.; Hernandez, O. 4-Dimethylaminopyridine: an efficient and selective catalyst for the silylation of alcohols. *Tetrahedron Lett.* **1979**, 99-102.

162. Barrack, S. A.; Gibbs, R. A.; Okamura, W. H. Potential inhibitors of vitamin D metabolism: An oxa analogue of vitamin D. *J. Org. Chem.* **1988**, *53,* 1790-1796.

163. Po-Lin So; Langston, A. W.; Daniallinia, N.; Hebert, J. L.; Fujimoto, M. A.; Khaimskiy, Y.; Aszterbaum, M.; Epstein Jr., E. H. Long-term establishment, characterization and manipulation of cell lines from mouse basal cell carcinoma tumors. *Exp. Dermatol.* **2006**, *15,* 742-750.

164. De Beule, K.; Van Gestel, J. Pharmacology of itraconazole. *Drugs* **2001**, *61,* 27-37.

165. Vanden, B. H.; Koymans, L.; Moereels, H. P450 inhibitors of use in medical treatment: focus on mechanisms of action. *Pharmacol Ther* **1995**, *67,* 79-100.

166. Girmenia, C. New generation azole antifungals in clinical investigation. *Expert Opin. Invest. Drugs* **2009**, *18,* 1279-1295.

121

167. Bennett, F.; Saksena, A. K.; Lovey, R. G.; Liu, Y.; Patel, N. M.; Pinto, P.; Pike, R.; Jao, E.; Girijavallabhan, V. M.; Ganguly, A. K.; Loebenberg, D.; Wang, H.; Cacciapuoti, A.; Moss, E.; Menzel, F.; Hare, R. S.; Nomeir, A. Hydroxylated analogues of the orally active broad spectrum antifungal, Sch 51048 (1), and the discovery of posaconazole [Sch 56592; 2 or (S,S)-5]. *Bioorg Med Chem Lett* **2006**, *16,* 186-190.

168. Tanoury, G. J.; Hett, R.; Wilkinson, H. S.; Wald, S. A.; Senanayake, C. H. Total synthesis of (2R,4S,2'S,3'R)-hydroxyitraconazole: implementations of a recycle protocol and a mild and safe phase-transfer reagent for preparation of the key chiral units. *Tetrahedron: Asymmetry* **2003**, *14,* 3487-3493.

169. Liu, J.; Chong, C. R.; Xu, J.; Lu, J.; Bhat, S. Patent Application Country: Application: WO; WO; Priority Application Country: US Patent WO2008124132, **2008**.

170. Shi, W.; Nacev, B. A.; Bhat, S.; Liu, J. O. Impact of Absolute Stereochemistry on the Antiangiogenic and Antifungal Activities of Itraconazole. *ACS Med. Chem. Lett.* **2010**, *1,* 155-159.

171. Uhmann, A.; Niemann, H.; Lammering, B.; Henkel, C.; Hess, I.; Nitzki, F.; Fritsch, A.; Pruefer, N.; Rosenberger, A.; Dullin, C.; Schraepler, A.; Reifenberger, J.; Schweyer, S.; Pietsch, T.; Strutz, F.; Schulz-Schaeffer, W.; Hahn, H. Antitumoral effects of calcitriol in basal cell carcinomas Involve Inhibition of Hedgehog signaling and Induction of Vitamin D receptor signaling and differentiation. *Mol. Cancer Ther.* **2011**, *10,* 2179-2188.

172. Markant, S. L.; Esparza, L. A.; Sun, J.; Barton, K. L.; McCoig, L. M.; Grant, G. A.; Crawford, J. R.; Levy, M. L.; Northcott, P. A.; Shih, D.; Remke, M.; Taylor, M. D.; Wechsler-Reya, R. J. Targeting Sonic Hedgehog-associated Medulloblastoma through inhibition of aurora and polo-like kinases. *Cancer Res.* **2013**, *73,* 6310-6322.

173. Wang, C. Y. Y.; Wei, Q.; Han, I.; Sato, S.; Ghanbari-Azarnier, R.; Whetstone, H.; Poon, R.; Hu, J.; Zheng, F.; Zhang, P.; Wang, W.; Wunder, J. S.; Alman, B. A. Hedgehog and Notch signaling regulate self-renewal of undifferentiated pleomorphic sarcomas. *Cancer Res.* **2012**, *72,* 1013-1022.

174. Jesus-Acosta, A. D.; O'Dwyer, P. J.; Ramanathan, R. K.; Von Hoff, D. D.; Maitra, A.; Rasheed, Z.; Zheng, L.; Rajeshkumar, N. V.; Le, D. T.; Hoering, A.; Bolejack, V.; Yabuuchi, D. T.; Laheru, D. A. A phase II study of Vismodegib, a Hedgehog (Hh) pathway inhibitor, combined with Gemcitabine and nab-Paclitaxel (nab-P) in patients (pts) with untreated metastatic pancreatic ductal adenocarcinoma (PDA). *J Clin Oncol* **2014**, *32,* Abstract 257.

APPENDIX A: Selected 1H & 13C NMR Spectral Data

mg-84b 2 1 /opt/topspin mghosh

11.9323
18.8625
22.2469
22.5637
22.8249
23.2693
23.8824
27.6355
28.0140
28.6629
30.8862
31.9815
36.1268
37.1401
37.7989
39.5073
40.3749
45.2621
55.7441
56.5371

76.7728
77.0960
77.2803

114.9319
115.0071

126.6824

141.6845
142.4608

167.9134

199.7753

[ppm]   200   150   100   50   0

[rel]   8   6   4   2   0

12.02
18.86
22.56
27.68
31.98
36.16
39.51
40.58
45.78
55.82
56.34
56.60
78.07
112.30
117.73
121.78
135.57
141.76
145.38

MeO

f1 (ppm)

127

13.72
18.03
22.41
22.70
23.03
27.29
29.72
30.53
30.72

39.82
41.92

51.60

58.53

72.62
76.76
77.01 CDCl3
77.27 CDCl3

116.31
119.94
121.96

129.68
132.36

155.78

166.47

13.77
18.21
18.75
19.36
22.86
27.25
29.88
30.72
35.40
38.27
40.10
42.11

51.80

56.69

72.83
76.92 CDCl3
77.18 CDCl3
77.37 CDCl3
77.43 CDCl3

116.50
120.09
122.12

129.84
132.52

155.92

166.58

f1 (ppm)

NAME   isobutyl derivative 96
EXPNO   1
PROCNO   1
Date_   20120726
Time   16.38
INSTRUM   spect
PROBHD   5 mm BBO BB-1H
PULPROG   zg30
TD   32768
SOLVENT   CDCl3
NS   16
DS   2
SWH   10030.578 Hz
FIDRES   0.315264 Hz
AQ   1.5860696 sec
RG   456.1
DW   48.400 usec
DE   6.00 usec
TE   298.2 K
D1   1.00000000 sec
TD0   1

======== CHANNEL f1 ========
NUC1   1H
P1   12.00 usec
PL1   -1.00 dB
SFO1   500.1330885 MHz
SI   32768
SF   500.1300000 MHz
WDW   EM
SSB   0
LB   0.30 Hz
GB   0
PC   1.00

ppm   1.0   1.5   2.0   2.5   3.0   3.5   4.0   4.5   5.0   5.5   6.0   6.5   7.0   7.5   8.0

1.00   0.92 0.94 0.92 0.93

NAME   isobutyl derivative 96
EXPNO   2
PROCNO   1
Date_   20120731
Time   17.30
INSTRUM   spect
PROBHD   5 mm TXI 1H/D-
PULPROG   zgpg30
TD   65536
SOLVENT   CDCl3
NS   20224
DS   4
SWH   30030.029 Hz
FIDRES   0.458222 Hz
AQ   1.0912410 sec
RG   14596.5
DW   16.650 usec
DE   6.50 usec
TE   298.2 K
D1   1.50000000 sec
D11   0.03000000 sec
TD0   1

======= CHANNEL f1 =======
NUC1   13C
P1   6.25 usec
PL1   0.00 dB
SFO1   125.7703643 MHz

======= CHANNEL f2 =======
CPDPRG2   waltz16
NUC2   1H
PCPD2   70.00 usec
PL2   -1.00 dB
PL12   13.76 dB
PL13   70.00 dB
SFO2   500.1320005 MHz
SI   32768
SF   125.7577890 MHz
WDW   EM
SSB   0
LB   1.00 Hz
GB   0
PC   1.40

ppm

13.62
18.03
18.61
22.67
27.04
30.53
32.54
35.27
37.86
39.92
41.98

51.60

56.24

72.61
76.76
77.02 CDCl3
77.27 CDCl3
77.27 CDCl3

116.33
119.96
121.93
125.54
128.27
128.35
129.69
132.30

143.25

155.77

166.43

-13000
-12000
-11000
-10000
-9000
-8000
-7000
-6000
-5000
-4000
-3000
-2000
-1000
0
-1000

-10
0
10
20
30
40
50
60
70
80
90
100
110
120
130
140
150
160
170
180
190
200
10

f1 (ppm)

13.88
14.19
18.20
22.19
22.57
22.86
23.19
27.45
29.88
30.70
30.88
39.99
42.09

51.77

58.71

72.79
76.93 CDCl3
77.18 CDCl3
77.43 CDCl3

116.48
120.07
122.16

129.86
132.54

155.87

166.35

13.77
14.30
18.21
18.79
22.86
22.92
25.88
27.24
30.71
32.54
35.56
35.84
40.09
42.09

51.78

56.62

72.92
76.92 CDCl3
77.18 CDCl3
77.43 CDCl3

116.55
120.16
122.06

129.85
132.44

156.00

166.71

f1 (ppm)

13.84
18.21
18.75
21.54
22.86
24.91
27.49
29.88
30.71
33.73
40.15
42.22
45.70
51.83
57.60
72.83
76.92 CDCl3
77.18 CDCl3
77.43 CDCl3
116.47
120.07
122.14
129.84
132.54
155.88
166.54

f1 (ppm)

13C NMR spectrum with peak labels:

13.76
13.88
18.20
18.79
22.57
22.87
27.45
29.56
29.84
29.89
30.34
30.70
30.88
33.90
39.99
42.09
51.77
58.71
72.85
116.54
120.16
122.02
129.84
132.45
156.07
166.70

f1 (ppm) axis: 210, 200, 190, 180, 170, 160, 150, 140, 130, 120, 110, 100, 90, 80, 70, 60, 50, 40, 30, 20, 10, 0, -10

Top axis: 1400, 1300, 1200, 1100, 1000, 900, 800, 700, 600, 500, 400, 300, 200, 100, 0, -100

450 400 350 300 250 200 150 100 50 0

10.75
1.43
1.50
0.89
0.59
1.51
5.69
2.71
0.63
1.39

1.00

0.60

0.97
1.30
1.88

9.5 9.0 8.5 8.0 7.5 7.0 6.5 6.0 5.5 5.0 4.5 4.0 3.5 3.0 2.5 2.0 1.5 1.0 0.5 0.0 -0.5 -1.0
f1 (ppm)

146

155.84

166.50

13.39
18.01
22.63
22.69

27.68
29.72
30.35
30.38
30.50
31.10
32.42
39.97
41.99

49.72
51.73

57.79

72.78
76.76
77.01 CDCl3
77.22 CDCl3
77.27 CDCl3

116.36
119.98
121.90

129.68
132.29

155.80

166.46

116.46
120.03
122.19

129.84
132.58

10.17
11.51
13.85
18.21
18.90
22.86
24.61
26.80
27.55
29.88
30.70
33.63
37.40
39.84
42.23

51.83

57.78

72.81
76.92 CDCl3
77.17 CDCl3
77.43 CDCl3

f1 (ppm)

13C NMR spectrum (f1 (ppm))

Chemical shift values:
13.57, 15.44, 17.58, 18.02, 18.77, 20.51, 22.68, 27.04, 27.70, 30.49, 30.53, 31.43, 33.47, 38.50, 39.04, 39.88, 41.90, 51.58, 56.29, 77.69, 116.32, 119.95, 121.91, 129.68, 132.28, 155.76, 166.46

13.48
13.52
17.45
18.56
18.62
22.54
22.68
22.80
23.77
23.81
27.16
28.00
33.61
35.29
35.40
35.94
35.99
39.48
39.51
40.40
42.01

51.60
52.62
56.53
56.74

69.45
72.51

108.24
111.87

120.73
122.48
125.18
127.49
127.94

136.84

162.05

f1 (ppm)

12.95
17.43
17.73
22.60
26.15
30.37
35.77
39.63
42.20

51.02
53.10

70.01
74.68
76.75
76.94 CDCl3
77.19 CDCl3
77.44 CDCl3

116.44
120.28
122.00

129.83
132.06

156.07

166.70

10000
9000
8000
7000
6000
5000
4000
3000
2000
1000
0

-10
0
10
20
30
40
50
60
70
80
90
100
110
120
130
140
150
160
170
180
190
200
10

f1 (ppm)

50000
45000
40000
35000
30000
25000
20000
15000
10000
5000
0

10.82
14.11
19.45
20.16
22.65

31.58

49.15
50.58
53.47
61.57
66.20
67.96
70.26
74.72
76.76 CDCl3
76.78
77.22 CDCl3
77.22 CDCl3
77.27 CDCl3

107.24
107.69
115.31
116.62
118.49
123.66
127.25
127.28
129.61
131.43
133.02
134.25
134.29
136.10
146.01
150.77
151.40
152.65
152.98

-10
0
10
20
30
40
50
60
70
80
90
100
110
120
130
140
150
160
170
180
190
200
210
f1 (ppm)

159